University of Twente

Characterisation of natural epicuticular wax

Norah Hornsveld

August 15th, 2014

Characterisation of natural epicuticular wax

By
Norah Hornsveld

To obtain the degree of Master of Science,
Applied Physics
August 15th, 2014

Abstract

The micro- and nanostructure of hydrophobic leaf surfaces, and in particular the leaves of *Euphorbia myrsinites* are examined. The leaves are characterised in terms of surface topography and wettability. The surface of the *E. myrsinites* leaves consist of papillae in the microscale with superimposed epicuticular wax platelets in the nanoscale. The hierarchical surface structure ensures superhydrophobicity of the leaf surface. Within the realm of surface science, the epicuticular wax is of main interest, because of the possibility to recrystallise the wax on top of artificial surfaces. *E. myrsinites* epicuticular wax is recrystallised on a silicon wafer. To obtain a nanostructured surface, a very thick layer of wax was needed. It is expected, that this is caused by the influence of the substrate on the wax. With the recrystallisation, a very hydrophobic surface with a static contact angle of ~155° is obtained. This extremely high contact angle partially occurs due to multiscale roughness caused by an uneven wax distribution on the substrate. The experiments are carried out with use of optical microscopy, atomic force microscopy, scanning electron microscopy, helium ion microscopy, gas chromatography, and contact angle goniometry.

Exam committee:

Professor:	Prof. dr. ir. Harold Zandvliet
Supervisor:	Dr. Stefan Kooij
External member:	Dr. Chao Sun

Work performed at:
Physics of Interfaces and Nanomaterials
Faculty of Science and Technology
University of Twente
P.O. Box 217
7500 AE, Enschede

Contents

1 Introduction **1**

2 Theory **3**

2.1 Surface wetting 3

2.2 Plant surfaces and hydrophobicity 5

2.3 Epicuticular waxes and their molecular structure 8

2.4 Wax extraction and recyrstallisation 12

3 Experimental details **14**

3.1 Material 14

3.2 Wax extraction and deposition 14

3.3 Characterisation tools 15

4 Euphorbia myrsinites leaves **18**

4.1 Introduction 18

4.2 Leaf surface structure analysis 18

4.3 Optimising the wax extraction 27

4.4 Chemical analysis of the wax 30

4.4 Analysis of deposited wax 30

4.5 Wettability analysis 43

5 Other plant leaves **47**

5.1 Introduction 47

5.2 Aquilegia Canadensis 47

5.3 Buxus sempervirens 50

6 Conclusions and outlook **53**

Bibliography **56**

Appendix **58**

Acknowledgements **64**

Chapter 1

Introduction

Inspired by their interesting properties, there is a strong drive to mimic natural surfaces. Natural surfaces provide a large diversity of structures and capabilities. One could think of a gecko which can climb up vertically, due to a reversible adhesion scale structure on the bottom of its feet [1], a pond skater walking on water, based on waxy hairs at the bottom of its legs [2], a skin structure of a shark reducing drag [3] or the nanostructure present on a moth's eye making it antireflective [4]. The unique structure is what gives the surfaces their characteristic properties. The structural diversity and properties evolved over several millions of years by a long lasting game of mutation and selection. Adaptations to different environments led to a huge structural variety and the development of multifunctional (protective) interfaces.

In the last decade still a lot of research is done on prominent natural occurring properties as water-repellency and self-cleaning of plant material. Those properties are desirable for a wide variety of artificial biological inspired materials, with (future) applications like water-free windows, waterproof (breathable) clothing, anti-icing coatings (on power lines/infrastructure), anti-corrosion coatings or microfluidic devices. Extreme water-repellency, i.e. superhydrophobicity, in nature, and in particular plants, is caused by two-level hierarchical surface structuring formed by papillose cell sculptures with smaller superimposed three-dimensional waxes on top [5]. The Lotus (*Nelumbo Nucifera*) leaf in figure 1.1 is the most famous example on which such a hydrophobic surface structure is present. Some superhydrophobic surfaces, like the *Salvinia Oblongifolia* (figure 1.1c-e), even provide a three level hierarchical structure. The first two levels are formed by the convex cells with superimposed three-dimensional wax crystalloids, and a third level of surface structuring is caused by large hairs. The three-dimensional wax-layer is called the epicuticular wax.
Epicuticular wax seems very interesting because of the great diversity of existing peculiar morphologies but it is mainly because these morphologies can result from self-assembly processes. Not only on the leaf surface itself, but also on artificial substrates, epicuticular waxes have been shown to grow without any external stimulus. It has been reported that wax can be subtracted from plants and by depositing it on various inorganic substrates the (original) wax morphology can reassemble [6]. In some cases certain environmental conditions are needed to activate or improve the reassembly [7]. In the theoretical chapter this is explained in more detail.

The research group Physics of Interfaces and Nanomaterials, where this master assignment is carried out, so far has no experience with research on plant waxes. Therefore, the aim of this project is first to develop the expertise on extracting and depositing wax and to explore the suitability of available characterisation tools on the basis of literature reports. Based on that, various experiments are carried out to create more understanding. The final goal of the experiments is to recrystallise plant waxes on artificial surfaces and follow the growth process over time after deposition. The morphology of the wax layers then needs to be characterised.

The majority of experiments are carried out with use of the plant named *Euphorbia myrsinites*. The *E. myrsinites* leaves are covered with an epicuticular platelet containing wax. In most of the recently published literature, experiments carried out with the use of Lotus leaf wax or other tubule containing waxes are described. This makes research to platelet waxes interesting. For comparison also other leaves, like the *Aquilegia canadensis*, are examined but not into detail.

The outline of this thesis is as follows. In the theoretical chapter, we provide relevant background on the topic of this thesis based on literature studies. Moreover, the most important findings of the last few years, pertaining to the recrystallisation of epicuticular wax layers are reviewed. In the next chapter the experimental procedures are discussed as well as the experimental tools and settings used in this work. The subsequent chapters are devoted to the actual experiments, the results and their analysis. We finish this report with an overall conclusion of this project and an outlook to possible future experiments.

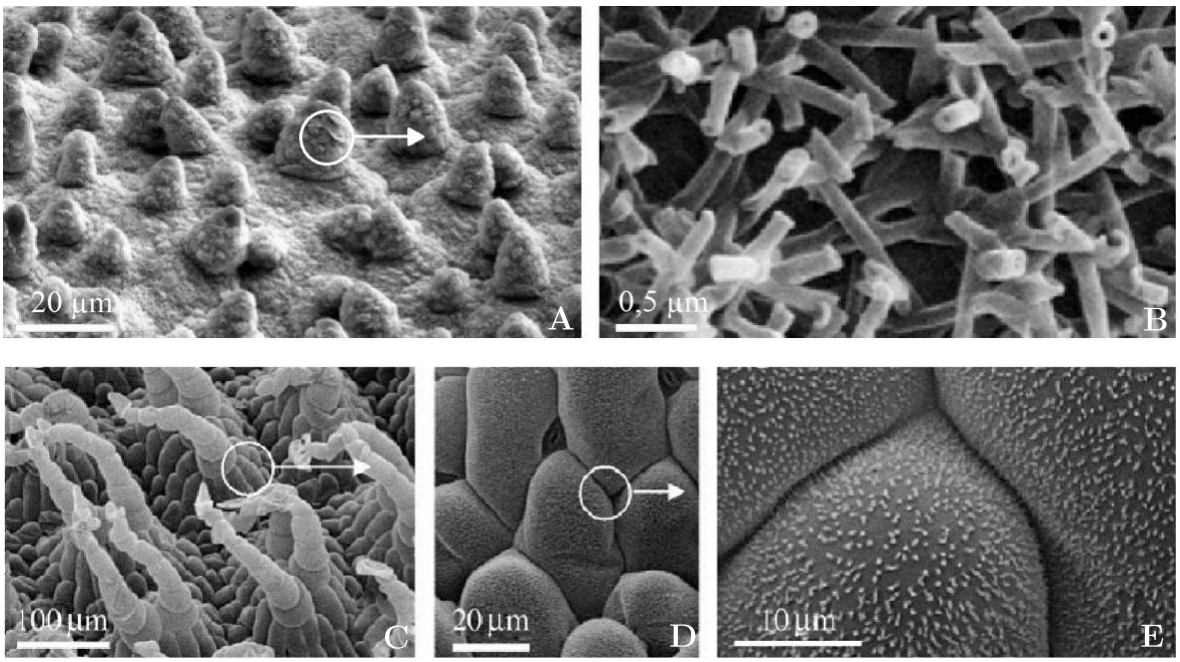

Figure 1.1: Nelumbo Nucifera (a & b) and Salvinia Oblongifolia (c,d & e) leaf surface structure at different magnifications. Figure adapted from [8].

Chapter 2

Theory and background

2.1 Surface wetting

When a droplet is deposited on surface it will spread to minimize its free energy. The way the droplet spreads is not only dependent on the type of liquid but also on properties of the solid and the fluid that surrounds the droplet. An important parameter of this process is the contact angle. The contact angle is the angle at which the liquid–fluid interface meets the solid–liquid interface as is shown in figure 2.1a and is determined by the interactions across the three interfaces. If the applied drop of water tends to spread, the wettable surface is described by a low contact angle and if the water droplet forms a spherical shape the contact angle will be high. The contact angle determines the wettability and is specific for any given system. For an ideal situation, the contact angle can be calculated with Young's equation [9].

$$cos(\theta_\gamma) = \frac{\gamma_{SF} - \gamma_{SL}}{\gamma_{LF}} \tag{2.1}$$

The formula defines the equilibrium between three interfacial tensions: liquid-fluid γ_{LF}, solid-fluid γ_{SF} and solid-liquid γ_{SL}, where θ_γ is the contact angle. This equation is only valid for an ideal solid surface which is smooth, rigid, chemically homogeneous, insoluble, and non-reactive. However, every surface has some degree of roughness. Roughness affects the measured contact angle and because of that it will differ from the actual contact angle. This is illustrated in figure 2.1b. The measured contact angle is referred to as the apparent contact angle θ_{AP}. The apparent contact angle is defined as the angle between the tangent to the liquid-fluid interface and the straight line that represents the surface. The actual contact θ_{AC} angle on the other hand, is determined locally and therefore takes the roughness into account. Because the interfacial tension works on a larger surface, the apparent contact angle is altered.

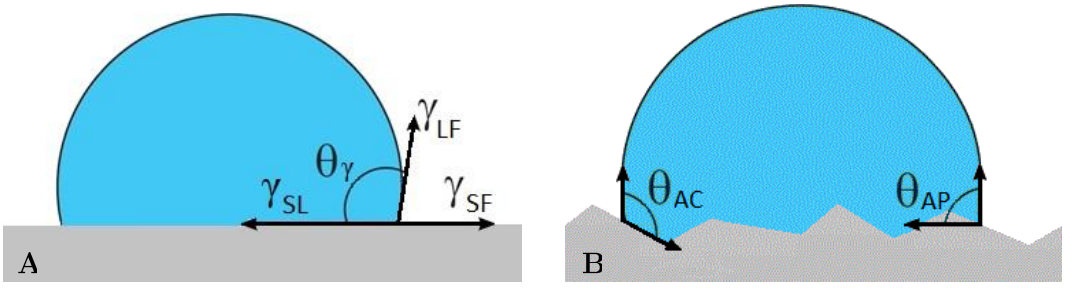

Figure 2.1: A schematic representation of droplets on a flat (a) and rough (b) surface. The three arrows in the left picture represent the three interfacial tensions: liquid-fluid γ_{LF}, solid-fluid γ_{SF} and solid-liquid γ_{SL}. The angle between the solid-liquid and liquid-fluid interface is known as the Young's contact angle θ_γ. The picture on the right shows the differences in the actual contact angle θ_{AC} and the apparent contact angle θ_{AP}.

To account for the effect of surface roughness the so-called Wenzel equation is established. The Wenzel contact angle θ_w is defined as the most stable apparent contact angle and can be calculated by taking the inverse cosine of the roughness factor r times the cosine of the ideal contact angle [10].

$$cos\ (\theta_\omega) = r\ cos(\theta_\gamma) \tag{2.2}$$

Here, the roughness factor is defined as the ratio between the true contact area and the projected apparent surface, which is always equal to or higher than 1. Roughness acts as an amplifier for the wetting characteristics. This implies that a surface which is easy to wet will have a θ_w smaller than θ_γ when roughness is added. The opposite holds for surfaces which are difficult to wet, the Wenzel contact angle will increase. The Wenzel equation will give a more realistic value of the contact angle for rough surfaces.

In the previous example it is assumed that a droplet completely wets the rough surface, referred to as the Wenzel state, but there is yet another possibility. Pockets of air can be trapped beneath the droplet; that is, inside the facets of the rough surface. In this case, the contact area of the solid surface is smaller than the projected area of the droplet. If the droplet is in contact with the surface in this manner it is referred to as the Cassie-Baxter state. In figure 2.2 a graphical illustration of both states is shown. The Cassie-Baxter state can be understood as a chemically heterogeneous surface, in which the contact area alternates between a solid surface and air. This results in a varying surface tension and thus varying Young's contact angle θ_γ. On this principle the Cassie-Baxter equation is based [11].

$$cos\ (\theta_{CB}) = f_1 cos(\theta_{\gamma 1}) + f_2 cos(\theta_{\gamma 2}) \tag{2.3}$$

In this equation θ_{CB} is the apparent Cassie-Baxter contact angle, f_1 and f_2 are the fractions of the areas of the two materials with respect to the total wetted area and $\theta_{\gamma 1}$ and $\theta_{\gamma 2}$ are their contact angles respectively. So what the Cassie-Baxter equation does essentially is calculating the contact angle by using a weighted average of the cosine of the different Young's contact angles (equation 2.1). The Cassie-Baxter state will always increase the contact angle, even for wetting surfaces. If a droplet would be deposited on the surfaces which are shown in the introduction chapter, it would be in the Cassie-Baxter state. The increase in contact angle can be shown as follows. Imagine a micro structured surface with only one type of pillars. To simplify the formula a bit, we set $f_1 = f$, so $f_2 = 1 - f$, where f is the areal fraction of the pillars. Now we assume that $\theta_{\gamma 2} = \theta_{air} = 180°$, i.e. perfectly non-wetting [9]. This gives:

$$cos(\theta_{CB}) = f cos(\theta_Y) + (1 - f)(-1) = f(1 + cos\ (\theta_Y)) - 1 \tag{2.4}$$

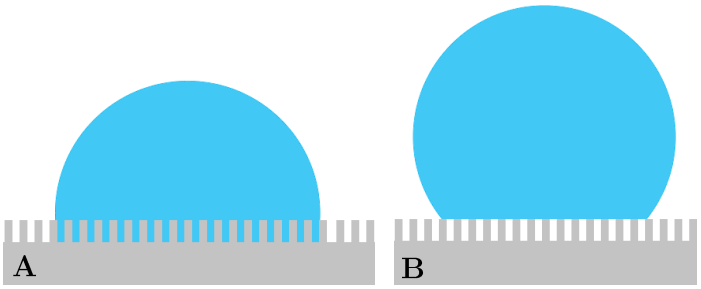

Figure 2.2: A graphical illustration of a droplet on a surface in the Wenzel (a) and Cassie-Baxter (b) state.

From equation 2.4 it can be understood that when the concentration of air pockets is very high in relation to the solid contact surface area, i.e. $f = 0$, the Cassie-Baxter contact angle θ_{CB} will come close to its upper limit of 180°. The Cassie-Baxter state, which can be created by small pillars with air pockets in between, is needed to get nearby such a high contact angle. It is energetically more favorable for the water to form a spherical drop because the water on such a surface gains very little energy through absorption. Both the contact area and the adhesion to the surface are dramatically reduced. The Cassie-Baxter state is metastable, because when enough pressure is applied a droplet in the Cassie-Baxter state will undergo a transition into a Wenzel state. In the Cassie-Baxter state the liquid air interface between the pillars is curved due to the Laplace pressure inside the droplet. If the hanging interface cannot remain pinned at the pillars, it will slide downward to the substrate, i.e. make a transition to the Wenzel state. This scenario can only occur when the contact angle at the liquid-air interface exceeds the actual contact angle. Also, when the pillars are not packed close enough or if the microstructure pillars are lower than the depth of the hanging interface the transition to the Wenzel state will occur [12].

Materials which are difficult to wet are called hydrophobic. The cause lies on the molecular level, molecules in hydrophobic materials are nonpolar and water molecules are polar. Because of this water molecules notice a stronger attraction to other water molecules than to the hydrophobic surface [13]. When a droplet is deposited on a hydrophobic surface, it wants as little contact with the surface as possible. As a result it will have a convex shape and thus a large contact angle. Materials which are easy to wet want to have as much contact with the droplet as possible. Those surfaces are called hydrophilic and droplets on such surfaces will have significantly smaller contact angles compared to contact angles on hydrophobic materials. The boundary between hydrophobic and hydrophilic is defined at 90°, because a surface that has an original contact angle greater than 90° becomes more hydrophobic when microstructured and a surface that has an original contact angle smaller than 90° becomes more hydrophilic when microstructured (see equation 2.2). If surfaces are extremely water-repellent they are called superhydrophobic. On a superhydrophobic surface the contact angle of a water droplet exceeds 150° according to the most recent reviews [14]. Moreover, on water-repellent surfaces, an applied droplet starts to roll off the surface when it is tilted to a specific angle. The angle where the droplet starts to move is called the tilt angle. Superhydrophobicity in combination with a low tilt angle can lead to self-cleaning properties. A tilt angle smaller than 10° is characteristic for superhydrophobic and self-cleaning surfaces [8].

2.2 Plant surfaces and hydrophobicity

Plant surfaces exhibit a great morphological diversity. The diversity of plant surface structures is based on the variability of cell shapes and micro- and nanostructures on top. All primary plant surfaces; e.g. leaves, petals, fruits and herbaceous stems have an outermost cell layer which is called the epidermis. In nearly all aerial tissues of land living plants the top layer of the epidermis is a thin extracellular membrane, called cuticle. The cuticle is basically composed of a polyester called cutin, and integrated (intracuticular) and superimposed (epicuticular) waxes. A schematic representation of the epidermal cells is shown in figure 2.3 as is observed on many plant surfaces. One of the most important attributes of the cuticle is its function as a transpiration barrier. Furthermore, the plant cuticle provides structural and chemical modifications to control surface wetting.

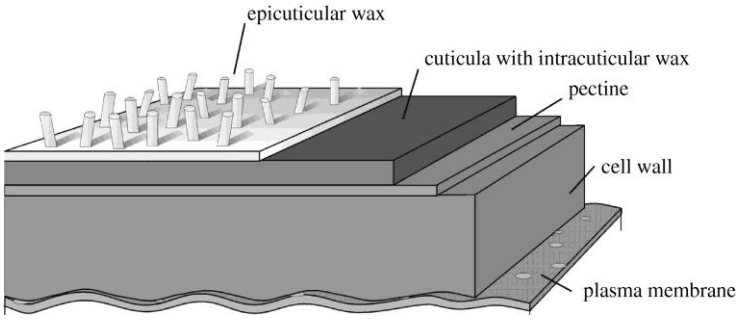

Figure 2.3: Schematic overview of the outermost layers of the plant epidermal cells. The cuticle is shown with an epicuticular wax layer in its most common form as a composite of three-dimensional waxes with an underlying wax film [8].

The cuticle with its integrated waxes is connected with the underlying cellulose wall by pectin, here simply visualized as a layer. Below the cell wall, the plasma membrane is shown. It separates the water-containing part of the epidermis cell from the outermost components of the epidermis above; i.e. it separates the living compartment of the water-containing cell from the outer non-living part of the epidermis [8].

The micro morphology of plant surfaces is formed by the outline and sculpture of a single epidermal cell. Cell curvatures can either be tabular (flat), convex (arced to the outside) or concave (arced to the inside), whereby the most common cell shape is the convex form. According to their shape and aspect ratio (height to width ratio), convex cells can be divided into several subtypes, such as hemisphere, cupola, cone, papilla, hair papilla and hair. Epidermal cells with an aspect ratio of 7:1 or higher are called hairs or trichomes [8]. Wetting in plants is influenced by the sculptures of the cells but also by the fine structure of the surfaces, which can be a cuticular pattern, or by epicuticular waxes. Cuticular patterns are very frequently found in the leaves of flowers (petals) and on seed surfaces. They occur as folding or tubercular (verrucate) patterns that originate due to the cuticle itself, by the expression of the bulk of the cell wall below, or by subcuticular inserts. Prüm et al. put together a schematic overview of several plant surface types [15]. This is shown in figure 2.4, where the horizontal pictograms indicate the epidermal cell shape and the vertical pictograms the substructure type. The epidermal cell shapes represented here are either flat, slightly convex or papillate; from left to right more convexity and more height difference is shown. The substructure is divided into: flat wax films/no structure, epicuticular wax and cuticle folding, respectively. This figure gives a nice overview of the diversity of combinations of plant surfaces that is present in nature. Every surface is useful for its own environmental conditions. Prüm et al. compared the surface types on insect attachment. They show that cuticular folds and epicuticular wax crystalloids strongly reduce traction forces, while smooth papillate epidermal cells improve the grip of pollinators. The difference in epidermal cell shape seems to have very little influence on the forces. What the authors didn't mention, but what is interesting about this schematic overview, is that every surface type also differs in wettability. The leaf surface of the *Magnolia grandiflora* (figure 2.4a) is hydrophilic with a static contact angle of 84° [16] while on the *Calathea zebrina* (figure 2.4c) with a relatively homogeneous structure of conical cells a CA of 0° is reached [8]. With extra roughness the hydrophilic nature is increased as explained in paragraph 2.1. Plant surfaces with high cuticular folds but also for example the *Diospyros kaki* (figure 2.4d) with superimposed epicuticular wax are approaching the superhydrophobic limit with contact angles just below 150°. The *Colocasia esculenta* on the other hand, with papillate cells and superimposed wax is superhydrophobic [16].

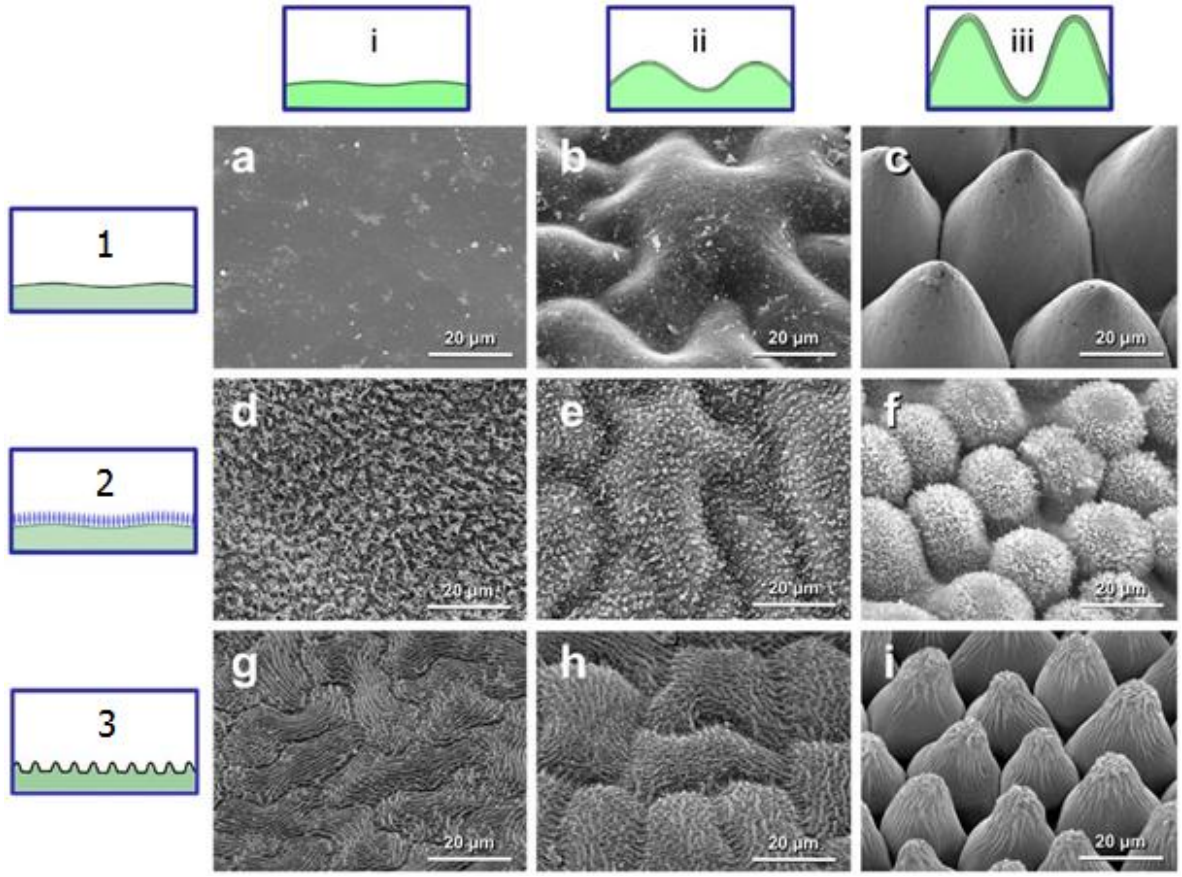

Figure 2.4: Plant surfaces showing different types of structuring. Pictograms on the top show the shape of the epidermal cells: Tabular cells (i), convex cells (ii) and papillate cells (iii). Pictograms on the left illustrate the level of superimposed microstructuring: Films of wax or no further structuring (1), epicuticular waxes (2) and cuticular folds (3). SEM micrographs of plant surfaces: *Magnolia grandiflora* (a), *Paeonia officinalis* (b), *Calathea zebrine* (c), *Diospyros kaki* (d), *Paeonia suffruticosa* (e), *Colocasia esculenta* (f), *Hevea brasiliensis* (g), *Vitis vinifera* (h), *Rosa hybrid Floribunda* (i) [15].

Superhydrophobicity of plants is caused by two-level hierarchical surface structuring. Most of the hydrophobic plant surfaces are formed by convex cell sculptures with smaller superimposed three-dimensional waxes on top [5]. In figure 2.5 a schematic representation of such a hierarchical structure is shown. Wetting of hierarchical surfaces is minimized, because air is trapped in the cavities as explained in the previous paragraph. The convex cell sculptures form the microstructure and the superimposed wax provides the nanostructure. The height and width of the nanostructuring is normally ranging from 10 to 50 µm. The roughness on microscale increases θ_{CB} to high values. The nanostructure on top of the microstructure mainly prohibits the impalement transition. It increases the stability of the Cassie-Baxter state and therefore a higher pressure is needed in order to induce a transition to the Wenzel state. Moreover, it ensures that the water–air interface becomes even larger because the solid–water interface is reduced. Simultaneously, the contact angle hysteresis is decreased, as the edges of micro structuring are covered with a nanostructure (more and smaller pinning sites).
In the article written by Koch and Barthlott in 2009 [8] many different leaves of plants are examined. Some leaves like the *Salvinia Oblongifolia* (figure 1.1), even provide a three-level hierarchical structure. The first two levels are formed by the convex cells with superimposed three-dimensional wax crystalloids, and a third level is caused by large hairs.

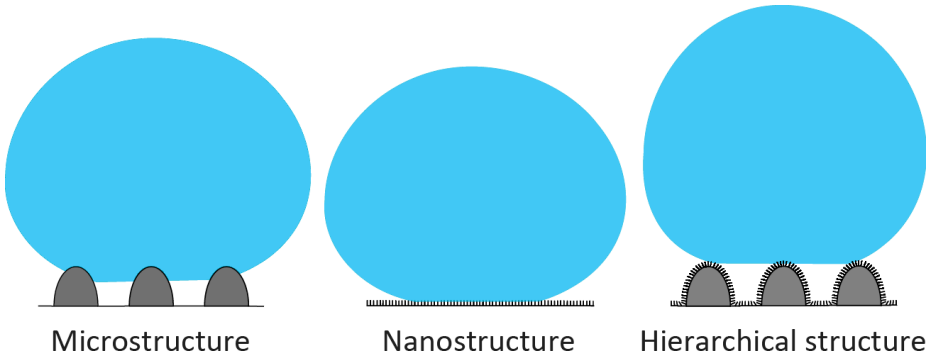

Figure 2.5: Graphical illustration of the hierarchical structure of superhydrophobic plants

2.3 Epicuticular waxes and their molecular structure

The superimposed wax layers on plant surfaces, called epicuticular waxes, show an enormous variety of functional structures. The waxes form thin films or thick crusts and very often superimposed three-dimensional (3D) crystalloids on an underlying wax film. The waxes with 3D crystalloids show a great morphological variability of 3D nano- and microprojections as platelets, rods and tubules in dimensions between hundreds of nanometers and some micrometers [17]. A number of examples are shown in figure 2.6. A dense layer of very small epicuticular wax crystalloids gives an extremely reduced contact area between the surface and the water drops and is therefore very hydrophobic. Superhydrophobicity of plants together with a small tilt angle can lead to self-cleaning properties. As droplets roll or bounce on the surface, droplets will bind with dirt on the substrate and thus will remove the dirt from the surface. Because the leaves of Lotus (*N. nucifera*) afford an impressive demonstration of this effect it is referred to as the Lotus effect [18]. Apart from self-cleaning, the epicuticular wax is responsible for a variety of functions, including the maintenance of stability, prevention of insect attachment and reflection of light at the cuticle interface.

It is believed that waxes diffuse through the cuticle via a lipidic pathway. After diffusion of the wax, the wax morphologies grow by self-assembly and plants are able to repair their wax layer. Typical plant waxes are mixtures of long-chain aliphatic compounds: *n*-alkanes and their derivatives with an oxygen containing functional group, mainly alcohols, ketones, aldehydes, fatty acids, or esters. Koch et al. [19] observed growth of wax layers and three-dimensional crystalloids on surfaces of living plants. They found that some wax sculptures grew directly on the cuticle or on the wax film. It may therefore be concluded that the independent growth processes between the wax film and the wax crystalloids in this experiment, is a separation of different chemical compounds. For some wax types, a correlation between the chemical composition and the morphology was found. Sometimes only one compound of the wax mixture is critical for the formation of a certain wax type [19]. For example waxes with a high content of secondary alcohols, mainly nonacosan-10-ol and nonacosan-diols, will usually form wax tubules (also called nonacosanol tubules). This also holds for waxes with a high content of beta-diketones, which look slightly different and are called beta-diketone tubules. Main components of platelet waxes are in most cases primary alcohols [20].

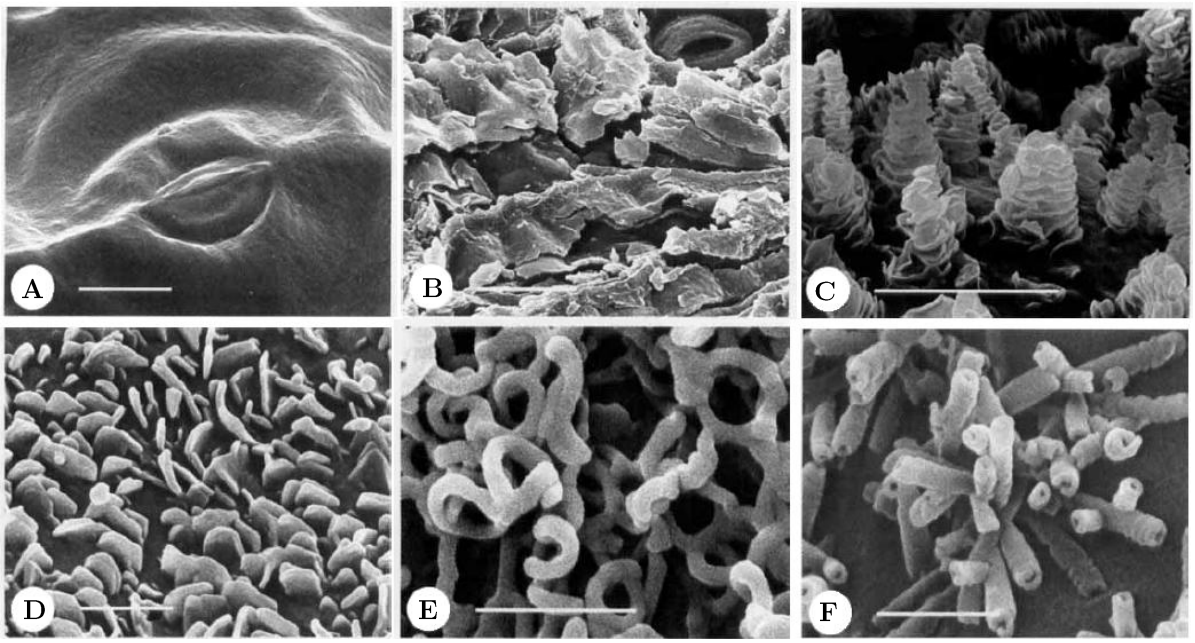

Figure 2.6: Several examples of picuticular waxes: *Hydrocotyle bonariensis* wax film, scale bar = 10 µm (a), *Cynanchum sarcostemma* wax crust, scale bar = 20 µm (b), *Williamodendron quadrilocellaturn* transversely ridged wax rodlets, scale bar = 5 pm (c), *Habropetalum dawei* wax platelets, scale bar = 1 pm (d), *Buxus sempervirens* coiled wax rodlets, scale bar = 1 µm (e), *Lonicera korolkovii* wax tubules, scale bar = 1 µm (f). Figure adapted from [21].

The characteristic aliphatic epicuticular waxes are solid at room temperature and soluble in organic solvents. Their melting point is defined between 60 and 95°C. The waxes are shown to have a crystalline nature, this however has not yet been generally proved for all types. The crystal structure of well known waxes, like the commercial paraffin wax (figure 2.7a), and also pure aliphatic wax compounds, show a parallel assembly of the straight molecules, whereby molecules of equal length usually form layers. An alkene structure model is shown in figure 2.7b, with which it becomes clear that the length of the molecules of the waxes determine the layer thickness. The model is used as a reference for the epicuticular waxes. The length of alkane molecules with n carbon atoms can be calculated by the formula [20]:

$$L = 1.273n + 1.875 \text{ Å} \tag{2.5}$$

Some plant epicuticular waxes crystallise in a bilayered structure, while others form a single-layer structure. Double layer structures result, when compounds with polar functional groups at the end of the molecules (fatty acids, aldehydes, prim. alcohols) assemble with a head-to-head orientation. The development of the layer order can vary if multiple components are present and depends on the chain length distribution and the separation of the components during crystallisation. Some wax morphologies show strong disorder of the molecular layers [20]. Different models of alkene molecular layer order are shown in figure 2.8.

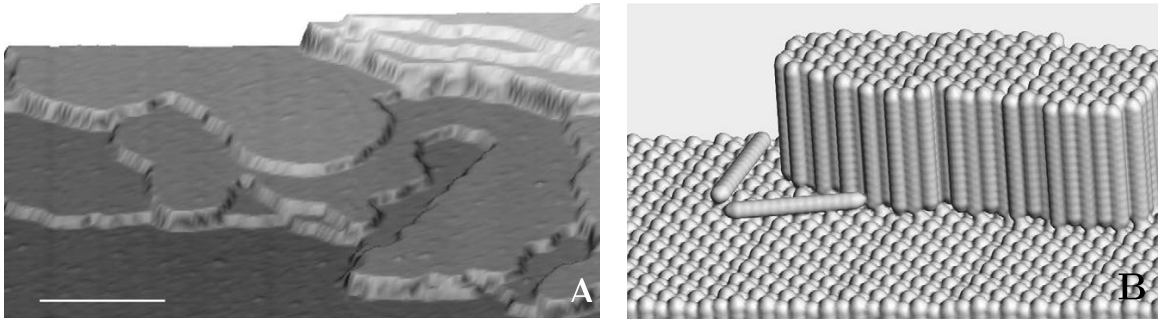

Figure 2.7: Typical wax layer structure: AFM image of paraffin (a) (not to scale; the lateral scan size is 5 µm and the height of small steps is ca. 40 Å) and the structure model of an alkane wax (b) [20].

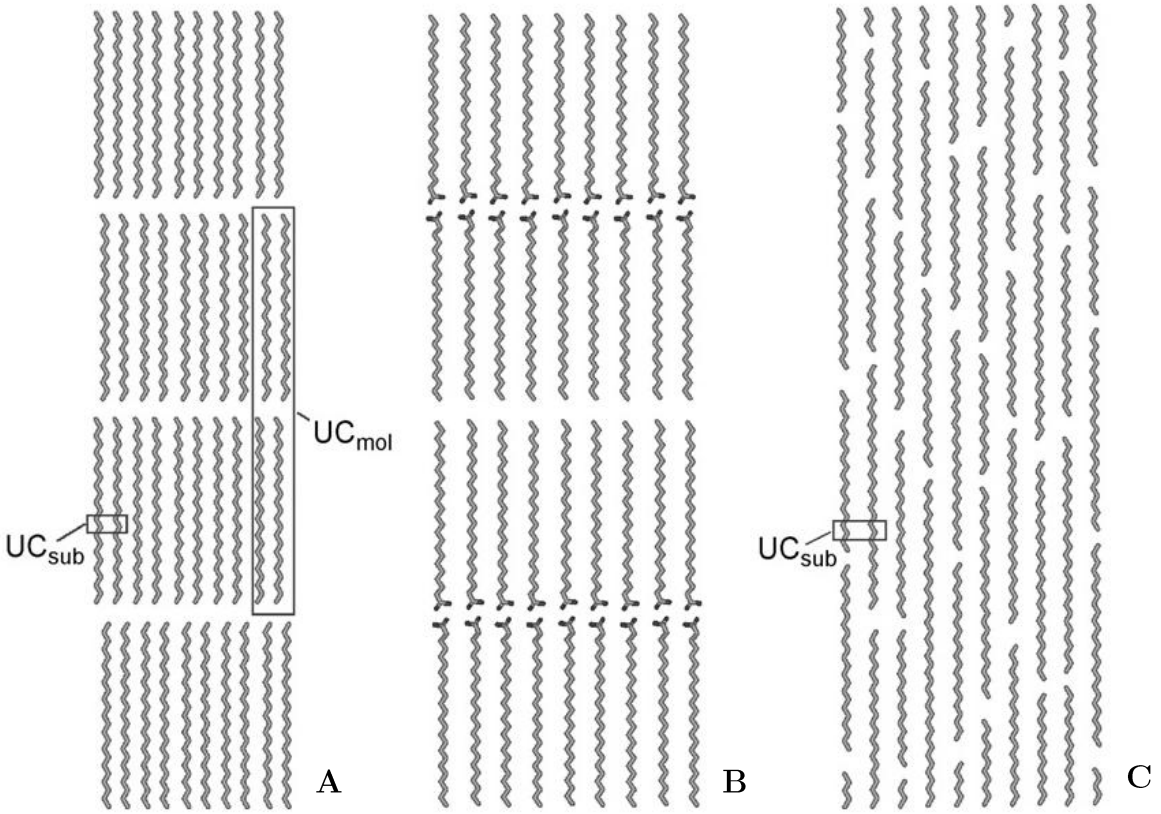

Figure 2.8: Model of regularly ordered alkane molecules (a), head-to-head orientation of the molecules, forming a double-layer structure (b) and a nematic structure without layer order (c). UC_{mol} is the unit cell of entire molecules; UC_{sub} the unit cell of methylene subcells [17].

Different crystal structure symmetries of the methylene subcells occur, when molecules take different orientations relative to their neighbours by rotation around their long axis. In most waxes the molecules are packed in a characteristic order which results in an orthorhombic symmetry of the subcells. In the orthorhombic structure the C-C zig-zag planes of the molecules occur in two orientations, almost perpendicular to their neighbours (see figure 2.9a). Other wax compounds crystallise preferentially in a triclinic order (figure 2.9b). A triclinic symmetry (or monoclinic, if the angles are 90 °) is also found e.g. in pure n-alkane compounds with even number of carbon chain lengths. In this structure the zig-zag planes are oriented parallel. Furthermore, a hexagonal structure occurs in the known commercial waxes, often as a high temperature form, just below the melting point. In this state the molecules are oriented in three directions or they can rotate around the long axis (rotator phase). Ensikat et al. did multiple diffraction experiments to determine the crystal structure of several epicuticular waxes. Most morphological features of the plant epicuticular waxes showed one of the three structures mentioned. Several morphological features seem to be incompatible with a three-dimensional periodical arrangement of the molecules [20].

Pure compounds usually form regular crystals with a periodic order in three dimensions. However, the plant waxes are mixtures of several compounds. If single components dominate, they may form separate crystals, while minor constituents remain mixed as a solid solution. The platelets Ensikat et al. [20] examined, appear as single particles, clusters or fused aggregates in combination with a basal wax layer. X-ray experiments showed interplanar spacings of 4.13 Å (in the 1 1 0 direction) and 3.73 Å (2 0 0 direction) which is characteristic for an orthorhombic crystal structure. Straight aliphatic molecules assemble preferentially side by side and form layers or platelets, since the growth speed is highest in the lateral direction. The recrystallised waxes of the platelet containing waxes of the *Euphorbia myrsinites* and *Sisyrinchium striatum* are found to have a periodical sequence of density differences in multiple layers of approximately 75 Å, indicating a double layer structure. Electron diffraction from separated single platelets acquired from several platelet containing waxes indicate that individual platelets usually appear as single crystals, but sometimes deformations of the platelets cause disturbed diffraction patterns. All wax films and crusts examined, also contain the orthorhombic structure (4.13 Å and 3.73 Å). But for the (periodical) layer sequence very different patterns were found, which indicates a varying development of the layer order.

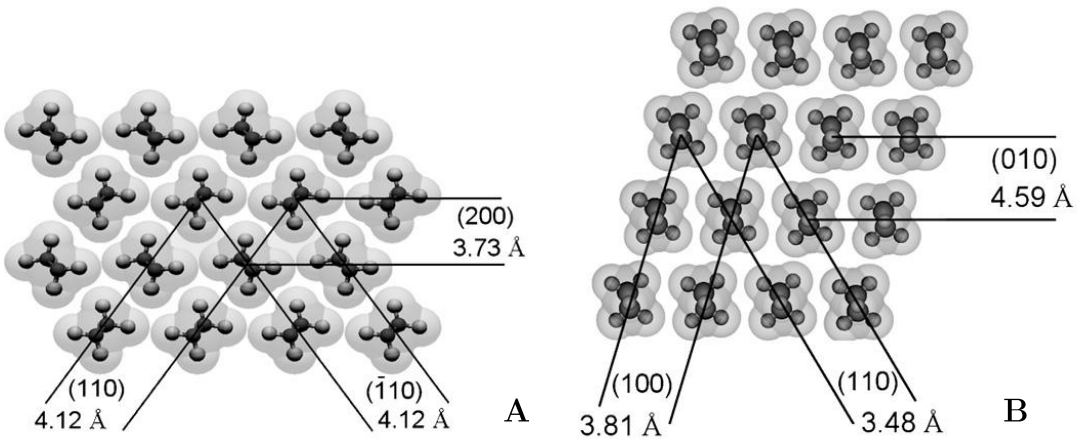

Figure 2.9: Models of the orthorhombic (a) and triclinic (b) symmetry of the methylene subcells. Indices and d-spacings are taken from XRD data of n-nonacosane and n-tetracosane (JCPDS) [20].

Great variations in the crystal morphology were found in waxes which contain components with lateral oxygen atoms as ketones and secondary alcohols. These components apparently hinder the formation of the orthorhombic structure, as the oxygen atoms require additional space. Tubules only show a periodic order on the short range, because the tubules grow with a circular or helical shape and are randomly oriented on the surface. Tubules containing mainly secondary alcohols show the characteristic diffraction peaks of triclinic alkanes. Ketones, in particular beta-diketone tubules, displayed the reflections of a hexagonal structure. Mixtures of different phases could be identified. Particularly ketone-containing waxes occur in different morphological forms such as transversely ridged, coiled, branched and triangular rodlets. Most tubules are associated with a basal wax film, which has an orthorhombic structure. Ensikat et al. assume that the different wax components cause the separation in structure [20].

2.4 Wax extraction and recrystallisation

The acquisition of plant waxes was performed either by dissolution in organic solvents or with mechanical isolation methods. Thick waxes can be scraped off, but in most cases the wax layers are too thin for this method. Various 'adhesive' methods have been developed to isolate the epicuticular waxes from the plants. The most common method, called cryo-adhesive method uses liquids such as triethylene glycol or glycerol which are applied to the plant surface. After freezing, the plant tissue is removed and the epicuticular wax remains embedded in the frozen liquid. After warming up to ambient temperature the wax can be transferred to the desired applications. For this purpose, one needs to cool down the leaf in contact with a preparation liquid to ca. -100 ℃. The most accessible way of quantitative wax extraction is to dissolve the wax. The epicuticular waxes are soluble in organic solvents and are completely dissolved within a few seconds. Some waxes contain components which are only slightly soluble at ambient temperature. Such waxes need to be dissolved in warm organic solvents. Generally, solvent-extracted waxes contain intracuticular waxes and can be contaminated by other organic solvent-soluble components from inside the tissues. Another disadvantage of this method is that insoluble or slowly soluble components may be lost. This could make it impossible to recover the original wax structure [17].

The simplest way to deposite the wax on the surface is by recrystallisation out of solution, but this leads to unequal mass distributions, with typical ring patterns (coffee-drop-effect) on the substrates. If it is preferred to have a homogenous distribution of the wax structures on the substrates, physical vapour deposition should be used. It should be considered that the mobility of the molecules is not the same for the two methods.

Crystallisation conditions on the plant surfaces are unique. A comparison between the wax crystallisation on plant surfaces and on artificial substrates shows great differences in the speed of crystallisation. The wax molecules move relatively slowly from inside of the living cell through the cuticle until they reach the surface, where they extrude from the cuticle and crystallise without a solvent on the dry surface. In this natural system the speed of the crystalloid growth is determined by the speed of wax synthesis and transport [19]. Some epicuticular wax crystalloids (e.g. tubules) can recrystallise on artificial substrates resulting in crystalloids of similar shape and dimension as on the plant surface. However, recrystallisation fails for many other crystalloids. The process of self-assembly in molecular systems is determined by five characteristics: the components, interactions, reversibility, environment and mass transport with agitation.

Temperature, solvent and substrate are environmental factors that might influence the recrystallisation, and their crystal habit on artificial substrates [17]. Waxes must be mobile until they reach edges or steps of the growing wax layers and crystalloids. On the artificial substrates, this can only be achieved when wax crystalloids are molten or dissolved in a solution. Three possible modes of crystallisation are found: crystallisation by unimpeded evaporation of the solvent, crystallisation by delayed evaporation of the solvent using a recrystallisation chamber, and crystallisation from the melt [7].

The influence of the substrate on the wax growth and morphology was found to depend on polarity and degree of crystallinity. This was observed for recrystallisation on highly ordered pyrolytic graphite (HOPG). It was found that on HOPG, tubules preferably grow standing vertically to the substrate in an ordered spatial distribution, while on silicon substrates, tubules preferably grow randomly orientated. Only on HOPG a time dependent increase in homogeneity of spatial distribution and tubule orientation was found [22]. Furthermore, a spatial pattern of reassembled wax platelets was found to strictly follow the hexagonal symmetry of the crystalline HOPG substrate [17, 23].

Chapter 3

Experimental details

3.1 Material

Material is collected from a small collection of plants with hydrophobic surfaces which were purchased specifically for this project. The majority of experiments are carried out with use of the plant named *Euphorbia myrsinites*. The leaves of the *E. myrsinites* are covered with a platelet containing epicuticular wax. In the following chapters it is precisely defined which plant leaf or wax is examined and for what purpose. Plants were chosen that are readily available in the commercial garden centers. The plant material used was fresh, fully developed and preferably uncontaminated. This is done by picking leaves that are dust-free and undamaged as observed by visual inspection. From those plants it was already known from literature which wax crystal structure is present on the leaves [8, 20, 21].

3.2 Wax extraction and deposition

As described in section 2.4, an organic solvent can be used to dissolve the wax. For this experiment, chloroform (Emsure, ≥ 99.0-99.4 % purity, Merck) is used as an organic solvent. The freshly harvested leaves were dipped into the solvent at room temperature (unless otherwise specified). A short immersion time should be chosen to reduce or ideally even to exclude the extraction of intracuticular wax compounds. Experiments done by Koch et al. [6] showed that wax tubules on the immersed leaves of for example Lotus dissolved within 2s. For the waxes determined in this project, this was approximately the same. The following chapter provides more detail on this. Intracuticular waxes can be chemically different from epicuticular ones. Those waxes are not as interesting as the epicuticular waxes because they do not form 3D crystallites.

When using chloroform, the precise amount of chloroform used is not important because it will evaporate very quickly when depositing the wax-chloroform solution on the sample. Still an uncontrollable small portion of the solvent might remain trapped within the deposited wax molecules which could influence the growth process. Solutions of 1.5 mg/ml wax in chloroform were prepared by Koch et al. [6]. For the wax extraction experiments in this project a minimum amount of chloroform is used, just enough to fully immerse the leaf. In the subsections which describe a specific experiment, the used amount of chloroform and the wax concentration are specified.
The wax-chloroform solutions were filtered with filter paper of grade 595 (Schleicher & Schuell) for removal of leaf contaminating particles from the extracted waxes. Larger particles, mostly dust, will be trapped in the filter paper. From experience it is learned that especially when working with an atomic force microscope (AFM) it is better to not have larger contaminating particles on the surface because it makes it a lot easier to move to a different scanning area without damaging the AFM tip.

To redeposit the wax, approximately 25 µL of the wax-chloroform solution was applied on top of a piece of silicon wafer or cover glass with a metal syringe. The chloroform will typically evaporate within 1 minute. The silicon wafer and cover glass pieces are cleaned by rinsing them first with ethanol (Assink Chemie, ≥ 99.8 % purity) and subsequently with chloroform (Emsure ≥ 99.0-99.4 % purity, Merck) before applying the wax solutions. To extend the evaporation time, a small chamber with chloroform vapour can be used (figure 3.1). If the bottom of the chamber is filled with chloroform, then the chloroform will partly evaporate while its vapour will distribute within the chamber. In this way, in general more wax remains on the sample surface. This chamber should not be closed entirely; otherwise the chloroform will never evaporate.

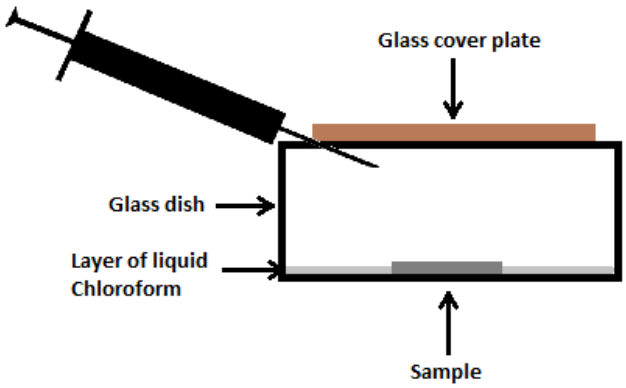

Figure 3.1: Wax deposition set-up to extend the evaporation time of chloroform on the sample

3.3 Characterisation tools

This paragraph describes the various characterisation tools which were used to characterise the samples. The samples include the substrates with deposited wax as explained before but also pieces of leaves. Small leaf pieces of typically 5 mm were cut and affixed to aluminum stubs by double-sided adhesive tape. The samples were examined by using optical microscopy, atomic force microscopy, scanning electron microscopy, helium ion microscopy, gas chromatography and contact angle measurements. In the subsequent sections the most important measurement details of the various techniques are described.

Optical microscope

A Leica DM2500 MH optical microscope (OM) was used to make top view pictures of the leaf surface and the deposited wax. The images were recorded with a PCO-Pixelfly camera together with PCO Camware software. Lenses of 20 times and 50 times enlargement were used to make top view pictures of the leaf surface. The images with smaller magnification were used for statistical analysis. A lens of 50 times enlargement is used to make pictures of the deposited wax.

Atomic force microscope

Atomic force microscopy (AFM) measurements were done with the Agilent 5100 atomic force microscope. All the measurements were done in tapping mode. The AFM cantilevers were Al-back-coated NSC36c Si_3N_4 probes from MikroMasch with a nominal spring constant of 0.6 N/m, resonance frequency of 65 kHz and tip radius of >8 nm. The set-point was kept high (~95%) and the amplitude between 20 nm and 25 nm in order to minimize deformation of the wax structure by the AFM tip. Picoview 1.14 software was used to operate the AFM.

Helium ion microscope

An ultra high vacuum (UHV) Orion Plus helium ion microscope (HIM) from Carl Zeiss was used to measure leaves as well as samples with deposited wax. Imaging with the HIM is based on the interaction of a He^+ ion beam with the sample. For this purpose the images were acquired by collecting secondary electrons (SEs) using an Everhart-Thornley (ET) detector. SE emission and neutralization of the positive helium ions with material electrons lead to a positive surface charging of insulating materials. This charge can be neutralized with low energy electrons. For imaging of insulating samples the ET detector can therefore be used in an interleaving way with an electron flood gun. Because the leaves as well as the wax are non-conducting the flood gun is used for the experiments.

Because the HIM works with ultra high vacuum, the main chamber should be pumped for a while in order to measure the plant leaves. It typically took one and a half hour (instead of the usual 20 minutes) to get to the desired pressure of in this case 5 x 10^{-7} mbar. This is mainly caused by the fact that the leaves contain a lot of water. Usually the HIM can reach even lower pressures of 1x10^{-8} mbar, however this is not necessary in order to measure the samples properly. Specific settings for a certain measurement can be found in the corresponding section. More details about HIM in general can be found in the review written by Hlawacek et al. [24].

Scanning electron microscope

The Zeiss Merlin high resolution scanning electron microscope (SEM) was also used to measure leaves and the deposited wax samples. This SEM works with low voltages (< 1 kV) which makes imaging of non-conducting samples possible. Imaging with the SEM is based on the interaction of an electron beam with the sample. Secondary electrons (SE) were collected with two different collectors, each with its own speciality. The so called in-lens SE detector has the highest resolution. This detector is situated in the same column as the incoming electron beam, which is right above and close to the surface. With this detection mode more details can be seen because more electrons are collected. However due to its position we obtain an image which gives a somewhat flat appearance. The high efficiency HE-SE2 detector is positioned to the side of the sample. This detector is much more suitable for topographical and morphological imaging. A combination of the two detectors gives a good overview of the surface structure. The voltage of the incoming beam determines how far it penetrates into the sample surface. By changing this value the optimal contrast can be reached. The highest obtainable resolution of this SEM is approximately 1 nm. The resolution of the images we made is slightly lower because of the organic sample composition. Specific settings for a certain measurement can be found in the corresponding section.

In contrast to the HIM, the SEM works with high vacuum. The leaves could be measured almost directly (it took at most one minute to pump the main chamber to high vacuum). In principle the same type of measurements can be carried out with both microscopes. Since we have the HIM available within our own research group it was preferred to use the HIM instead of the SEM. Unfortunately the HIM had some technical problems during the project, and therefore sometimes it didn't work properly to do the experiments. Furthermore, sometimes it's preferred to use the SEM instead of the HIM because the samples may degenerate more in the HIM which may be unfavorable (this is also explained in chapter 4).

Data processing

The measured AFM data is processed with the software package Gwyddion. To optimize the contrast of images obtained from the OM, HIM and SEM the software package Fiji [25] is used. This software package is also used to measure distances in images, to detect individual objects on the surface and to calculate the position and area of the objects. A home-built Matlab script is used to process the data files obtained from Fiji and for doing additional calculations. Another home-built Matlab script is used to make movies from individual OM or AFM images measured at different times.

Gas chromatograph mass spectrometer

Prior to the gas chromatography and mass spectrometry (GC/MS) experiment, *Euphorbia myrsinites* wax is obtained by dipping 100 leaves, one by one, into 4 ml of chloroform. After the extraction, the wax-chloroform solution is filtered as described in section 3.2. The chloroform was removed under a gentle stream of nitrogen and silylation was achieved by adding 75 µl BSTFA (bis(trimethylsilyl)-trifluoroacetamide) and 25 µl andydrous pyridine. This process involves the replacement of a proton with trimethylsilyl. Silyl derivatives are generally less polar, more volatile and more thermally stable than their precursor organic compound. The introduction of a silyl group therefore makes the derivatives suitable for analysis by gas chromatography. The samples were heated to 70°C for 30 min. for completion of the reaction. Subsequently, the samples were again dried and dissolved in 1 ml of chloroform to bring the concentration up to 1 mg/ml of chloroform for chromatographic analysis.

Quantification of the wax components was performed on a programmable GC/MS (5975C, Agilent Technologies). The temperature program was set as follows: on-column injection at 50 °C, then held for 2 min. at 50 °C, then increased at 40 °C/min. to 200 °C, then held at 200 °C for 2 min., then increased at 3 °C/min. to 280 °C and finally held at 280 °C for half an hour. The sample volume was 1 µl containing 1 µg of wax. The exact amount is not very important since the wax components are reported as a percentage of the total injection. Comparison of wax components was based on retention time (R_t) and known standards from the computer database. Mass spectrometry was used to verify the identity of found compounds.

Optical contact angle goniometer

Contact angles are measured with an OCA15+ goniometer (Dataphysics, Germany). Microliter droplets of 5-8 µl are created by employing a computer-controlled syringe; the droplet volume, typically in the microliter range, is accurate to within 5%. A build-in ccd sideview camera is used to characterize the droplet shape in terms of the dimensions and contact angles; the latter are accurate to within 0.5°.

Chapter 4

Euphorbia myrsinites leaves

4.1 Introduction

The *Euphorbia myrsinites* is an evergreen perennial with trailing to ascending stems of 20-50 cm long when fully grown. The mature leaves are 1-4 cm long and arranged in close spirals around the stems. When fresh, the leaves are pale glaucous bluish-green (see figure 4.1). The *E. myrsinites* is an interesting plant within the scope of this project because of its leaf surface structure. The leaves of the *E. myrsinites* are in fact superhydrophobic. This chapter describes multiple experiments done with the *E, myrsinites* leaves, starting with an examination of the leaf structure itself, followed by experiments done with extracted *E. myrstinites* (epicuticular) wax. The main goal is to recover the epicuticular wax structure present on the leaves on artificial substrates. In the following sections, several experiments are independently described and discussed.

4.2 Leaf surface structure analysis

The leaf surface is examined in order to determine the surface micro- and nanostructure. Herewith we examine if any specific arrangement of the micro- and nanofeatures is present. For characterisation of the surface structure, scanning electron microscopy (SEM) and optical microscopy (OM) are used. Top view optical microscopy images of the leaf were used to do statistical measurements. With this technique we can accurately determine the dimensions of surface features on the microscale at a certain height on the surface. With the SEM the surface morphology is determined. The SEM images give a very realistic overview of the surface viewed from different angles. To start with, the SEM experiments will be described and discussed.

Figure 4.1: *E. myrsinites* stems (a) and close-up of the stem tip with a droplet on the leaf surface (b)

The surface of the *E. myrsinites* consists of convex (papillose) cells with a superimposed epicuticular wax layer. This can be seen in the SEM picture in figure 4.2. The convex cells, i.e. surface papillae contain a very high density of thin wax platelets oriented perpendicular to the papilla surface. A surface papilla on top of a well-developed fresh leaf is fully covered with wax platelets as shown in figure 4.3a. The wax layer on the tops can be damaged when the leaf surface comes into contact with something hard/rough in its environment. In figure 4.3b it can be seen that the wax platelets are smeared off the surface. The lower-lying surface will be damaged less easily. When the leaf is still attached to the living plant the wax platelets will eventually re-grow. On the basis of multiple SEM images, it is estimated that the thickness of the platelets is approximately 50 nm and the height is 0.5-3 µm, i.e. the aspect ratio is very high. Figure 4.3b shows the measurement results of the full wax platelet layer thickness measured with a build in tool of the SEM. Sometimes the wax platelets cross each other. In figure 4.4a an example of this is shown indicated with the red arrow. It looks like the platelet on the surface, which is pointing from the left bottom to the right top of the picture, goes right through the platelet which is perpendicular to it.

The SEM images of high magnification (figure 4.4) show that the platelets exhibit features which are characteristic for a crystalline structure. From figure 4.4b it becomes clear that the wax platelets have straight edges of approximately 90°. The straight edges suggest that the wax platelets have a crystalline structure. From literature, it is known that the epicuticular wax of the *E. myrsinites* does indeed have orthorhombic molecular crystal structure (see chapter 2.3). The Lotus leaf as a comparison, which is covered with wax tubules, has been shown to have characteristic diffraction peaks of triclinc alkanes in XRD experiments. This also holds for other tubule forming waxes which contain secondary alcohols. Platelet waxes on the other hand, most of the time contain primary alcohols. Unlike the primary alcohols, secondary alcohols have a lateral oxygen atom. These components apparently hinder the formation of the orthorhombic structure, as the oxygen atoms require additional space.

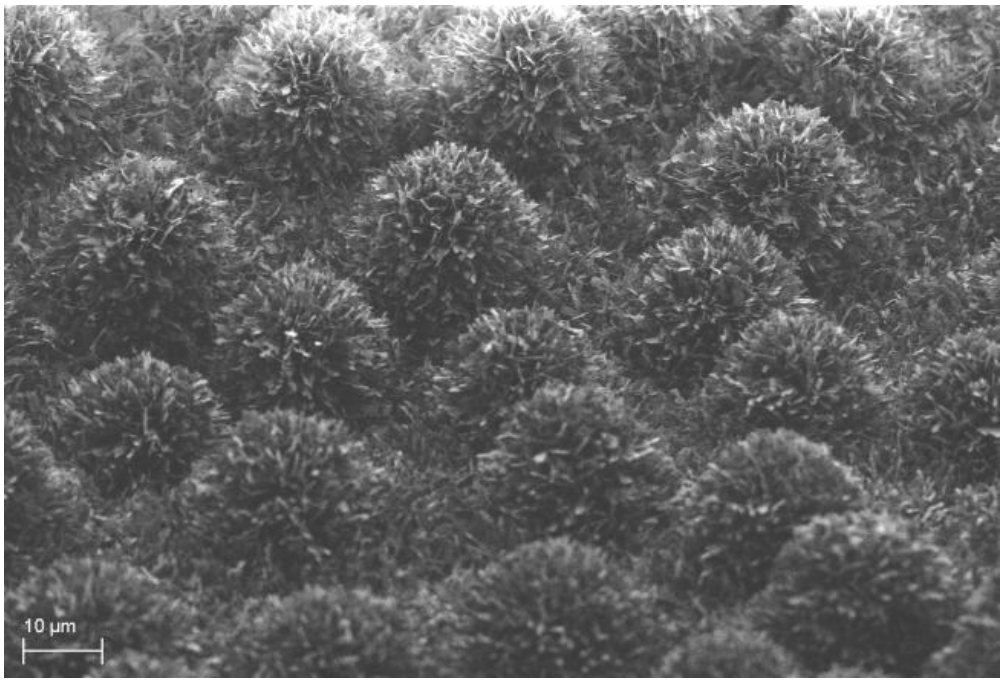

Figure 4.2: SEM HE-SE2 image at 0.85 kV and 70 pA of multiple *E. myrsinites* surface papillae with superimposed wax platelets on top

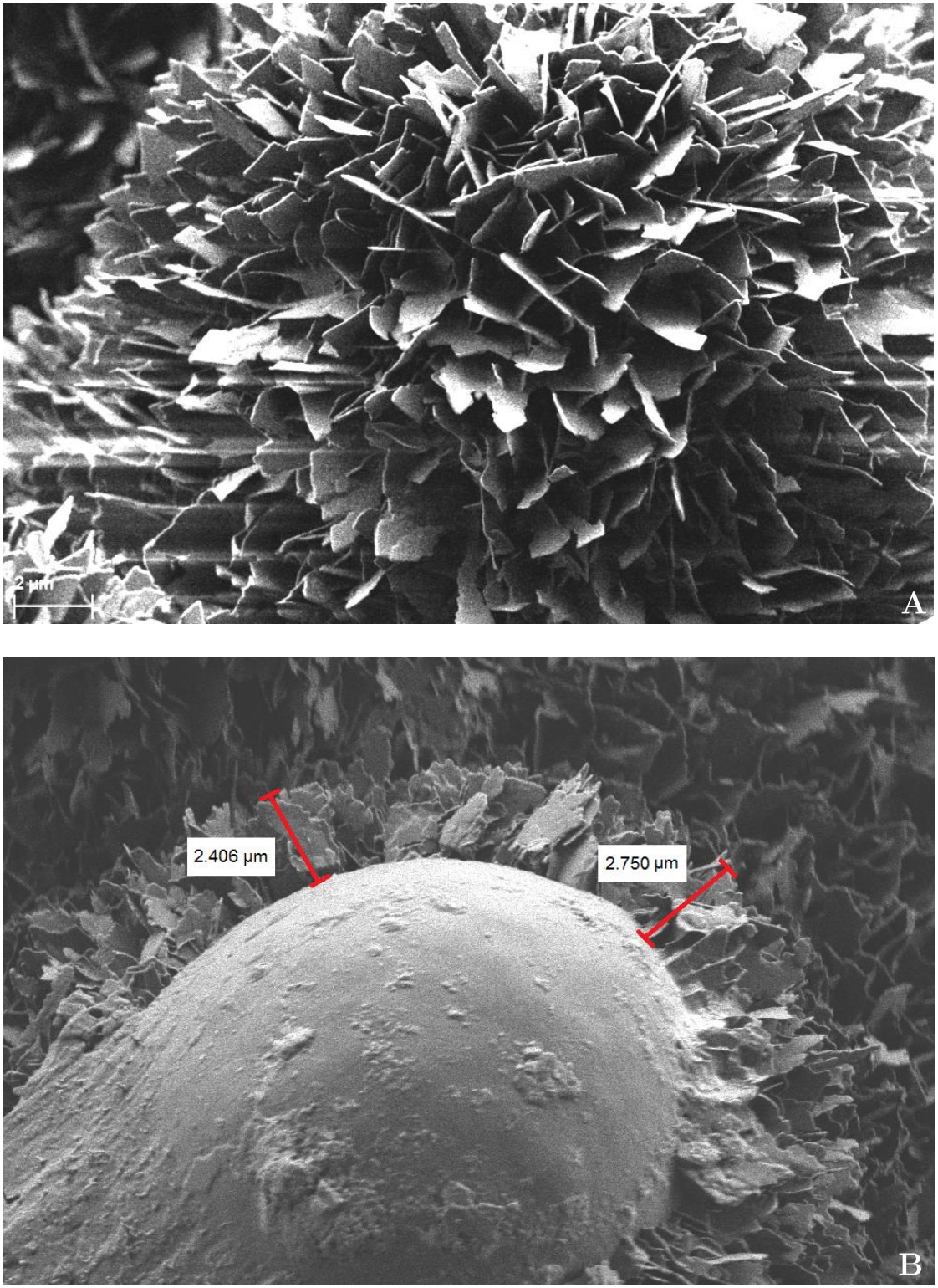

Figure 4.3: SEM HE-SE2 images at 0.85 kV and 70 pA of an undamaged (a) and damaged (b) top of the *E. myrsinites* papilla.

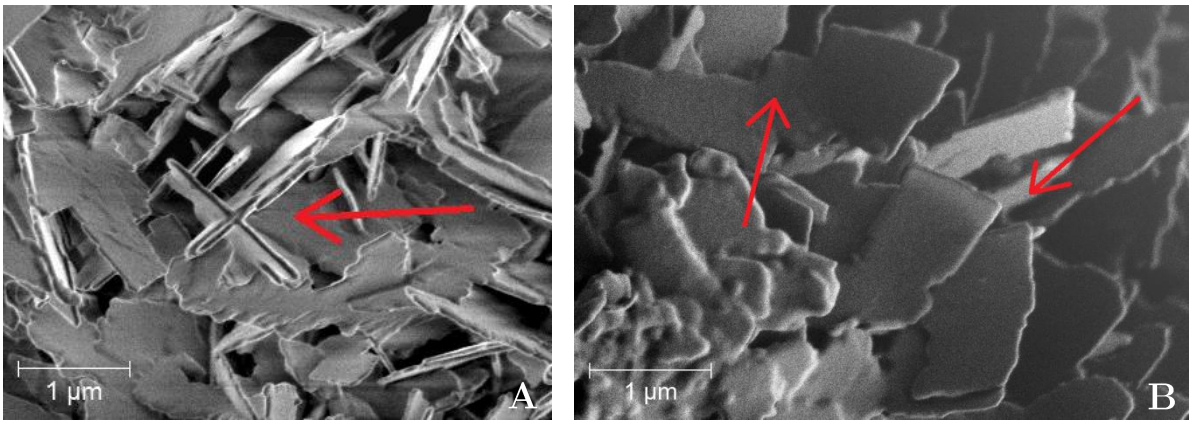

Figure 4.4: High magnification SEM images of *E. myrsinites* platelets: edges of 90°, measured with the In-lens SE detector (a), platelets crossing each other, measured with the high efficiency HE-SE2 detector (b). The incoming electron beam voltage amounted to 0.40 kV and the current to 70 pA.

When the leaves are stored under ambient conditions for two weeks they will dry out and become brittle. The surface micro- and nanostructure is maintained, but the platelet shape will slightly change compared to the fresh and well-developed leaves. In figure 4.5 we can see that the platelets are bended and have rounded edges. It seems like the platelets are partly destroyed. In paragraph 4.5 the wetting properties of these stored leaves are discussed.

When measured with HIM, the surfaces of fresh leaves look quite similar to the dried leaf surface shown in figure 4.5, although not as degenerated. The degeneration is caused by the ultra high vacuum pumping of the HIM main chamber. Another possibility to determine surface topography is with the use of AFM. However, measuring the *E. myrsinites* with AFM is very hard due to huge papilla height differences (~20 µm) and sloping surfaces. It might be possible to measure the nanostructured wax when the AFM tip is placed on top of a papilla. Unfortunately, it is impossible to see the surface with the AFM built-in top-view camera, because the leaf surface does not reflect any light, which makes it difficult to locate the AFM tip. Because the tip easily damages due to the above mentioned reasons, we did not use the AFM for this purpose.

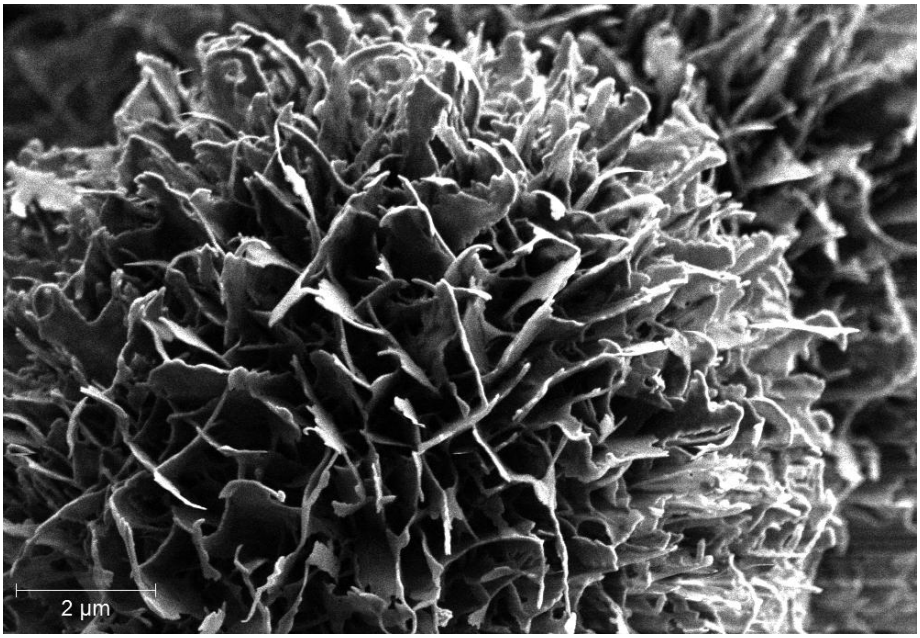

Figure 4.5: SEM HE-SE2 image at 1.20 kV and 60 pA of a surface papilla stored for two weeks

Optical microscope images were processed in order to detect and measure individual surface papillae. Of course, due to the limited resolution, the individual wax platelets cannot be resolved. The images where taken with the optical microscope described in paragraph 3.3, with the use of a lens of 20 times enlargement. An example image is shown in figure 4.6. The images are processed in several steps such that individual objects on the surface can be detected. Several statistical measurements are carried out with the obtained data.

In figure 4.6 it can be seen that the surface is covered with a large number of papillae in the micrometer range. The actual papillae density is measured to be 1087±50 per mm^2, which is quite large compared to some other hydrophobic leaf surfaces. For a quantitative comparison the papillae density of the *Aquilegia canadensis* is measured. This leaf has a papilla density of 430±30 per mm^2. More information on this plant can be found in chapter 5. The measurement errors of the above mentioned densities are estimated and based on an error in the counting of the papillae which are at the boundary of the picture. However, if we compare the results to the famous Lotus leaf, as shown in the SEM micrograph in the introduction (figure 1.1), a surface papillae density of ~3400 per mm^2 is found. Even though great differences in papillae density are found, all of the three plants have superhydrophobic leaves with static contact angles >150° and tilt angles so small it's impossible to measure them with the available characterisation tools in our research group. However, a high density of the surface structuring is necessary to ensure hydrophobicity, because it reduces the contact area between the surface and water drops. Not only the density is important, but also the diameter, papillae height and height differences between the papillae. The Lotus leaf for example has a higher density and the papillae diameter is a lot smaller then for the *E. myrsinites*. To make a more qualitative comparison of the surfaces, more research has to be done. But this is beyond the scope of this project. It is expected that also for example the impact of droplets on the surface will differ for the different plants and self-cleaning properties are more developed for leaves with higher papillae densities. More about the wetting properties of the *E. myrsinites* leaves will be discussed in paragraph 4.5.

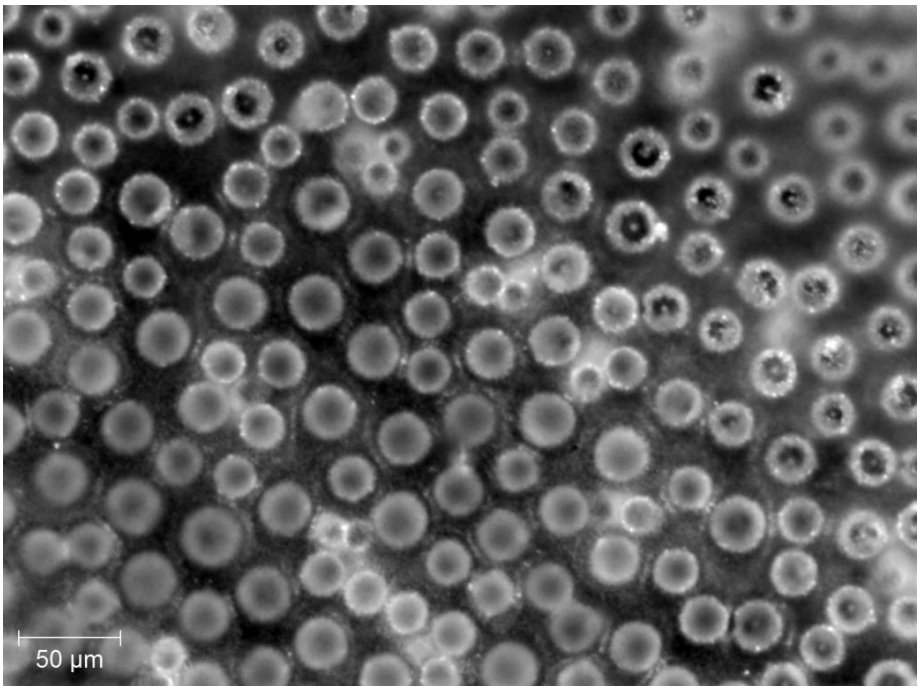

Figure 4.6: Example of an OM image of the *E. myrsinites* surface used for statistical analysis

We analyzed the papillae diameters as determined from images such as that in figure 4.6. The diameter slightly varies between different papillae. A histogram of this distribution clearly illustrates this (see figure 4.7). The average papillae diameter is 22.4±1.0 µm. The measurement error is estimated and based on errors in the detection of the particles and the assumption that the papillae tops are perfectly circular. The first half of the graph seems to represent a normal distribution but the second half does not seem to fit. The dispersion of papillae diameter smaller than the average papillae is a lot larger than the dispersion for the larger ones. The most frequently found diameter (mode) rounded to an integer value is found to be 24 µm. This means that a lot of papillae do actually have large diameters. The papillae diameter is measured at the bottom of the papillae at the height at which the surface becomes almost flat. In addition, the diameter is measured including the superimposed wax and might therefore differ from values found elsewhere if the 'real' papilla diameter is measured. To measure the 'real' papilla diameter one could for example cut multiple leafs in half and measure them in a side view with SEM.

If we look at the SEM micrograph of the surface papillae shown in figure 4.2 it looks as if the papillae have a preferred nearest neighbour distance. For this specific reason a Matlab script is written in order to find the radial distribution of the papillae. Herewith the radial distribution function is used. The result is a measure of the probability of finding a 'particle' at distance r away from a given reference particle [26]. It is determined by calculating the distance between all particle pairs and binning them into a histogram. The histogram is then normalized with respect to an ideal gas, where particle histograms are completely uncorrelated. The result of this measurement is shown in figure 4.8, where the radial distribution is calculated in the range of 0-80 µm from the reference particle. The results in figure 4.8 indicate that the papillae distribution exhibits a limited degree of order. The graph only shows the data from the distances $0<r<80$ µm from the reference particle. The dimensions of the picture used for this calculation are in fact limited to 442.5 µm. Therefore the graph will be inaccurate if r_{max} becomes too large. The data is filtered with a moving average filter with a high span of 31 to specifically point out the order characteristics of the data. This is shown with a red line in the figure.

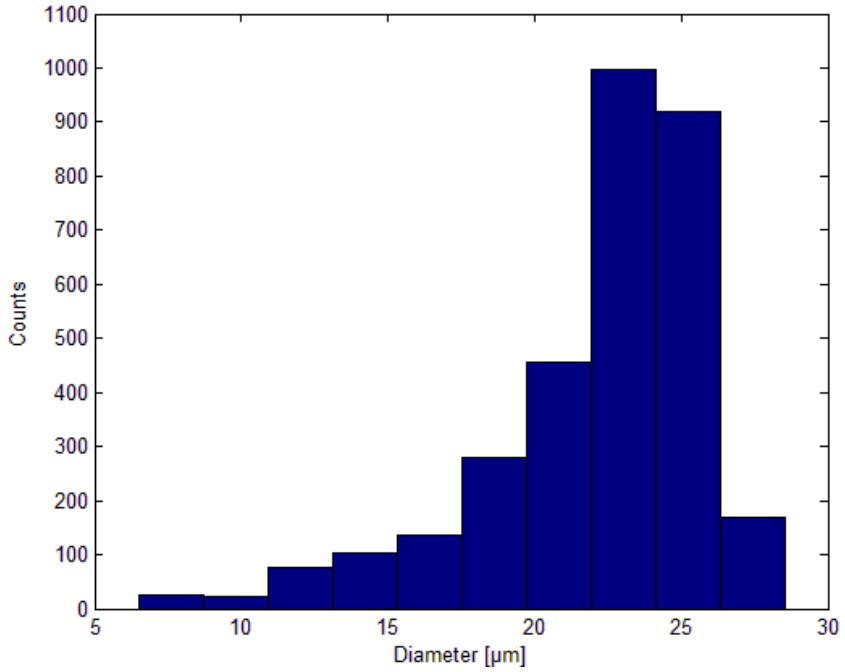

Figure 4.7: Diameter distribution of surface papillae on the *E. myrsinites* leaf surface

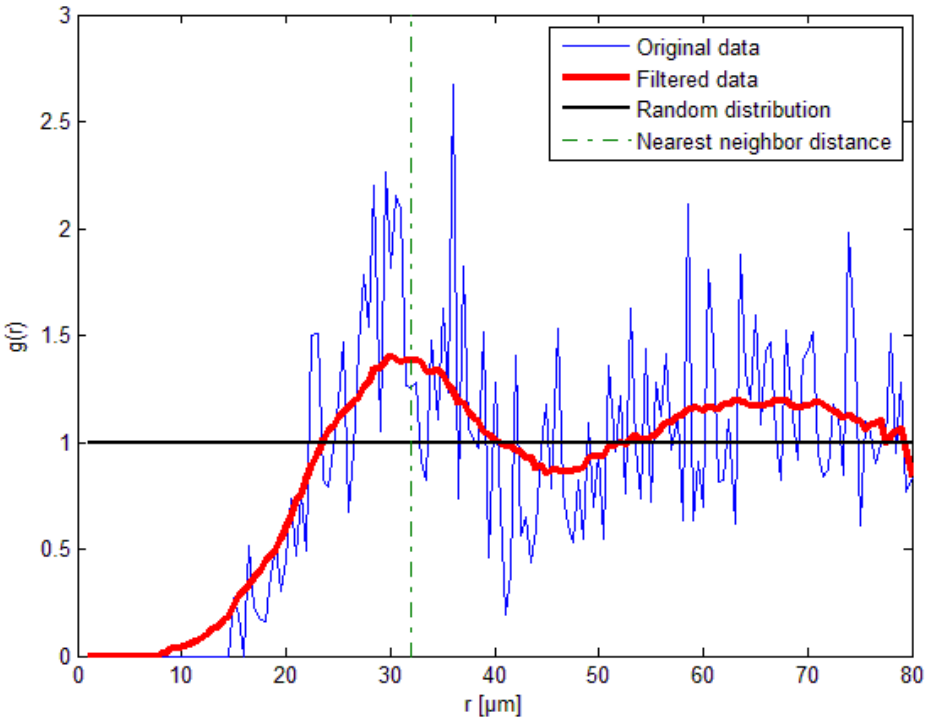

Figure 4.8: Radial distribution function of the *E. myrsinites* surface papillae. The data is filtered with a moving average filter.

From the figure we read that the papillae have a nearest neighbour distance of approximately 32 µm (green dashed-dotted line). This result is verified, on the basis of the measured number of particles per square millimeter. If we would make a hypothetical division of the surface into small hexagons of equal size, one around each equally sized papilla, then the height of the hexagons is equal to the nearest neighbour distance. Therefore, the area of the hexagon is directly related to the number of papillae that fit onto the surface. If we have 1087 papillae per square meter it follows that the nearest neighbour distance is approximately 32.5 µm.

However, it has not yet been discussed what the shape of this radial distribution function means. By comparison to the functions of known particle distributions this will become clearer. First, the results are compared to the standard distribution function of a liquid (see figure 4.9). The circles in the illustration inside the graph indicate which distance r belongs to which peak. It is clear from this figure that the shape is quite alike, but the relative height difference between the first two peaks is a lot smaller. This means that at larger distances from the reference particle, we find more correlations, than for the standard liquid model. A certain structure might be present.
We calculated the radial distribution function of a cubic and hexagonal particle distribution. The results are shown in figure 4.10. The radial distribution function of a cubic crystal structure shows four sharp peaks. These peaks correspond to distances r where we find the next ring of particles from the perfectly aligned lattice. The magenta colored line in figure 4.10 shows the plot of the typical hexagonal lattice. The measured graph for the surface papillae seems to show some characteristics of the hexagonal structure. The second peak is in fact found somewhere next to r=50 µm, like for the hexagonal distribution function. The radial distribution function of the surface papillae shows a broad peak between $50<r<80$, whereas the hexagonal structure shows more ordering at larger distances from the reference particle.

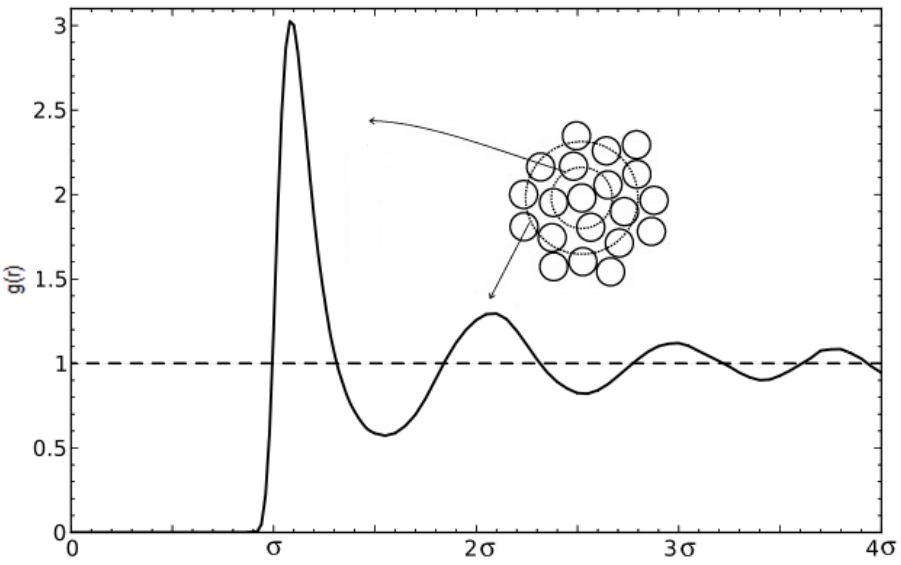

Figure 4.9: Radial distribution function of a simple liquid of size σ. This graph shows an absence of amplitude of $g(r)$ for $r<<\sigma$, which is called the exclusion radius. Figure adapted from [27].

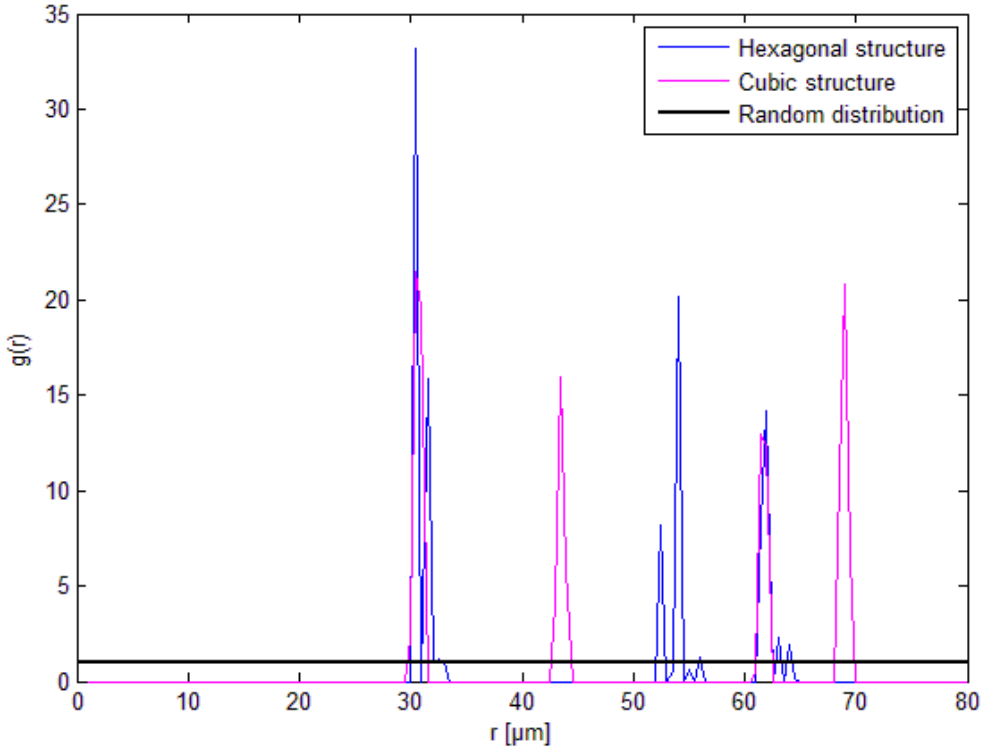

Figure 4.10: Radial distribution functions calculated for particles distributed in a cubic structure and hexagonal structure,

Furthermore, the Matlab script is expanded to see if this preferred nearest neighbour distance is dependent on the size of the papillae. In figure 4.11 the average diameter of papillae for a certain r-value is plotted. The data shows us that in general it holds that the larger the diameter of the papillae, the larger the nearest neighbour distance is. The green line in the figure represents the average papillae diameter. If we look at distances further away, e.q. r>40 µm, the average diameter still dominates as the most frequently occurring value and the graph saturates. The few particles which are larger than the average papillae might also have a larger center-to-center distance, but this effect might be suppressed by the overall average value.

There are two possibilities for the size dependency; either the space between two papillae stays the same, but since the diameter changes, the center-to-center distance changes, or the space between the papillae is related to the papillae diameter. Between 15<r<31 the line is approximately linear with a slope of 0.37 µm average diameter increase per 1 µm increase of the radial distance. This is indicated by the red dotted line in figure 4.11. It means that, if the distance r is changed, the relative change of the average diameter of the particle is only small. This means that the space between the papillae changes and therefore we conclude that the space between the papillae is related to the papillae diameter and not a constant value.

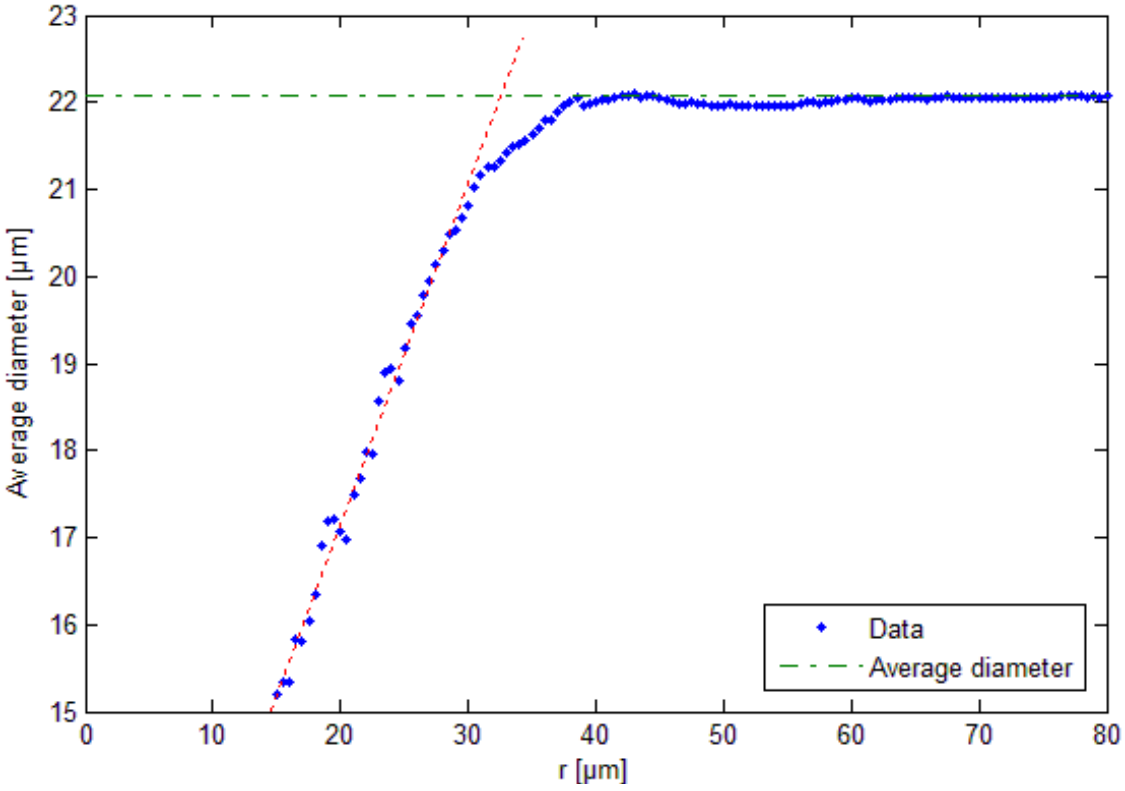

Figure 4.11: Dependence of the average diameter of the *E. myrsinites* papillae on their nearest neighbour distance

4.3 Optimising the wax extraction

We now turn to the extraction of the wax from the leaf surface. It is important to know what the ideal immersion time of the leaves in chloroform is, because extraction of intracuticular wax compounds should be reduced or ideally even excluded. Intracuticular waxes can be chemically different from epicuticular ones and in the context of this project those waxes are not as interesting as the epicuticular waxes because they do not form 3D crystallites. In order to find the optimal immersion time, an experiment is done to see what happens to the leaf surface if we immerse it in chloroform. The helium ion microscope (HIM) is used to image the surface structure after immersing the leaf in chloroform for different time periods. The leaf surfaces are also compared in terms of the static contact angle. This is shown in paragraph 4.5.

First, the leaf is immersed in chloroform for one second. As can be seen in figure 4.12, all the platelets are removed from the surface. From literature it is known that epicuticular wax usually consists of superimposed wax crystals on top an underlying wax film (see paragraph 2.2). Underneath the wax film the intracuticular wax can be found. It looks as if still some wax is remaining on the surface, because of the small features which are present in between, and on top of the papillae. It is hard to say whether we did dissolve some of the intracuticular layers or not, but most of the platelets are probably left in the chloroform solution. For longer immersion times, the leaf surface becomes smoother. This is shown in figure 4.13, which shows part of the leaf surface which is dissolved in chloroform for 1 minute.

However, it is very rare to find an intact surface structure with well defined papillae when immersed leaves are measured with the HIM. Most of the time the surface papillae measured seem 'collapsed' (see figure 4.14). Normally the cells of the leaves are filled with water. The loss of water from the cells can lead to such collapsing. The collapsing can be caused by dissolution in chloroform, by the vacuum pumping or by a combination of both. The HIM works with ultra high vacuum and pumping to such low pressures, may destroy the original leaf surface. No further research has been done on this because it lies out of the scope of this project. If we immerse the leaves for more than 1 minute, holes start to form in the papillae. In figure 4.14b a HIM image of a leaf immersed for 5 minutes is shown. Small round holes form around the papillae surface. It seems as if the holes are caused by surface tension, because the papilla wall will get thinner by the immersion and the spot where the holes occur is the weakest part of the papilla. From all the measured data it is concluded that the optimal immersion time should be 1-2 seconds. This is sufficient to dissolve the platelets, and probably most of the epicuticular wax, on top of the papillae.

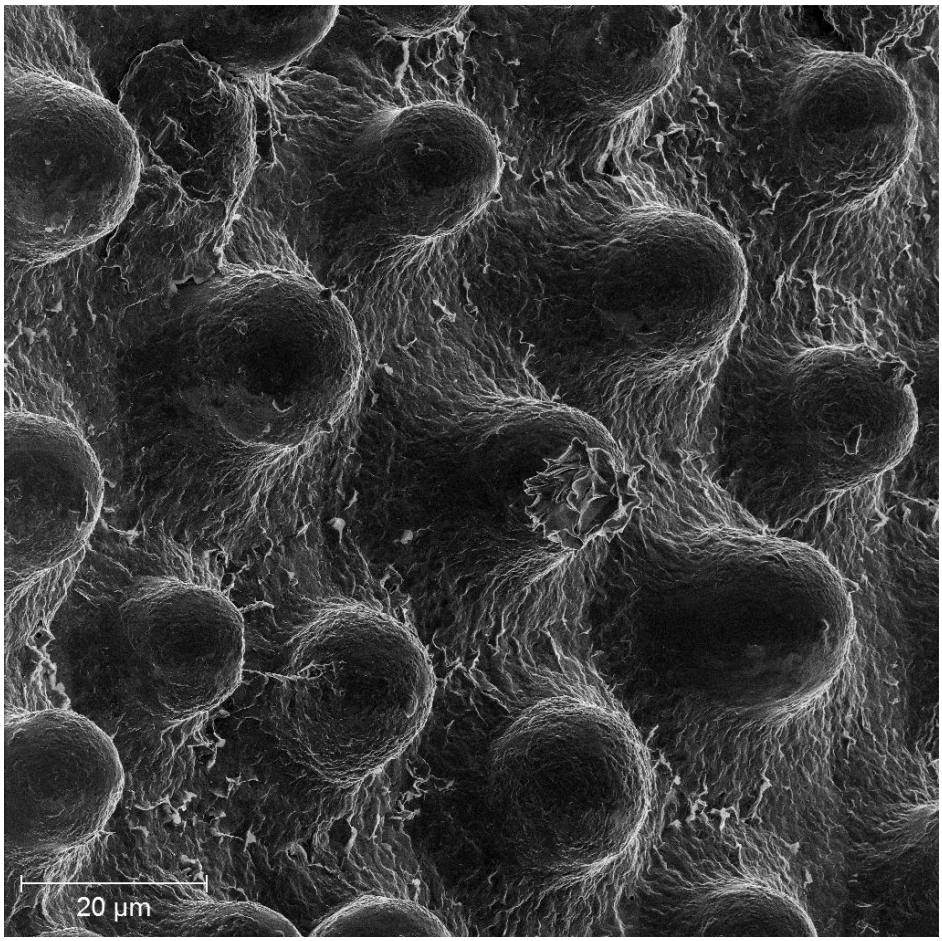

Figure 4.12: HIM image of an *E. myrsinites* leaf surface immersed for 1 sec. in chloroform. The acceleration voltage for this image was 30 kV, the current 0.1 pA and the dwell time of 128 µs.

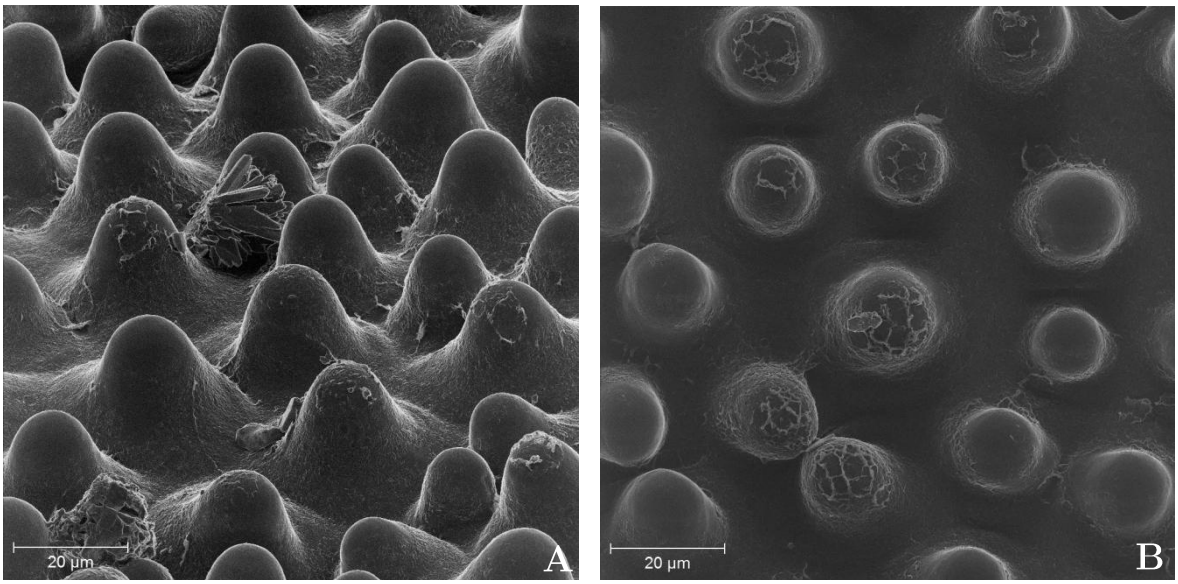

Figure 4.13 : *E. myrsinites* leaf surface immersed for 1 min. in chloroform measured with HIM. Figure 4.13a shows a sideview while figure 4.13b shows a topview. The acceleration voltage, current and dwell time were 30 kV, 0.1 pA and 128 µs respectively.

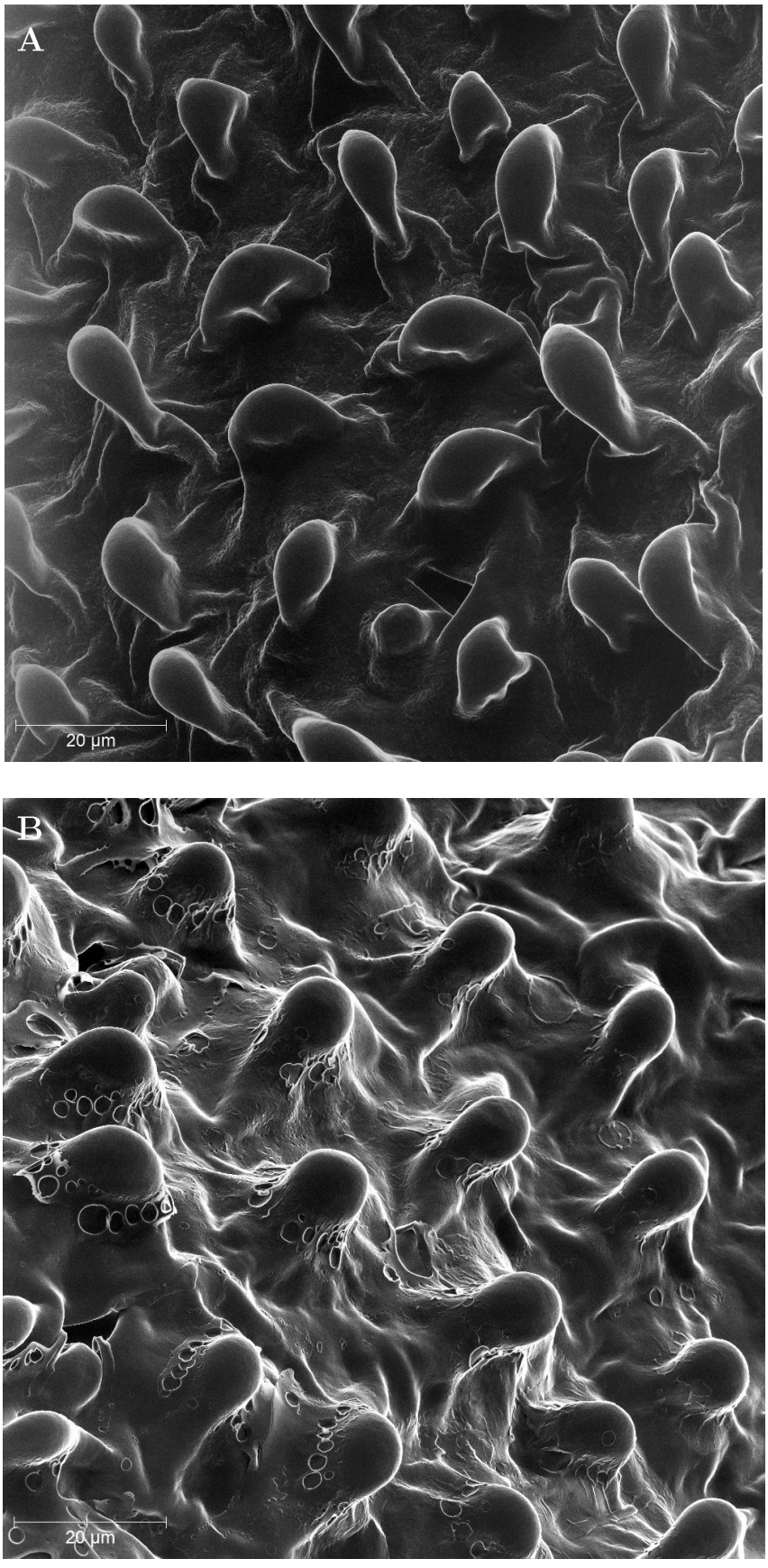

Figure 4.14: HIM images of destroyed *E. myrsinites* papillae caused by collapsing of the epidermal cells. The images were taken of leaves immersed for 1 min. (a) and 5 min. (b) in chloroform. In the 5 min. immersed leaf small holes form around the papillae tops. The acceleration voltage, current and dwell time for this measurement were 30 kV, 1.4 pA and 64 µs respectively.

4.4 Chemical analysis of the wax

From literature it was known that the main component of the epicuticular wax on top of the *Euphorbia myrsinites* leaves is the primary alcohol hexacosan-1-ol [20]. To verify if the extracted wax also contains this as the main component, a chemical analysis was done. The chemical identification of the composition was done with gas chromatography and mass spectrometry. The measurement is carried out as described in the experimental section (paragraph 3.3). The *E. myrsinites* wax is extracted with 1-2 sec immersion in room temperature and warm (50°C) chloroform, because it might be possible that components are less soluble at room temperature.

The gas chromatography measurement shows us the signal detected as a function of time. Both measurements, from the cold as well as the warm extracted wax, only showed a few peaks, namely: one from the solvent, some traces of the chemicals used for stabilisation and one other peak at 41.5 minutes. From the only interesting peak at 41.5 minutes, most likely caused by a wax component, the mass spectrum was analysed. The spectrum showed that in the most probably case this peak was formed by the presence of (i) silane, (hexacosyloxy)trimethyl- (76% chance) or (ii) silane, (1,1-dimethylethyl)hexacosyloxydimethyl- (49% chance) in the epicuticular wax. The graphs are shown in appendix 1. These components are silyl-derivatives of hexacosan-1-ol. Therefore we conclude that this component is the main component of our wax, as expected.

4.5 Analysis of the deposited wax

From paragraph 4.3 we learned that 1-2 seconds immersion of the leaves in chloroform is sufficient to extract the epicuticular wax. In the next experiment, dissolved *Euphorbia myrsinites* wax is deposited on artificial inorganic surfaces. The wax solution will distribute itself on the surface after deposition. The goal of this experiment is to investigate if the epicuticular *E. myrsinites* wax recrystallised and 3-dimensional nanocrystallic features are formed.

The *E. myrsinites* wax is obtained by dipping 50 leaves, one by one, into 4 ml of chloroform. This amount of chloroform was sufficient to fully immerse one leaf. After the extraction, the wax-chloroform solution is filtered as described in section 3.2. In the first attempt to recrystallise the epicuticular wax, the solution with an unknown concentration is simply deposited on the substrates (a silicon wafer and cover glass) under ambient conditions and without any further processing. A glass syringe with a metal needle is used for deposition. In order to determine the surface structure of the artificial surfaces with deposited wax on top, we examined the surfaces using helium ion microscopy (HIM) and atomic force microscopy (AFM).

Overall we observe from the HIM experiments that the wax is unevenly distributed on the surfaces. In figure 4.15 a HIM image is shown of the deposited *E. myrsinites* wax on a silicon wafer. From the different grey shades of individual terraces, it is clearly visible that multiple wax layers grow on top of each other. In figure 4.16a another HIM image is shown of the deposited wax. On this spot slightly more wax is present and striped features are found on the surface. The deposited wax shows us no recognizable nanostructure as we have seen for plant surfaces as described in chapter 2.3. Figure 4.16b shows a HIM image of deposited wax on top of a cover glass. The superimposed wax also shows the stripy behavior. Although there seems to be more of a patterning on this surface, again no typical crystal nano-objects could be found.

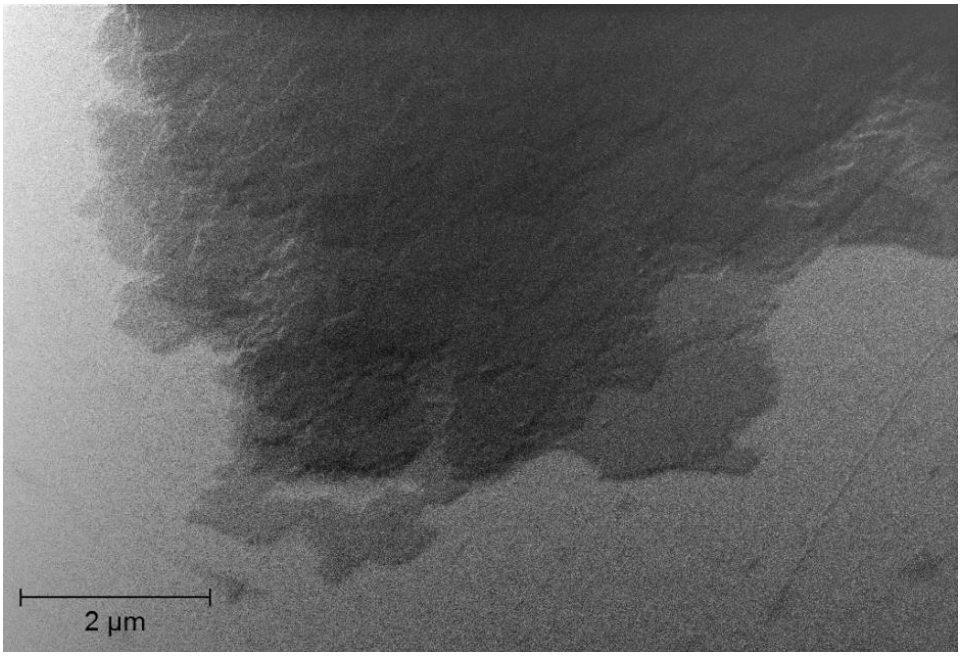

Figure 4.15: HIM image of *E. myrsinites* wax deposited on a Silicon wafer. For this image the acceleration voltage was 35 kV, the current 0.5 pA and the dwell time of 128 µs.

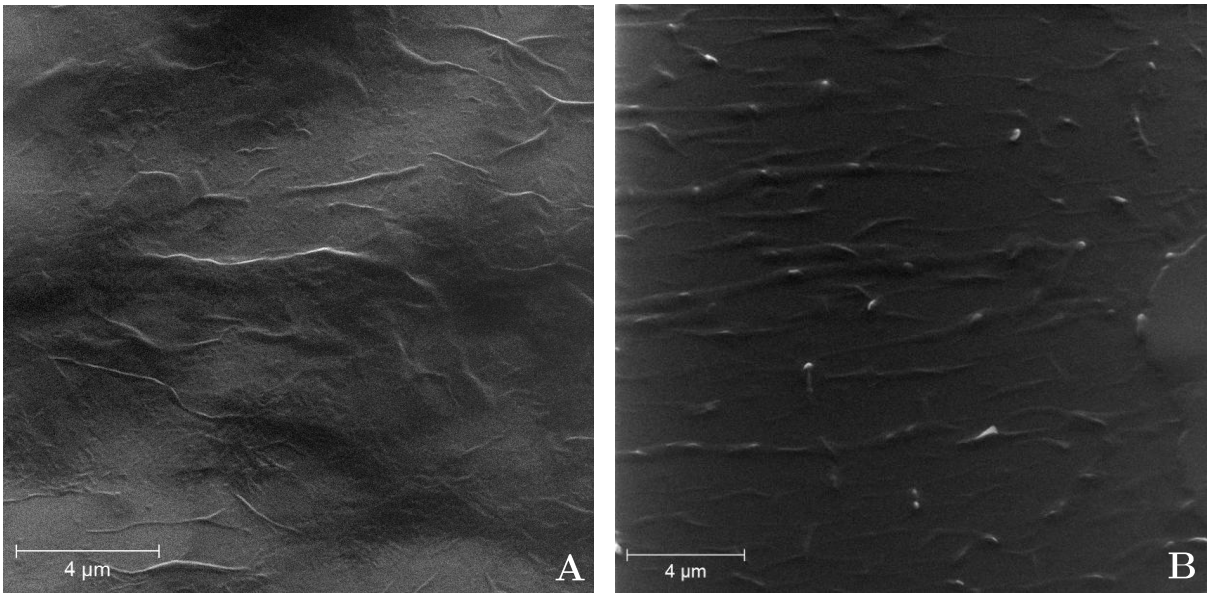

Figure 4.16: HIM image of *E. myrsinites* wax deposited on a silicon wafer (a) and cover glass (b). For these images the acceleration voltage was 35 kV, the current 0.6 pA and the dwell time of 128 µs.

Details on the surface are more visible with AFM. In the AFM pictures it can be confirmed once more that the wax on the surface is very unevenly distributed, and multiple layers grow on top of each other (figure 4.17). We find step edges of approximately 7 nm high, but also larger ones of varying lengths. To demonstrate this, a cross-sectional view of multiple step edges is given in figure 4.18a. In the topography image we observe eight different step edges; this can be confirmed with the graph in figure 4.18b.

Wax molecules usually stand vertically upwards and form layers. The chemical analysis, in paragraph 4.4 verifies that the main component of *E. myrsinites* epicuticular wax is the primary alcohol hexacosan-1-ol. The primary alcohol has a polar group at the end of the molecule and therefore prefers to assemble with a head-to-head orientation as explained in paragraph 2.3. Due to this orientation preference it is more likely that the molecules form a double layer structure, as shown in figure 2.8b. The development of the layer order can vary, because multiple components are present and depends on the chain length distribution and the separation of the components during crystallisation. The chain length of hexacosan-1-ol (C26) is 3.50 nm, according to equation 2.5. Multiples of this chain length are often found for the *E. myrsinites* wax. This is probably the double layered structure (see also figure 4.18b).

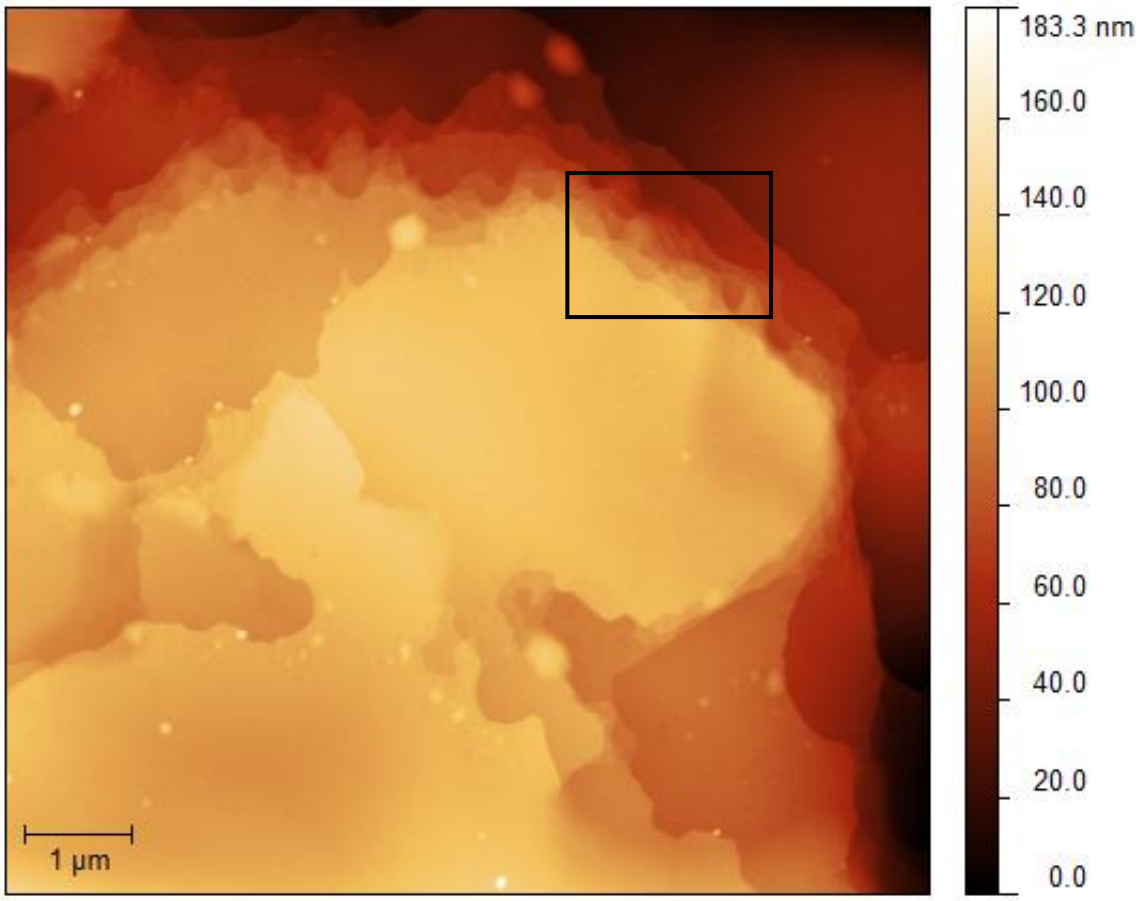

Figure 4.17: AFM topography image of *E. myrsinites* layered wax structure on top of a silicon wafer

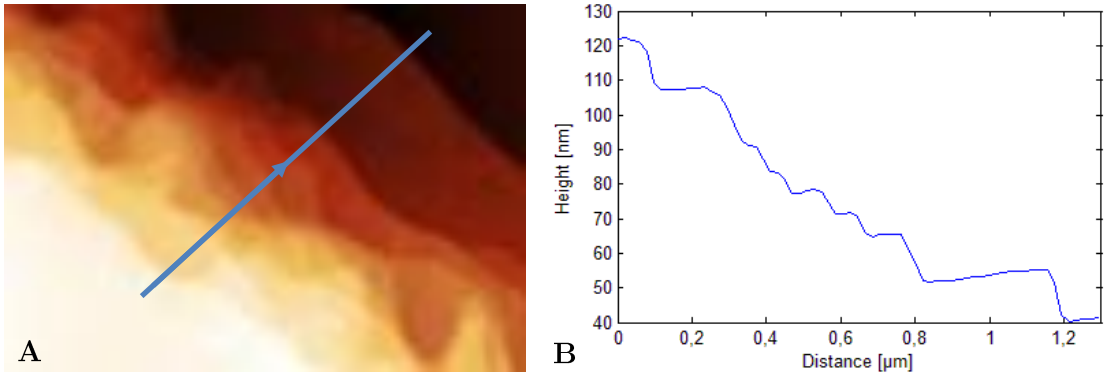

Figure 4.18: Magnification of the area in the black square in figure 4.18 (a) and a cross section along the blue line (b) to demonstrate the step heights.

The larger 'stripes' found with the HIM do not seem to be individual features when measured with AFM, but rather an accumulation of wax layers (figure 4.19). The surface in figure 4.19 differs a lot from figure 4.17, because the surface is rougher at this spot. We observe a lot of wax layers on top of each other. The morphologies are a result of anisotropic crystal growth. This is probably due to the fact that the wax is crystallised out of solution. During crystal growth, the assembly of the molecules in the x and y direction (parallel to the surface) occurs rapidly and independent from the chain length. The formation of a periodic layer structure in the z-direction requires more time particularly in wax mixtures with different molecule lengths where a separation of the components takes place. If we extended the evaporation time for several minutes, less of these stripy features are found on the surface. Still we do not find any typical nanostructured features.

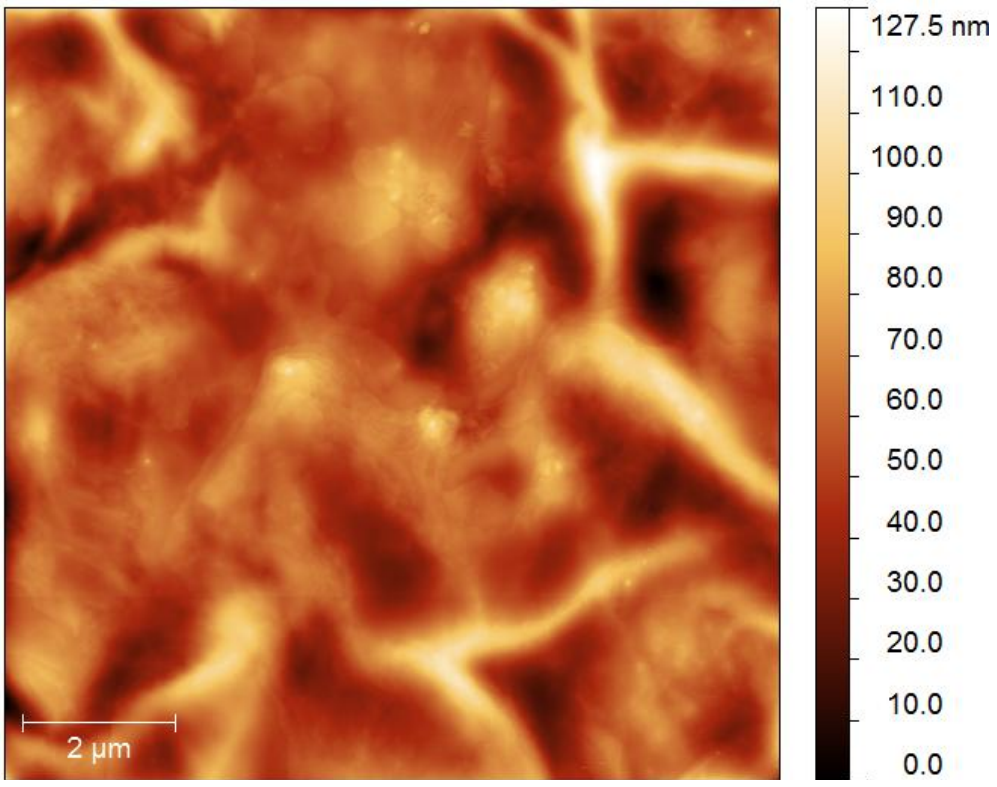

Figure 4.19: AFM topography image of *E. myrsinites* wax on top of a silicon wafer.

Influence of heating on deposited wax

The previous experiments did not lead to the formation of a recognizable nanostructure. No crystal-like features could be discerned on the surfaces. It is well known that at higher temperatures, molecules will be more mobile. This increased molecule mobility could perhaps lead to the formation of platelets. To examine this, new experiments were done with the use of several methods to increase the temperature of the wax sample. A Peltier heating plate, an AFM heating stage and an oven are used for various experiments. The surfaces are examined with AFM, SEM and OM to get more insight in the surface topography and morphology.

Because the wax should not evaporate from the surface, first the wax melting- and boiling point were determined. The temperature of the wax samples was increased with the Peltier heating plate by 2 ℃/min. from 25 to 80 °C. Over 1000 images in total of the surface were collected by using an optical microscope, with magnification of 50 times. Because the wax is deposited on the sample on top of the heating plate, and the thermocouple is located at the bottom of the heating plate, the temperature displayed on the Peltier computer interface will differ from the actual wax temperature. This means that the Peltier heating stage should be calibrated. For this purpose we use two different methods. The first method is to slowly increase the temperature of the heating plate while measuring the top of the silicon wafer with a temperature sensor. This measurement shows that the top of the plate is usually between 0-5°C lower than the displayed temperature. The second method is to use a piece of silicon wafer with paraffin wax (BDH Ltd.) and a piece of silicon wafer with tap water on top and measure their melting and solidification points. The Peltier element can heat the sample but is also able to cool down to low temperatures. A drop of water on top of the wafer is cooled from room temperature to -10 °C and then again raised in temperature and a piece of solid paraffin is heated to 100 °C and cooled down after. We are interested at the point where water (0 °C), and paraffin (55 °C) change phases. From this experiment we find an average error in the temperature of ±4 °C. In both experimental set-ups the heating plate with the sample on top is covered with a glass chamber to prevent room temperature air stream from changing the temperature.

The melting temperature of the *E. myrsinites* epicuticular wax is found to be 65±5 °C. Other experimentalists state the *E. myrsinites* epicuticular wax melting temperature to be 75-76 ℃ [20]. It is not mentioned in the article if the determined melting point of the recrystallised epicuticular wax was from solvent extracted wax or the mechanically isolated wax, so therefore we cannot compare the melting points. In addition to the fact that the extraction method could have been different, slight differences in the determined melting point could be caused by a different amount of wax, heating rate or measuring method.
Just after the melting phase occurs, we observe that the wax forms small droplets on the surface, which means complete dewetting of the sample. The liquid-liquid interactions are stronger than the liquid-solid (wax-silicon wafer) interactions. This is shown in figure 4.20. In the experiment shown, the temperature is raised even after the melting point is reached. The droplets will appear even if we keep the temperature constant above 65 °C and are stable at these temperatures. If the temperature is decreased very fast the wax will form solid bumps on the surface. If we decrease the temperature slowly the wax will spread more over the surface.

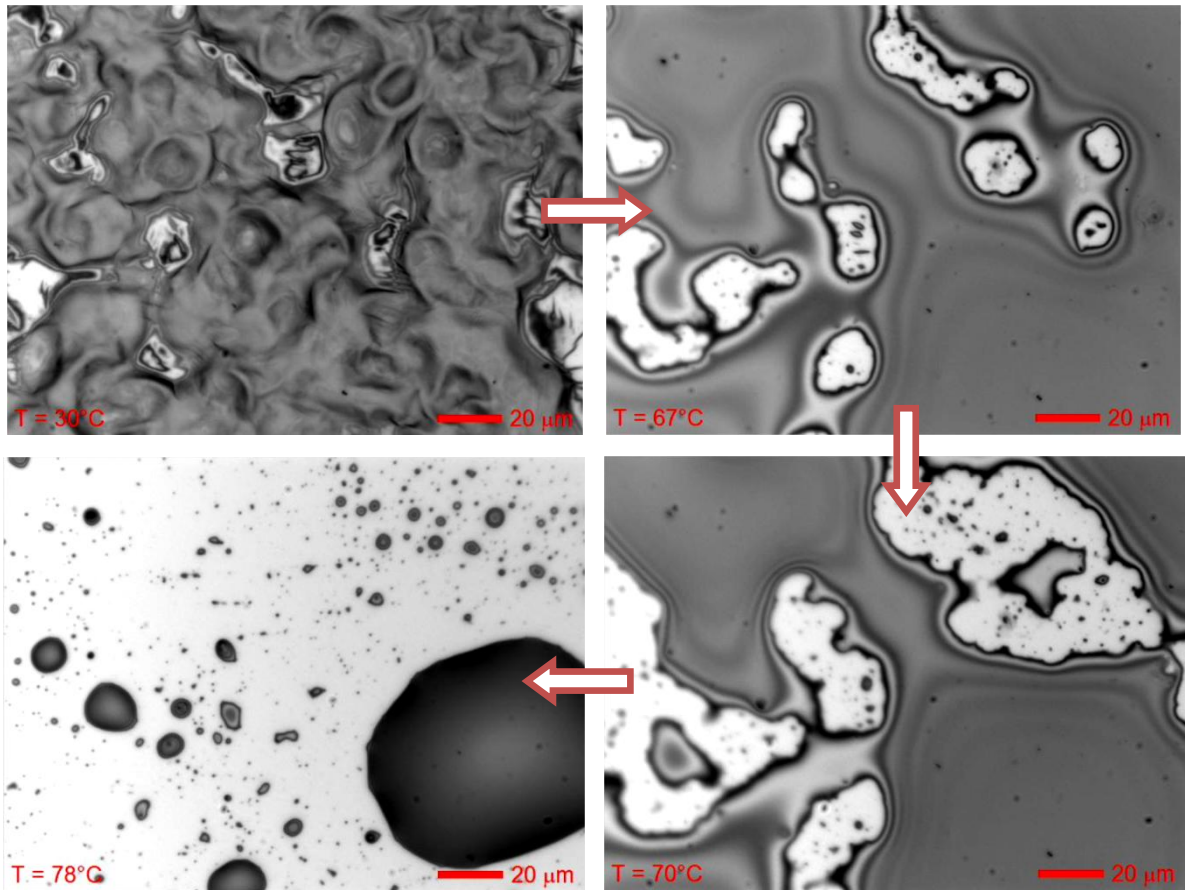

Figure 4.20: OM images of *E. myrsinites* wax on top of a silicon wafer. The wax is heated from 25 to 80 °C. After melting the wax forms droplets on the surface. The white region represents the silicon wafer while the darker parts represent the superimposed epicuticular wax.

The melting temperature plus 5 °C is used as the absolute maximum temperature for heating the sample. In the first heating experiment we increased the temperature of the sample gradually from room temperature up to 50 °C by an AFM heating stage while measuring the topography in situ. Apart from some molecules growing onto the existing layers or moving away from it, not a lot of dynamics is observed. An example of this is shown in figure 4.21. Sometimes the layers have approximately straight edges, as the triangle shaped layers in the example shown. The growing layers activated by heat grow in oak leaf shaped forms. Changes in the wax layers could only be observed if the temperature was increased, in time no sufficient changes to the surface are found. Even if we leave the sample for 24 hours at the heating stage of 50 °C, we don't observe significant differences. As such, we conclude that heating the sample to 50 °C, did not lead to the formation of platelets on the surface.
Furthermore, an attempt is made to activate the platelet growth by placing the sample with the wax solution on top in the oven at 50 °C for one week. This is done because a heated environment might have a different effect on the wax then the heating plate. With this method we also did not find any recognizable structure apart from wax layers growing on top of each other as was shown in figure 4.17.

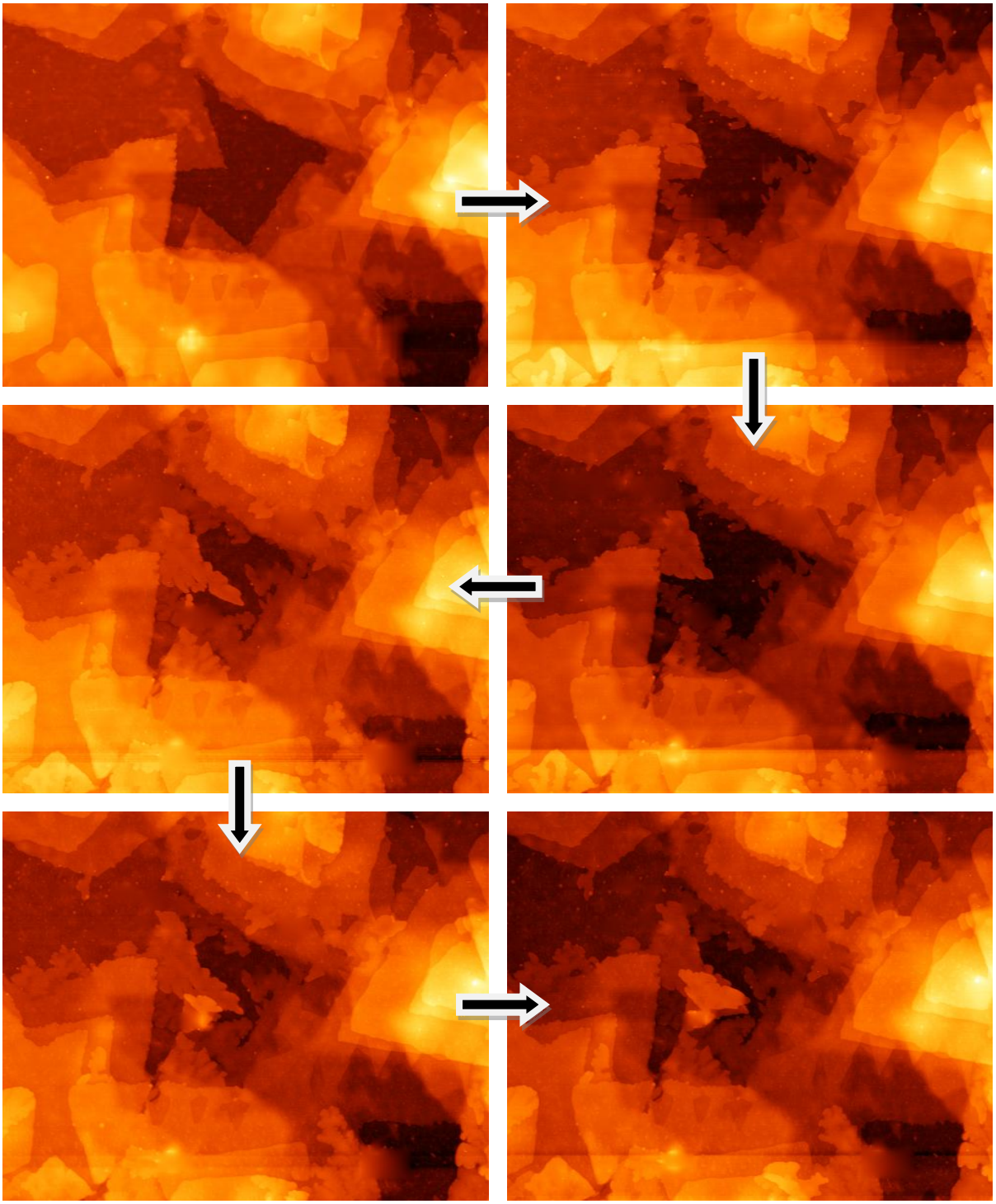

Figure 4.21: AFM topography images of layer growth of the *E. myrsinites* epicuticular wax on top of a silicon wafer activated by heating. The wax is heated from 25 to 50 °C in approximately 2.5 hours. Most changes were observed for temperatures close to 50 °C.

In the next experiment we increase the temperature to just above the melting temperature of the wax. From 25 to 57 °C heating, no sufficient changes to the surface are observed (figure 4.22a). From approximately 58 °C, spontaneous displacement of layers was found. The layers now partly point in the upward direction (figure 4.22b). The height difference of these displaced layers compared to the lower lying surface is approximately 100-200 nm. In the areas of the layer displacement we observe that the AFM phase image has changed (see figure 4.22b). Right after the displacement we observe that the height of this region becomes smooth. The displacing does not lead to the formation of platelets.
If the temperature is raised even further, the smooth area becomes larger and larger (figure 4.22c). In the AFM phase image of figure 4.22c, which refers to the phase shift of the cantilever oscillation, three different phases are found. The oscillation phases in the middle of the picture are both very uniform and smooth, while the other phase (shown with the red color) shows the features which correspond to height differences in the topography image. From the appearance of the AFM phase shifts, we conclude that the wax is melted at certain spots on the surface. The spots where the AFM phase image is uniform and smooth, corresponds to the melted surface, whereas the other part of the surface is solid. Two different melting phases are observed. This might be due to the fact that, when melted, the wax separates into two phases with different compositions or the compositions are the same but the molecules are oriented in different directions. From the figure we cannot draw any conclusion on which of the two is more likely to be the case. However, in the chemical analysis only hexacosan-1-ol could be observed. There are probably more components present in the wax, but in relation to the hexacosan-1-ol this is a very small portion. Therefore, we expect that the molecules are oriented in a different direction in the phase image.
Above 65 °C, it was impossible to measure with the AFM because the surface was completely melted and there was too much drift in the image induced by heat. From 70 °C, the wax is cooled down to room temperature by 3 °C per second. The surface topography and phase are measured again at 25 °C. The surface structure completely changed: sharp ridged surface roughness is observed (see figure 4.23). Interestingly, these features are not very likely to occur for waxes extracted with longer immersion times, as shown in figure 4.23b. This means there clearly is a difference in the composition of waxes extracted with longer immersion times. The height of the surface structuring is measured and shown in figure 4.24. The aspect ratio of this roughness is very small compared to the aspect ratio of the original leaf platelet structure. To get more insight in the surface morphology the surface is measured with SEM (figure 4.25). The sharp ridged surface roughness surface roughness appears where we find some wax accumulation; this is indicated with the green arrow. On surface spots where the wax accumulation is highest, we find superimposed features which look quite similar to the original platelets. In contrast to the original, vertical platelets on the leaves, these ‘platelets’ grow parallel to the surface. This is indicated in figure 4.25 with the blue arrow. Apparently recrystallisation from the melting phase does not lead to the formation of a nanostructure similar to that on the leaf surface.

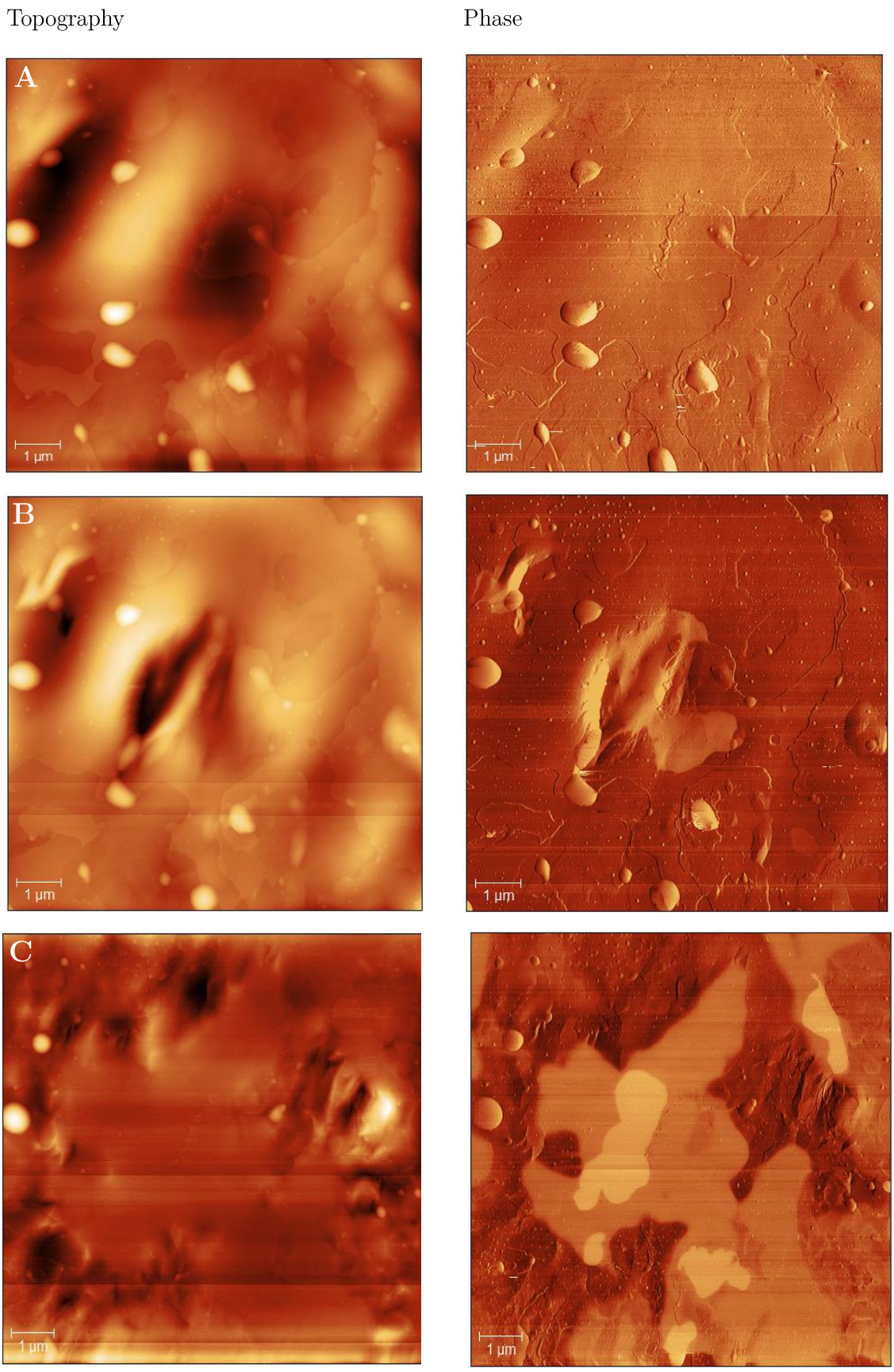

Figure 4.22: AFM topography (left) and phase (right) images of *E. myrsinites* wax on a silicon wafer on top of a heating plate. The contrast in the topography image gives the height of the surface from approximately 0 (black) to 200 (white) nm. The contrast differences in the phase images show regions of different phase. The images are taken at 56 °C (a), 58 °C (b) and 65 °C (c) respectively.

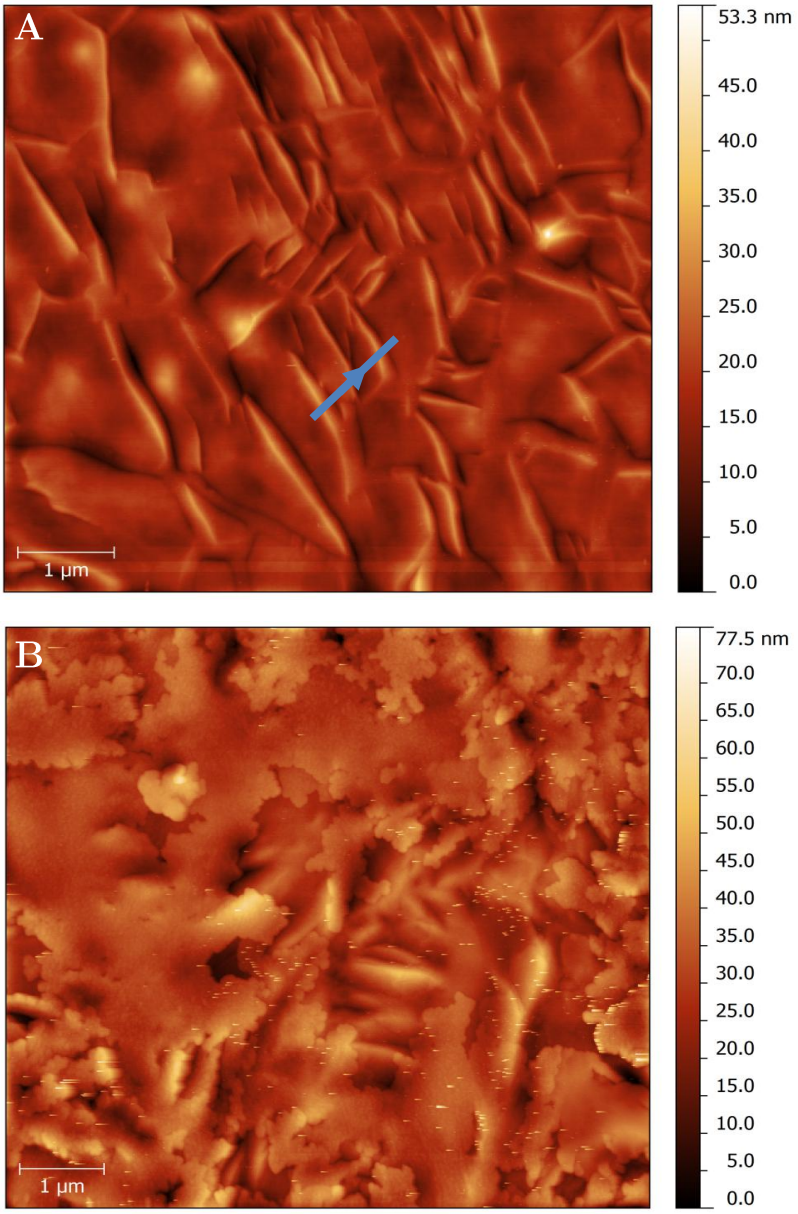

Figure 4.23: AFM topography image of *E. myrsinites* wax after cooling down from the melting phase. The waxes extracted with 1-2 sec. leaf immersion (a) and 1 min. leaf immersion (b) respectively.

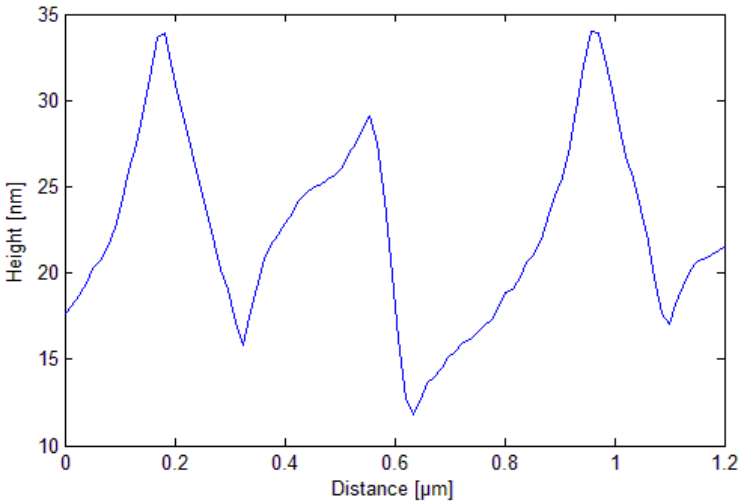

Figure 4.24: Height profile of the *E. myrsinites* wax structure along the blue line in figure 4.24a.

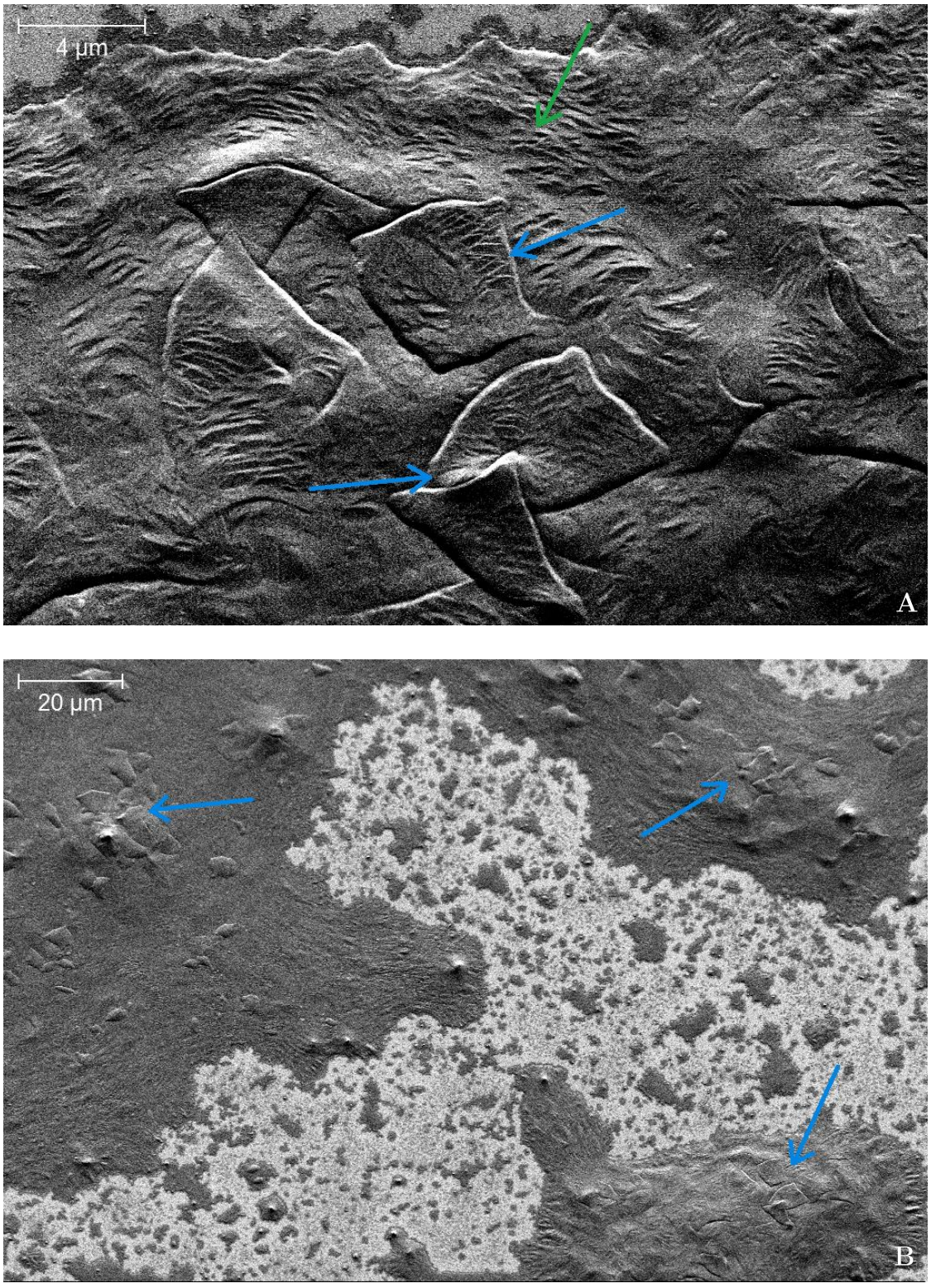

Figure 4.25: SEM HE-SE2 images at 0.55 kV and 60 pA of *E. myrsinites* epicuticular wax after cooling down from the melting phase. The upper picture is a magnification of the right bottom of the lower picture. The green arrows indicate the rough surface features and the blue arrows indicate the platelet like features.

High wax concentrations

It was found in the previous experiment that at the spots where the wax accumulation was very high, horizontally directed 'plates' appear after the melting phase. Because these features appear only when the wax density was high, i.e. in the middle of the areas where wax has accumulated, the wax concentration was increased in the next experiment.

The chloroform wax solution was dried under a gentle stream of nitrogen. The dry wax was dissolved in 0.1 ml chloroform. The wax chloroform solution is now measured to have a concentration of approximately 10 mg/ml. This concentration is almost seven times higher as the tubule wax concentration prepared by Koch et al. [6]. 25 µl of the high concentrated wax solution was deposited on a silicon wafer. The wax introduces a white rough layer of unequal distribution and height on the surface as observed by the eye. Measuring with AFM was impossible; the AFM tip very easily snapped into the surface or picked up material from the surface. Therefore the surface was measured with the SEM. From SEM images it becomes clear that high aspect ratio surface features were the cause of this.
Measurements with the SEM indeed reveal that the higher wax density parts on the surface consist of small features in the nanoscale. In figure 4.26 a highly magnified picture of the surface is shown, where these features are visible. At first sight, it seems as if the recrystallised wax is very different from the original wax platelets. If we take a closer look, we actually see that they are much alike in several aspects: the growth for example. We did not actually measure the time dependence of the growth, but in figure 4.27 we can see clearly that the nanostructure grows from an underlying wax layer. When we compare this for example to figure 4.3 we can see that this is quite similar.

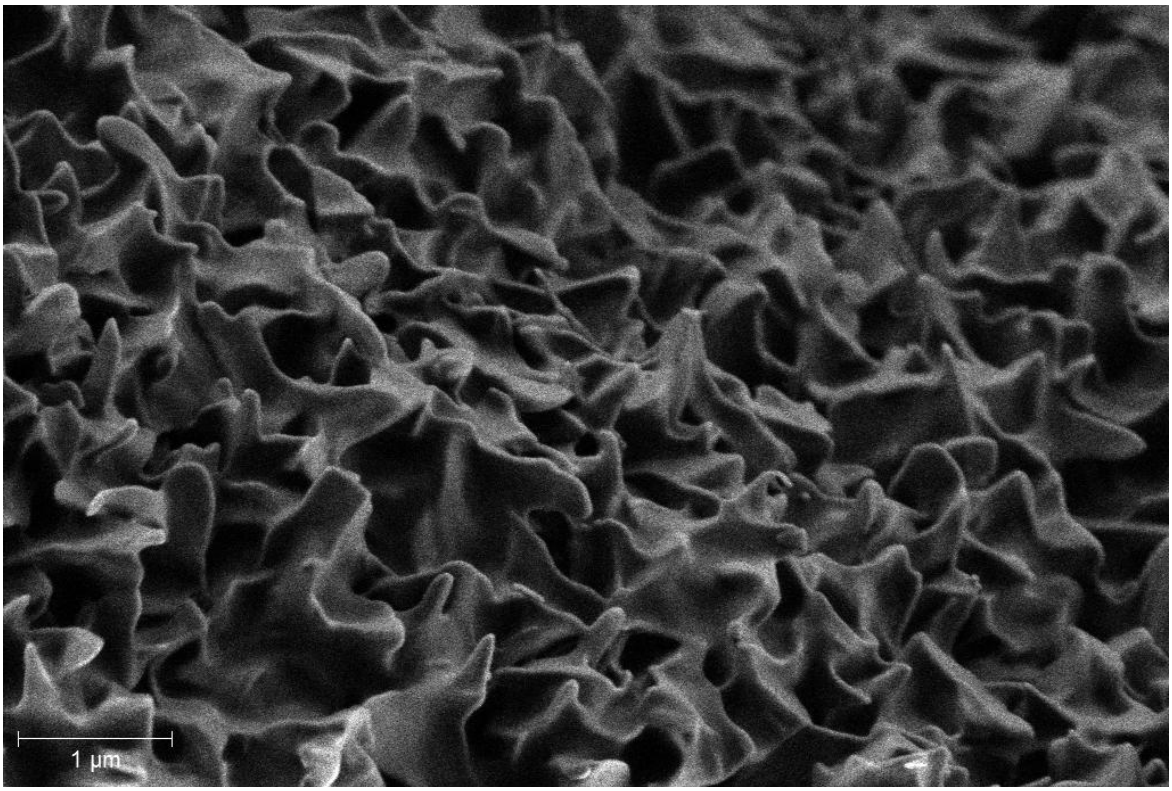

Figure 4.26: SEM HE-SE2 images at 1.00 kV and 30 pA of an increased amount of *E. myrsinites* epicuticular wax on top of a silicon wafer. This image is a high magnification of the surface, where the nanostructure can be seen.

The height of the layer is measured with the built-in SEM tool. The measured values seem to be in the same range as for the original platelets. From the pictures of the leaves in paragraph 4.2 we could see that the platelets might overlap each other, which makes the nanostructured layer higher. This also seems to be the case for the recrystallised wax layer. Also the thickness of these features seems similar. Furthermore it was found that the features might cross each other, like the platelets. This is shown in figure 4.27b. However, we do not recognize much of the straight edges we found for the original platelets on the leaves.

The structure might be best described as partially fused platelets. The question arises of course why the recrystallised wax nanostructure is different from the epicuticular wax on the leaves? If we look at the edges of the structuring, we observe round bended edges. This is comparable to the nanostructure on the leaf which was stored for 2 weeks (figure 4.5). Therefore, it could be that the recrystallised wax degenerated by the environment. To see if the structure changes over time, a sample which was stored for 4 weeks under ambient conditions was measured. This showed us the same structure as seen for the newer wax samples. Hence we assume that the wax recrystallises in this fashion and does not change over time. The straight-edged and well-defined epicuticular platelets do exist on a living plant though. If the leaf is cut from the plant, we see the epicuticular wax structure changing. It might be that the platelet structure only exists on the living plant. The environmental conditions for the living plants are different. The plant ensures that the epicuticular will be renewed by diffusion through the cuticle via a lipidic pathway (as is believed). Also it could be that it is not possible to retrieve this platelet epicuticular wax structure by deposition from solution. However, Koch et al. [23] showed that the primary alcohol octacosan-1-ol dissolved in chloroform can crystallise out of chloroform solution in octacosan-1-ol platelets on HOPG. This compound does crystallise on HOPG without a thick underlying wax layer. Of HOPG the polarity and degree of crystallinity are different when compared to silicon wafers. As mentioned in the theoretical chapter, HOPG influences the molecular orientation and alignment. It is assumed that this also holds for the plant cuticle. Unfortunately, this could not be investigated within the duration of the project.

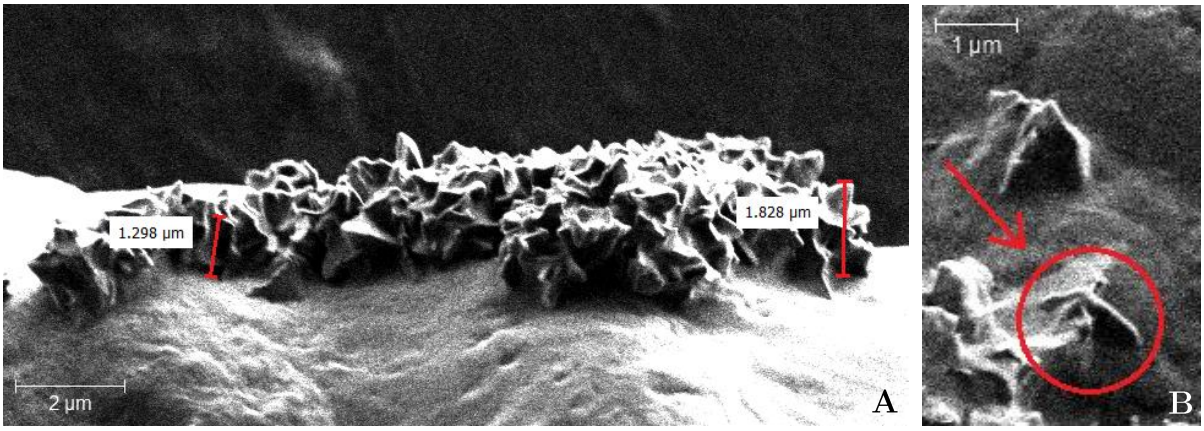

Figure 4.27: SEM HE-SE2 images at 1.00 kV and 30 pA of the nanostructured layer on top of a relative flat layer of the epicuticular *E. myrsinites* wax.

4.6 Wettability analysis

In the second paragraph of this chapter, it could be seen that the *Euphorbia myrsinites* leaves have a hierarchical surface structure. These surface structures can lead to superhydrophobicity and self-cleaning properties. To get a better understanding of this, the wettability of the *E. myrsinites* is examined. Herewith, we also look at the wetting properties of dried leaves and leaves immersed in chloroform. Those surfaces were also shown in paragraph 4.2. Furthermore, we make an attempt in determining the wetting properties of the deposited wax. The wetting properties are measured in terms of the contact angle between a deposited water droplet and the surface to be examined. The contact angles are measured with the instrument described in paragraph 3.3.

In order to measure the contact angles of the leaf surfaces, small pieces of approximately 0.5 by 0.5 cm are cut from the leaf. The leaf surface is slightly curved to the middle, where we find a grain. The grain lies just slightly lower than the part of the leaf more to the boundary. If we do not cut the leaf, the droplets will just roll to the grain. The static contact angle of the *E. myrsinites* leaves is measured to be 160.8±2.5° for droplets of approximately 8 µl. This is the average taken for over 20 pieces of leaf. The original measurement data is shown in appendix 2. The high contact angle means that the surface is superhydrophobic. The roll-off angle is very small because even when the leaf surface (which is slightly curved though) lies on a horizontal plate, it is very hard to even make sure that the droplet will stay on the surface. If the drop sticks on the surface it will easily roll off by even slightly bumping the table. These characteristics are typical for self-cleaning surfaces. Because the droplet rather adhered to the metal needle than that it would stick to the surface (like shown in figure 4.28a), we were not able to measure the advancing and receding contact angle of the leaf surface.

Furthermore, it is found that when the piece of leaf is stored under ambient conditions, the contact angle will decrease, but only just a few degrees. Even after a couple of weeks, when the leaf becomes all yellowing and brittle, the contact angle was found to only decrease by 2-4° on average measured over 10 samples. This can be explained by the SEM image in figure 4.5, which shows the leaf surface after 2 weeks of storage. The papillae are still completely undamaged and the nanostructure is still present, although a bit degenerated. The contact area between the water droplet and the surface will still be very small. We expect the leaf to maintain this superhydrophobic behavior until the nanostructure is completely caved (which might not even happen) or when the leave becomes so dry that it shrinks or just breaks apart, which we think is more likely to be the case.

When the leaves are immersed into chloroform, the platelets are removed from the papillae as shown in chapter 4.3. It was expected that this will decrease the contact angle because the contact area between the water droplet and the surface is then increased. Also it seems plausible that the contact angle will decrease even more when immersing the leaf for a little longer because the surface will initially get smoother, more wax will be removed and the papillae will get smaller. Leaves of the *E. myrsinites* plant were immersed in chloroform for different time periods, and small pieces of the leaves where used to measure the static contact angle as shown in figure 4.29. The original measurement data is given in appendix 2. The measurement was repeated 15 times for every immersion time.

As can be seen from the graph the initial contact angle of the fresh leaf decreases a lot when immersing in chloroform. The initial nanostructure is removed and the droplet probably comes into the Wenzel state. It was found that the surface becomes sticky. If we turn the leaf upside down the droplet will still be stuck to the surface. This is shown in figure 4.28b. From the graph it turned out that our expectations were not completely right. Surprisingly the static contact angle seems to increase for longer immersion times, while the surface will remain sticky. This means that the adhesion force between the surface and the water droplet has increased a lot. This could be caused by a change in chemical composition of the outermost surface layer. For 1-2 sec immersion we assume that the epicuticular wax is removed, followed by the removal of the cuticular waxes and eventually other parts of the cuticle will be removed. The static contact angle could then increase if the surface roughness is increased. Adhesive superhydrophobic surfaces were fabricated by Guo et al. [28] and this effect can also be seen for example for red rose petals. For longer immersion times the papillae structure and aspect ratio are different due to increased removal of the outermost epidermal layers, but eventually also due to the possible collapsing of the papillae. The mutual papillae height difference is larger and the collapsing increases the surface roughness.

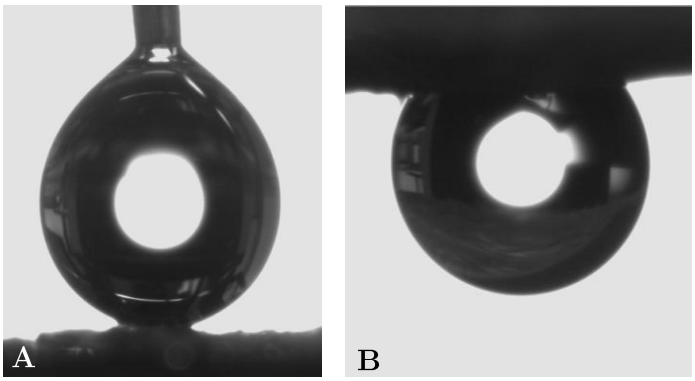

Figure 4.28: Water droplet of 5 µl which refuses to stick on a very hydrophobic surface and one that is hanging on a sticky *E. myrsinites* leaf surface which is immersed for 5 sec in chloroform.

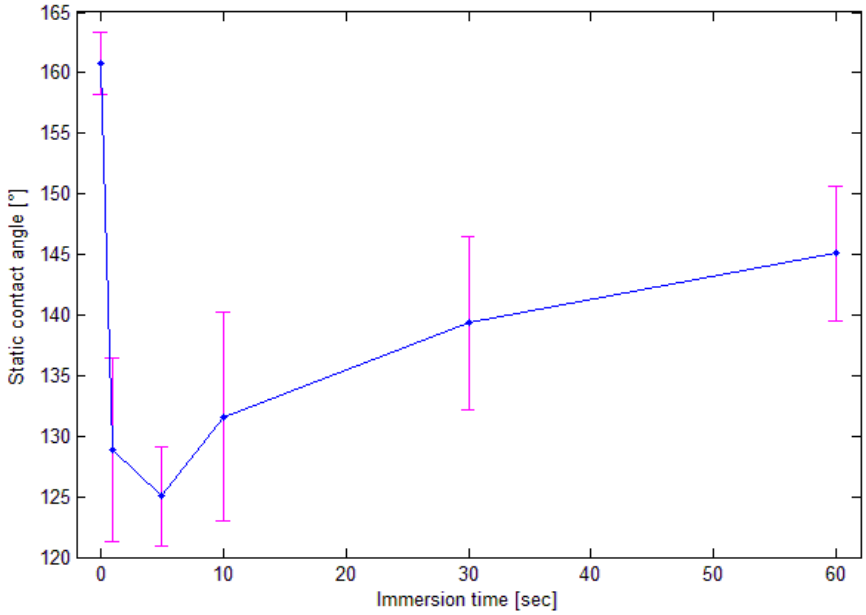

Figure 4.29: Contact angle as a function of leaf immersion time in chloroform. The data points are averaged over 15 measurements. The purple error bars are based on standard deviation.

The static contact angle of the *E. myrsinites* wax without any typical nanostructured features on top of a silicon wafer (which is described in the first part of chapter 4.4 and shown in figure 4.15 tm 4.19) is measured to be 110.1±3.2°. The measurement data is shown in appendix 2. To make sure that we are actually measuring the contact angle of superimposed wax, also the static contact angles of a bare silicon wafer and a silicon wafer on which a drop of 20 µl chloroform was deposited are measured. The chloroform evaporates within a few seconds and the contact angle is measured afterwards. The different samples with water droplets on top are shown in figure 4.30. Prior to the measurements and chloroform/wax deposition, the silicon wafers were cleaned by rinsing them first with ethanol and after with chloroform and drying them with a stream of nitrogen. This makes the surfaces well-nigh clean when imaging them with the optical microscope. As shown in the figure, the silicon wafer itself is measured to have a static contact angle of approximately 35°. For the silicon wafer on which a chloroform droplet was deposited the static contact angle has increased significantly. Because chloroform easily dissolves all kinds of compounds, it leaves contamination on the silicon surface when it evaporates. This contamination contributed to extra roughness on the surface. If the wafer is rinsed with chloroform and dried with nitrogen, this effect is largely retained. Even though the droplet induces extra roughness on the surface, still an increased contact angle could be found for the sample with deposited wax.
Since the surface is only partly covered with wax, the measured static contact angle is only an indication of how large it can be. For a smooth surface a contact angle of ~110° would be very high. But epicuticular waxes, for example on the leaf surface shown in figure 2.4d and which is only slightly curved, can show contact angles approaching 150°. This increase in contact angle is caused by the wax nanofeatures. This also confirms that we did not reveal the epicuticular wax nanostructure on this surface.

To compare this epicuticular wax to commercial wax, the static contact angle of paraffin wax (BDH Ltd.) is measured. The contact angle of solid paraffin and also deposited paraffin wax is measured. For the deposited paraffin a solid piece of wax cut in a cube with sides of approximately 40 mm was melted on an approximately 1 by 1 cm large silicon wafer. The wafer is placed on top of a heating stage and cooled down slowly to get a substantially uniform wax distribution on the surface. The static contact angle for the solid wax as well as the solidified wax is measured to be 114±5°. This contact angle is quite similar to the measured contact angle of the approximately smooth epicuticular wax layer. It is known that flat surfaces can have static contact angles up to 120°. This also further demonstrates the unique wetting properties that the epicuticular wax with superimposed nanocrystalloids may have.

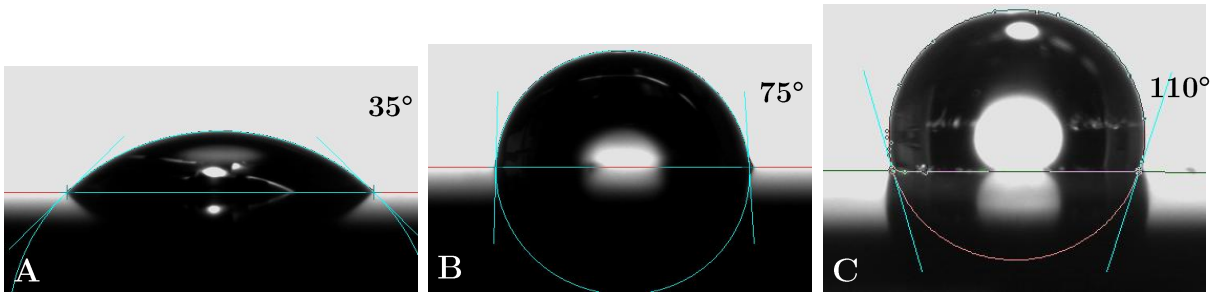

Figure 4.30: Static contact angles of water droplets on top of a silicon wafer (a), on a silicon wafer with a deposited chloroform droplet (b) and on a silicon wafer with deposited *E. myrsinites* epicuticular wax without nanocrystalloids.

As described in the previous paragraph the higher concentrated *E. myrsinites* wax solution recystrallises in thick rough spots of accumulated wax as observed by the eye. The static contact angle of the higher concentrated wax is measured to be 154.6°±3.9. Because making the wax samples is quite time consuming, it was only measured for five different samples. The measurement data is shown in appendix 2. The droplets are deposited on spots where the wax density is high, whereby the measured value in all probability would be approximately the same if the surface would be fully covered with the wax. Even though we managed to measure some static contact angles, it was very hard to deposit a droplet on top of the wax layer, because it rather adhered to the metallic deposition needle. Even the larger droplets refused to stick on the surface, like in figure 4.28a. This image, which was also used to explain the superhydrophobic properties of the leaves before, is actually taken from a droplet on top of the recrystallised wax layer.
The high contact angle indicates that a surface nanostructure is present. This is also confirmed by the SEM image in figure 4.26, by which we found that the surface is covered with nanocrystalloids. The crystalloids reduce the contact between the surface and the water droplet. As described in the theoretical chapter, epicuticular waxes on almost flat surfaces can have contact angles approaching 150° (close to the superhydrophobic limit). Our measurement data show an even higher contact angle. Because the wax does have an unequal distribution, extra roughness is created. These large height differences cause microscale roughness, which increase the contact angle.
The static surface contact angle was also measured for this thicker layer of *E. myrsinites* epicuticular wax after storage for 4 weeks. The contact angle did not change. This can of course be explained by the fact that the surface structure did not change as observed by SEM.

The theoretical chapter describes that the papillae provide the tool to magnify the contact angle based on the Wenzel model. The static contact angle of the leaves was measured to be ~160°. So which contact angle would the *E. myrsinites* epicuticular wax need to ensure such a high contact angle? This can be calculated by equation 2.4, which gives a rewritten Cassie-Baxter equation. Because the tilt angle of the *E. myrsinites* leaf surface is extremely low, we can assume that the droplet is in the Cassie-Baxter state. In this equation it is assumed that we have perfectly non-wetting, i.e. $\theta_{air} = 180°$. Input values for the equation are the Cassie-Baxter contact angle θ_{CB} and the areal fraction of the papillae f. The areal fraction of the papillae is estimated to be 0.3, based on optical microscopy images, like the one shown in figure 4.6 and the scanning electron microscope images. This is of course only an estimate, since we do not know how the droplet exactly covers the papillae. The Youngs contact angle of the wetted area θ_Y, i.e. the papillae tops, is then calculated to be 143°. This very well suits the outcome of our measured static contact angle.

Chapter 5

Other plant leaves

5.1 Introduction

Besides the research on the *Euphorbia myrsinites* leaves, some other plant material is examined: the *Aquilegia canadensis* and *Buxus sempervirens* leaves. This makes it possible to compare different self-studied plant leaves and their waxes. The measurements on this plant material covered only a small part of the project, since limited research is done on these plants. The observations and results are only briefly described. For both plant leaves the leaf surface is examined with the optical microscope (OM), the papillae density is calculated and the static contact angle is determined. Furthermore, an attempt is made to recrystallise the epicuticular wax on silicon wafers. After wax deposition the surfaces are measured with atomic force microscopy (AFM).

5.2 Aquilegia canadensis

The *A. canadensis* is an erect, branching perennial which can grow up to 2 meter height. The green to blue-green leaves are 1-3 cm long, as shown in figure 5.1. The leaves are lobed and grouped together with three. First, the leaf surface of the *A. canadensis* is examined with the optical microscope (OM). For the imaging a lens of 20 times enlargement was used. As observed from the OM image, the surface of the *A. canadensis* is not covered with well-defined surface papillae like the *E. myrsinites*. In figure 2.4 from the theoretical chapter different types of surface structuring are shown, where it can be seen that we rather have convex cells or something in between convex cells and papillae. Just as in the previous chapter, the density of these protruding cell shapes is calculated, which amounted to 430±30 per mm^2.

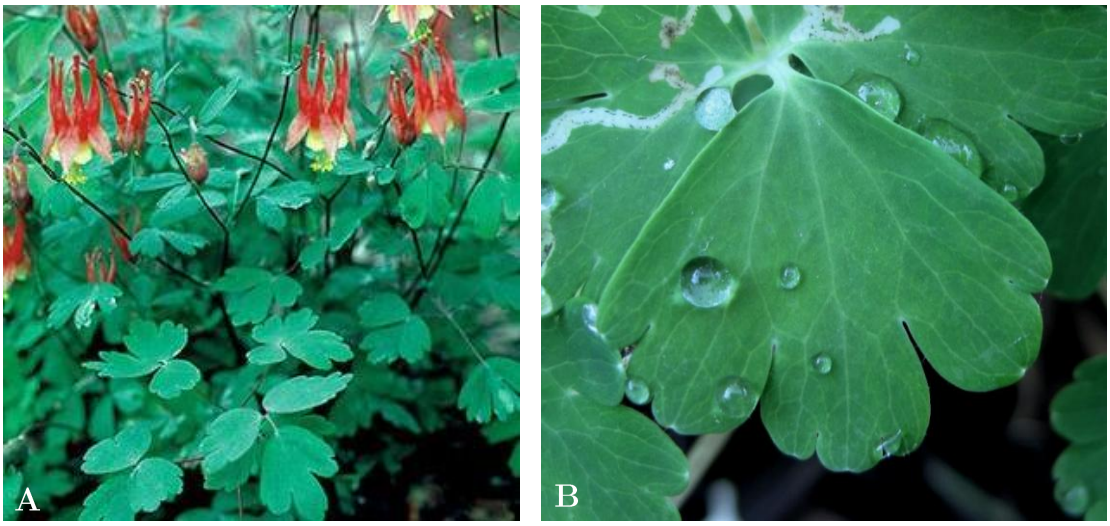

Figure 5.1: Picture of the *A. canadensis* plant with leaves and flowers (a) and a close up of the leaf with a water droplet on top (b).

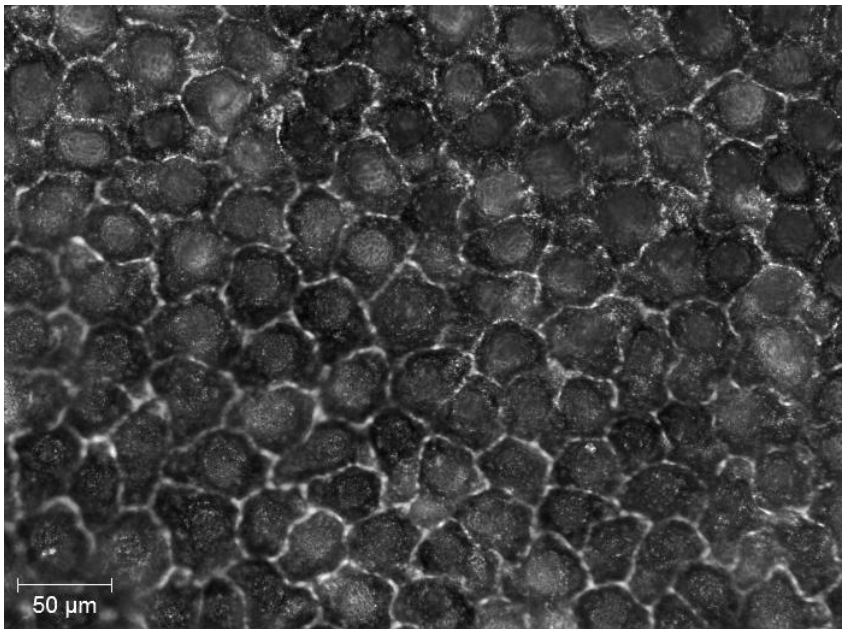

Figure 5.2: OM image of the *A. canadensis* leaf surface also used for statistical analysis

The static contact angle of the *A. canadensis* is measured to be 156±5°. It was already described in section 4.2 that the tilt angle is extremely low. The static contact angle is almost as high as the static contact angle of the *E. myrsinites*. The difference could be caused by the fact that the *E. myrsinites* surface consists of well-defined surface papillae and their papillae have a higher density.

It was not examined which epicuticular wax structure is present on the *A. canadensis*. From literature it is known that the *A. canadensis* epicuticular wax recrystallises in nonacosanol tubules and some platelets in ethanol [20]. Some experimentalists [6, 22] measured the time dependent growth of nanocosanol tubules extracted from Lotus leaves. Because the *A. canadensis* also recrystallises with tubules, our intention was to measure the time dependent growth of our wax. The *A. canadensis* epicuticular wax is made by immersing 50 leaves one by one in 4 ml chloroform. The immersion time amounted to 1-2 seconds. The wax is deposited on the surface out of solution like the *E. myrsinites* wax. We measure the surface with AFM after deposition. The measured data is shown in figure 5.3.
The image acquisition started as soon as possible after the chloroform evaporation, typically after 10 minutes. In figure 5.3 we see that the surface is covered with a dense layer of very small wax tubules. The wax tubules grow in the horizontal direction on the surface, and from an underlying wax layer. In the picture of the smaller scan area in figure 5.4, we observe that the tubules are hollow and consist of multiple layers. This is in accordance with the tubule structure model as is described by Ensikat. et al. [29]. The average outer diameter of the vast majority of Lotus wax tubules varied between 200–300 nm, which corresponds to our wax tubule width. Also the length of approximately 800 nm and layer thickness of approximately 20 nm, seem to agree. Over time, no sufficient changes to the surface were observed. The tubules were already present on the surface. However, in the experiments from literature where time dependent growth was examined, the wax was deposited on non-polar crystalline substrates. It was shown also in the article by Koch et al. [6], that wax tubules on silicon recrystallised predominantly on thicker bulks of wax mass. Mainly on HOPG, vertical orientation of the tubules was found. An epitaxial growth of the wax on flat lying wax molecules must have led to vertically oriented tubules on HOPG.

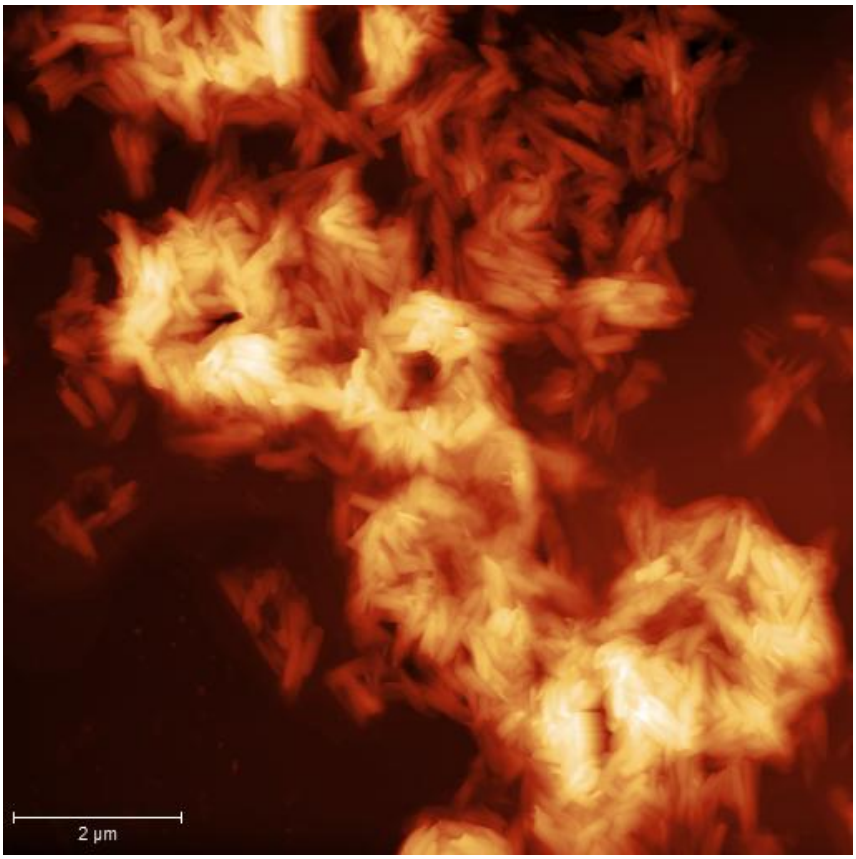

Figure 5.3: AFM topography image of A. canadensis wax tubules on top of underlying wax layers.

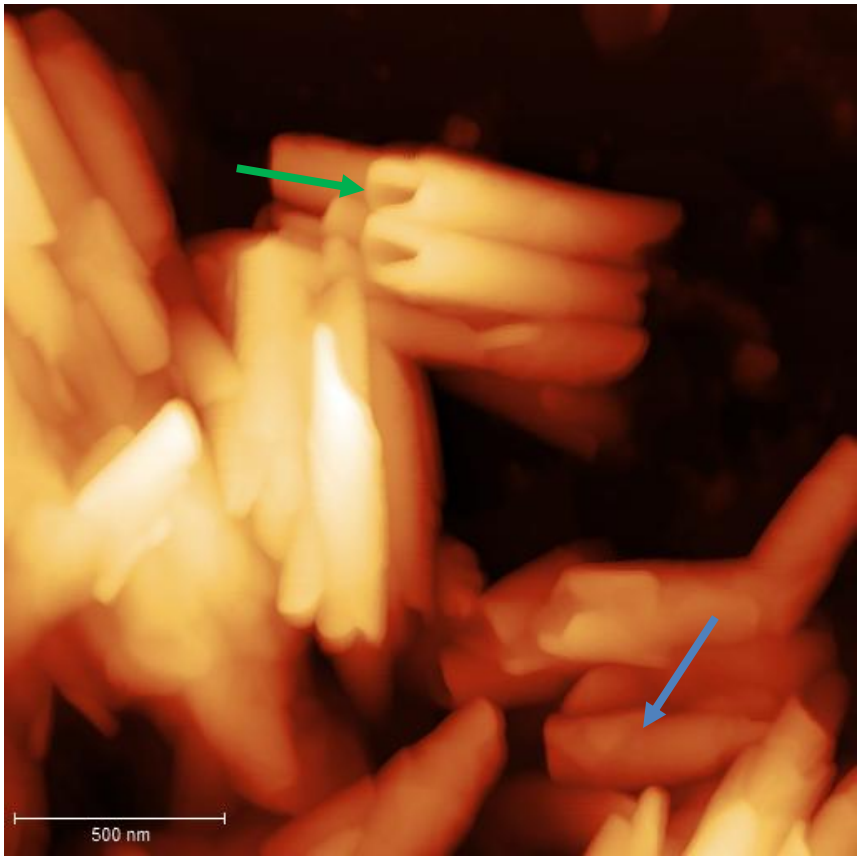

Figure 5.4: AFM topography image of *A. canadensis* wax tubules at high magnification. In this image we observe that the tubules are hollow (green arrow) and consist of multiple layers (blue arrow).

5.3 Buxus sempervirens

The well-known *Buxus sempervirens* is an evergreen shrub or small tree growing 1-9 m tall. The trunk is up to 20 cm in diameter. Arranged in opposite pairs along the stems, the leaves are green to yellow-green, 1.5–3 cm long, and 0.5–1.3 cm broad. The *B. sempervirens* stems with a high density of leaves are shown in figure 5.5. Like in the previous example, we first examined the leaves with the OM, where we used a lens of 20 times enlargement. The result is shown in figure 5.6. The epidermal outer cell shape is again different from the well-defined papillae of the *E. myrsinites*. The protruding epidermal cell shapes seem like convex cells but when we focus on a certain height, it becomes visible that there is a small papillose top present. From the OM picture you get the impression that not the entire surface is covered with papillae. This is due to the fact that the optical microscope can only focus on a certain height and the surface is not completely flat. Therefore, to determine the papillae density, smaller images made with a lens of 50 times enlargement are used. The measured papillae density amounted to 2494±150 per mm^2. The measurement error is estimated and based on an error in the counting of the papillae which are at the boundary of the picture. The error is relatively larger compared to the previous experiments because we used smaller images for the calculation.

The maximum static contact angle of the *B. sempervirens* was found to be 157±5°. This contact angle is in the same range as the contact angle measured for the *A. Canadensis* and the *E. myrsinites* leaves, although slight differences are found. The *E. myrsinites* probably has the best water repellent surface, due to the high density of papillae with relatively small tip radii. For the *A. Canadensis*, the density of papillae is smaller, which means a lower capillary pressure is necessary for the intrusion of water. Also, since the tip radii are higher, this will reduce the water repellency and stability. The *B. sempervirens* has the highest density of papillae with the smallest tip radii, but the papillae are also very small in height. At higher pressures, for example the impact of raindrops, the water intrudes deeper between the papillae. The highest water repellency occurs when the water drops touch the tips of the epicuticular wax crystals only. The waxes are, however, relatively soft materials so that older leaves often show patches of eroded or damaged wax, which cause an increased adhesion of water. For the Buxes leaves, this means that the droplets can very easily intrude between the papillae. To make a more differentiated comparison, the adhesion between surface and water during retraction of a drop could be measured [29].

Figure 5.5: *B. sempervirens* stems full with leaves (a) and a close up of a Buxus stem top with older (dark green) and newer leaves (bright green) (b),

The measured *B. sempervirens* contact angles were very different for each leaf. An example of this difference is shown in figure 5.7. Both pictures show a water droplet on top of the *B. sempervirens* leaf. The image on the left shows a droplet on top of a leaf that is more light green as shown in the photograph in figure 5.5, whereas the image on the right shows a droplet on top of a more dark green leaf. Literature studies reveal that the *B. sempervirens l.*, which is a cultivar of the normal *B. sempervirens* does not maintain water-repellency for the whole lifetime of the leaf [30]. We assume that this is also the case for our *B. sempervirens*.

The epicuticular wax of the *B. Sempervirens* leaves was reported to consist of coiled rodlets, as shown in figure 2.6. However, this leaf structure could not be observed in the nanoscale images shown in the article of Gostin et al. [30].
For our experiment, epicuticular wax of the *B. sempervirens* leaf surface is extracted by immersing 50 leaves for 1-2 seconds in chloroform just as in the previous experiment. The wax solution, which is deposited on a silicon wafer, is shown in figure 5.8. The height differences in the picture range between 0 nm and 165 nm. The wax surface structure we obtained did not change over time. Although we do not observe any repeating crystalloid features on the surface, like the coiled rodlets, the surface shows a similar appearance as the leaf surfaces shown in the article by Gostin et al.. By this we mean a rough lumpy layer structure. Because the Buxus leaf surface structure shows ontogenetic development and also the adaxial and abaxial leaf surfaces are reported to show different epicuticular waxes [30], the formation of rodlets might not occur.

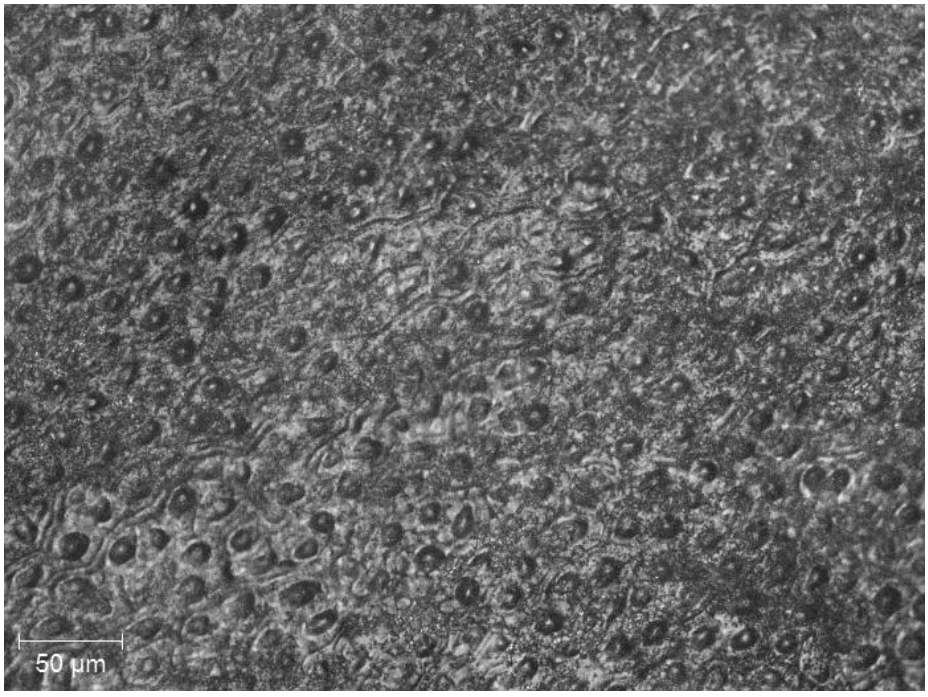

Figure 5.6: OM image of the *B. sempervirens* leaf surface with a high density of protruding epidermal cells.

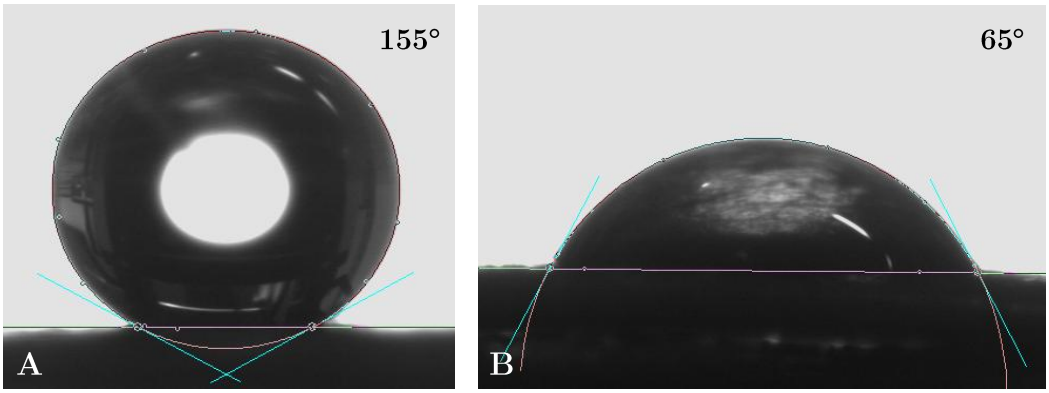

Figure 5.7: Droplets on top of a younger (a) and older (b) piece of *B. sempervirens* leaf

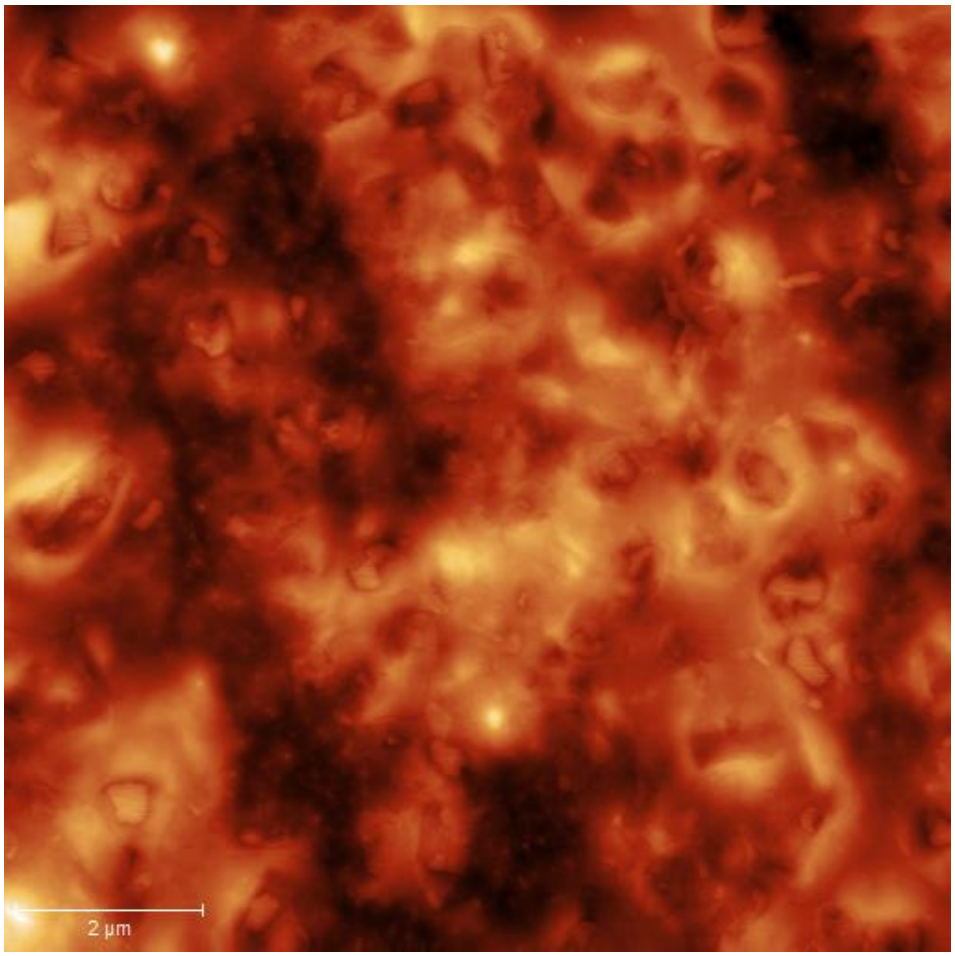

Figure 5.8: AFM topography image of *B. sempervirens* wax on top of a silicon wafer. The maximum height difference in the picture is 165 nm.

Chapter 6

Conclusions and outlook

In this project, hydrophobic leaf surfaces and their epicuticular waxes are examined. In particular the leaves of *Euphorbia myrsinites* have been extensively studied. The epicuticular wax on the *E. myrsinites* leaves contain hexacosan-1-ol platelets in the nanoscale. On the one hand, the goal of this project was to acquire more knowledge on the deposition of epicuticular waxes, and on the other hand, the goal was to actually recrystallise the epicuticular wax and measure the time dependent growth. On both aims we will give a brief conclusion and an outlook for future experiments will be given.

Sample fabrication and suitability of characterisation tools

Within the project it was chosen to extract the waxes with an organic solvent and deposit them out of solution. With the use of this method, fabrication of the epicuticular wax is relatively simple. Most epicuticular waxes are removed within 1-2 sec. immersion in chloroform. However, the deposition out of solution creates a very unequal distributed wax on the samples. This could complicate the measurements on the sample. For example the atomic force microscopy measurement on the *E. myrsinites* epicuticular wax could not be carried out. This might also have been difficult because the nanostructure aspect ratio was too high, but mainly the extreme height differences in the larger scale caused problems. Furthermore, we were not able to measure the contact angle of just the epicuticular wax nanostructure, because the height differences in the underlying wax layers caused microscale roughness. In addition, if the layers would have been smooth, we could have used the ellipsometer to exactly determine layer thicknesses.

The optical microscope was found to be very suitable for quickly carrying out multiple surface structure measurements in the microscale. A lens of 20 times enlargement is sufficient to easily determine the surface structuring, and a lens of 50 times enlargement gives a little more detail. The AFM is a useful technique to measure topographical nanoscale features with high resolution. The tubules of the Aquilegia canadensis wax could be measured very precisely and also layer growth from the *E. myrsinites* wax could be observed in enough detail. However, for measuring platelet waxes with high aspect ratios, we would not recommend this technique. The scanning electron microscope is extremely suitable for the characterisation of epicuticular waxes. The SEM gives a morphological overview of the surface that gives more information than any of the other techniques. Also, this technique could be used to explore the surface primary to other experiments, which might be helpful to start with. For measuring leaves and waxes, we would not recommend to use the helium ion microscope. The ultra high vacuum pumping could influence the sample. The ion and electron beam (SEM) did also influence the sample. When the sample was irradiated with the beam for some time, the features on the sample were slightly moving induced by heat. However, the observed changes to the surface seem negligible. Furthermore, gas chromatography is found to be very useful to determine main components and the well-known contact angle goniometer very helpful to easily get an impression of the wetting properties.

Wax recrystallisation

The final goal of the experiments was to recrystallise plant epicuticular waxes on artificial surfaces and follow the growth process over time after deposition. For the different deposited waxes within this project, no time dependent change (except for layer growth) of the epituticular wax could be observed. The *E. myrsinites* wax was recrystallised on top of a silicon wafer with a certain nanostructure. We found that the obtained nanostructure was different then for the real leaf surface. However, we could also observe many similarities, such as the growth on top of multiple wax layers, the height and width of the features, the overlapping and the mutual crossing.
The differences in the nanostructure could be influenced by the rapid crystallisation when the chloroform evaporates, but we think the substrate has a larger influence. Already in the first deposition experiments, we observed that the substrate does influence the wax growth by the slight differences of *E. myrsinites* wax growth on a cover glass compared to the growth on silicon. The first molecular layer of, mostly, hexacosan-1-ol molecules on silicon will grow on an amorphous layer. We observed that, only when a very thick layer of wax has been formed, nanostructure was present. In this case, the silicon has no influence on the growth of the molecules, but only the mutual interactions between the molecules themselves have. It was reported in literature that recrystallisation of epicuticular waxes on non-polar substrates with a crystalline structure, leads to different crystal growth and morphology. The molecular orientation and spatial distribution of crystals is shown to be different on these substrates.
It is therefore expected that also the *E. myrsinites* platelet growth will be different on non-polar, crystalline substrates. We expect to obtain more structuring and less epicuticular wax will be necessary to obtain a nanostructured surface. This is not examined within this project.

Additional findings

During the project some additional ideas arose. Therefore, additional surface aspects are examined, like the ordering of papillae on the *E. myrsinites* leaves. This experiment showed us that the papillae are distributed across the surface in a certain fashion and that the distribution also depends on the size of the papillae. As far as we know this has not been reported before in literature.
Furthermore, quite some contact angle measurements of different surfaces are carried out. Some remarkable finding we got was that the immersed leaves will become sticky and the static contact angle is raised for long immersion times in chloroform. This is due to the fact that the adhesive forces of the leaf surfaces will become stronger and the surface will get rougher.

Outlook

This report can be used as a guide for further research on epicuticular waxes. The report provides a global overview of many things that can be examined for hydrophobic plants. Unfortunately, not all our experimental ideas could be carried out within the project period. If we consider the current results, mainly the deposition of *E. myrsinites* wax on different substrates would be interesting to examine. We would recommend using HOPG as a substrate for the next experiments and observe how the growth takes place. This could give new insights in the growth and dynamics of the wax. It was already found that the polarity and crystallinety influence the growth, although the relation to the growth on plant surfaces is not fully understood.

Furthermore, using a more advanced deposition method, as physical vapor deposition, would ensure a smooth layer of wax on the surfaces. This could make certain measurements easier to carry out and/or more reliable. Also, using a more advanced AFM could make sure that it would be possible to measure surfaces right after deposition of the wax and take images faster. This could give more additional information on the growth. Besides, also other techniques as diffraction should be considered. With this technique molecular arrangement can be determined.

In addition, it would be interesting to calculate the radial distribution function of several other plants and compare them to the *E. myrsinites* leaf. We expect to also find ordering on other leaf surfaces.

Bibliography

1. Gao, H., et al., *Mechanics of hierarchical adhesion structures of geckos.* Mechanics of Materials, 2005. **37**(2-3): p. 275-285.
2. Gao, X. and L. Jiang, *Biophysics: Water-repellent legs of water striders.* Nature, 2004. **432**(7013): p. 36-36.
3. Reif, W.-E., *Squamation and ecology of sharks.* 1985, Frankfurt am Main: Senckenbergische Naturforschende Gesellschaft.
4. Genzer, J. and K. Efimenko, *Recent developments in superhydrophobic surfaces and their relevance to marine fouling: a review.* Biofouling, 2006. **22**(5): p. 339-360.
5. Koch, K., H.F. Bohn, and W. Barthlott, *Hierarchically Sculptured Plant Surfaces and Superhydrophobicity.* Langmuir, 2009. **25**(24): p. 14116-14120.
6. Koch, K., A. Dommisse, and W. Barthlott, *Chemistry and Crystal Growth of Plant Wax Tubules of Lotus (Nelumbo nucifera) and Nasturtium (Tropaeolum majus) Leaves on Technical Substrates.* Crystal Growth & Design, 2006. **6**(11): p. 2571-2578.
7. Meusel, I., et al., *Chemical Composition and Recrystallization of Epicuticular Waxes: Coiled Rodlets and Tubules.* Plant biology, 2000. **2**(04): p. 462-470.
8. Koch, K. and W. Barthlott, *Superhydrophobic and superhydrophilic plant surfaces: an inspiration for biomimetic materials.* Philosophical Transactions of the Royal Society A: Mathematical, Physical and Engineering Sciences, 2009. **367**(1893): p. 1487-1509.
9. de Gennes, P.G., F. Brochard-Wyart, and D. Quere, *Capillarity and Wetting Phenomena: Drops, Bubbles, Pearls, Waves.* 2004: Springer.
10. Wenzel, R.N., *Resistance of solid surfaces to wetting by water.* Industrial & Engineering Chemistry, 1936. **28**(8): p. 988-994.
11. Cassie, A.B.D. and S. Baxter, *Wettability of porous surfaces.* Transactions of the Faraday Society, 1944. **40**(0): p. 546-551.
12. Bartolo, D., et al., *Bouncing or sticky droplets: Impalement transitions on superhydrophobic micropatterned surfaces.* Europhysics Letters (EPL), 2006. **74**(2): p. 299-305.
13. Israelachvili, J.N., *4 - Interactions Involving Polar Molecules*, in *Intermolecular and Surface Forces (Third Edition)*, J.N. Israelachvili, Editor. 2011, Academic Press: San Diego. p. 71-90.
14. Latthe, S.S., et al., *Superhydrophobic surfaces developed by mimicking hierarchical surface morphology of lotus leaf.* Molecules, 2014. **19**(4): p. 4256-83.
15. Prum, B., et al., *Impact of cell shape in hierarchically structured plant surfaces on the attachment of male Colorado potato beetles (Leptinotarsa decemlineata).* Beilstein J Nanotechnol, 2012. **3**: p. 57-64.
16. Bhushan, B. and Y.C. Jung, *Micro- and nanoscale characterization of hydrophobic and hydrophilic leaf surfaces.* Nanotechnology, 2006. **17**(11): p. 2758.
17. Koch, K. and H.-J. Ensikat, *The hydrophobic coatings of plant surfaces: Epicuticular wax crystals and their morphologies, crystallinity and molecular self-assembly.* Micron, 2008. **39**(7): p. 759-772.

18. Barthlott, W. and C. Neinhuis, *Purity of the sacred lotus, or escape from contamination in biological surfaces.* Planta, 1997. **202**(1): p. 1-8.
19. Koch, K., et al., *Self assembly of epicuticular waxes on living plant surfaces imaged by atomic force microscopy (AFM).* Journal of Experimental Botany, 2004. **55**(397): p. 711-718.
20. Ensikat, H.J., et al., *Crystallinity of plant epicuticular waxes: electron and X-ray diffraction studies.* Chemistry and Physics of Lipids, 2006. **144**(1): p. 45-59.
21. Barthlott, W., et al., *Classification and terminology of plant epicuticular waxes.* Botanical Journal of the Linnean Society, 1998. **126**(3): p. 237-260.
22. Dora, S.K. and K. Wandelt, *Recrystallization of tubules from natural lotus (Nelumbo nucifera) wax on a Au(111) surface.* Beilstein Journal of Nanotechnology, 2011. **2**: p. 261-267.
23. Koch, K., et al., *The use of plant waxes as templates for micro- and nanopatterning of surfaces.* Acta Biomaterialia, 2007. **3**(6): p. 905-909.
24. Hlawacek, G., et al., *Helium ion microscopy.* Journal of Vacuum Science & Technology B, 2014. **32**(2).
25. Schindelin, J., et al., *Fiji: an open-source platform for biological-image analysis.* Nat Meth, 2012. **9**(7): p. 676-682.
26. Kirkwood, J.G. and E.M. Boggs, *The Radial Distribution Function in Liquids.* The Journal of Chemical Physics, 1942. **10**(6): p. 394-402.
27. Reichman, D.R. and P. Charbonneau, *Mode-coupling theory.* Journal of Statistical Mechanics: Theory and Experiment, 2005. **2005**(05): p. P05013.
28. Guo, Z.-G. and W.-M. Liu, *Sticky superhydrophobic surface.* Applied Physics Letters, 2007. **90**(22).
29. Ensikat, H.J., et al., *Superhydrophobicity in perfection: the outstanding properties of the lotus leaf.* Beilstein Journal of Nanotechnology, 2011. **2**: p. 152-161.
30. Gostin, I.N., *Leaf micromorphology in Buxus sempervirens L. during the ontogenesis.* Analele Universităţii din Oradea, Fascicula Biologie, 2009. **16**(1): p. 57-60.

Appendix 1

Chemical analysis

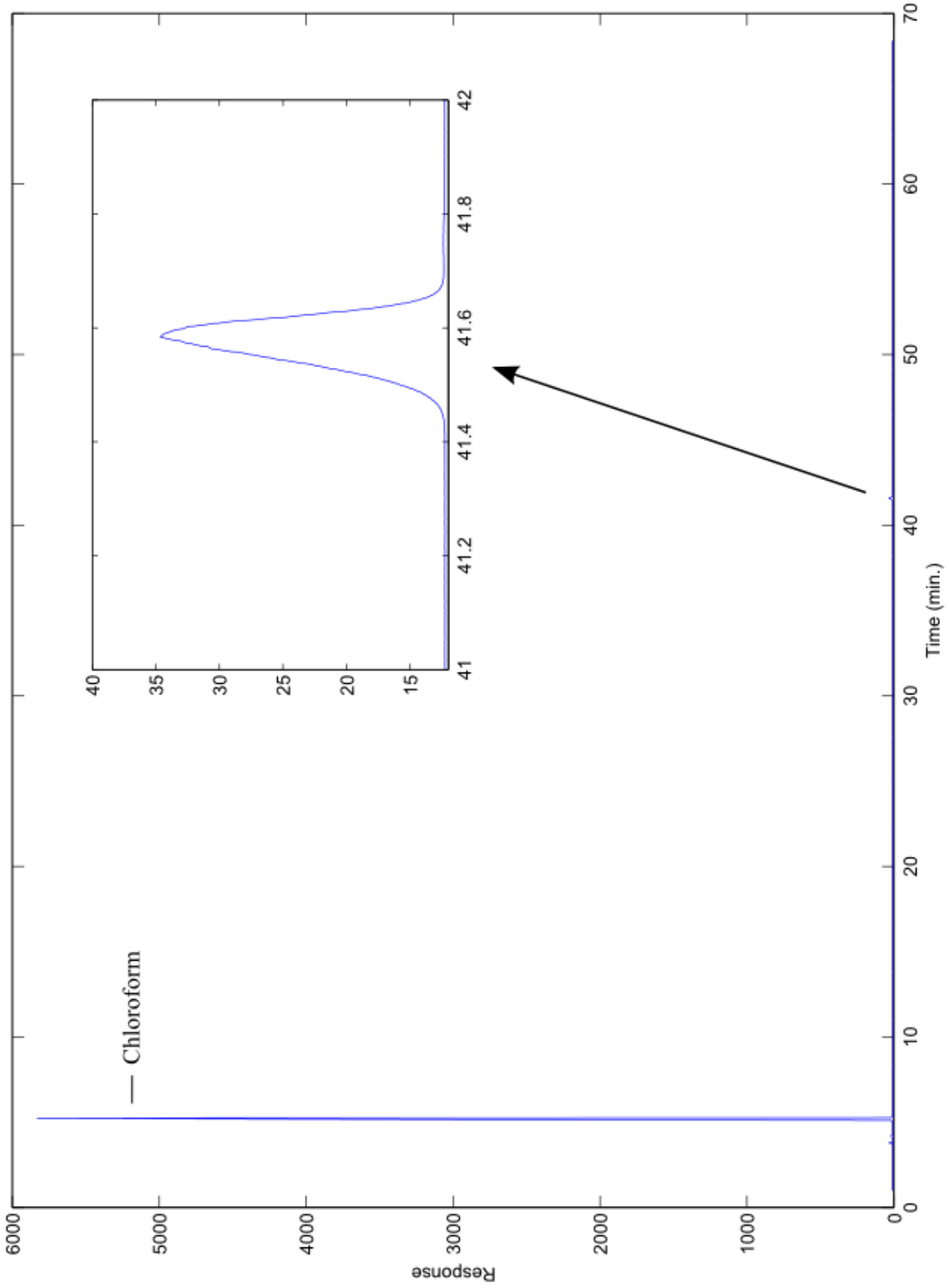

Figure A 1: Gas chromatography measurement of the wax which was extracted with room temperature chloroform.

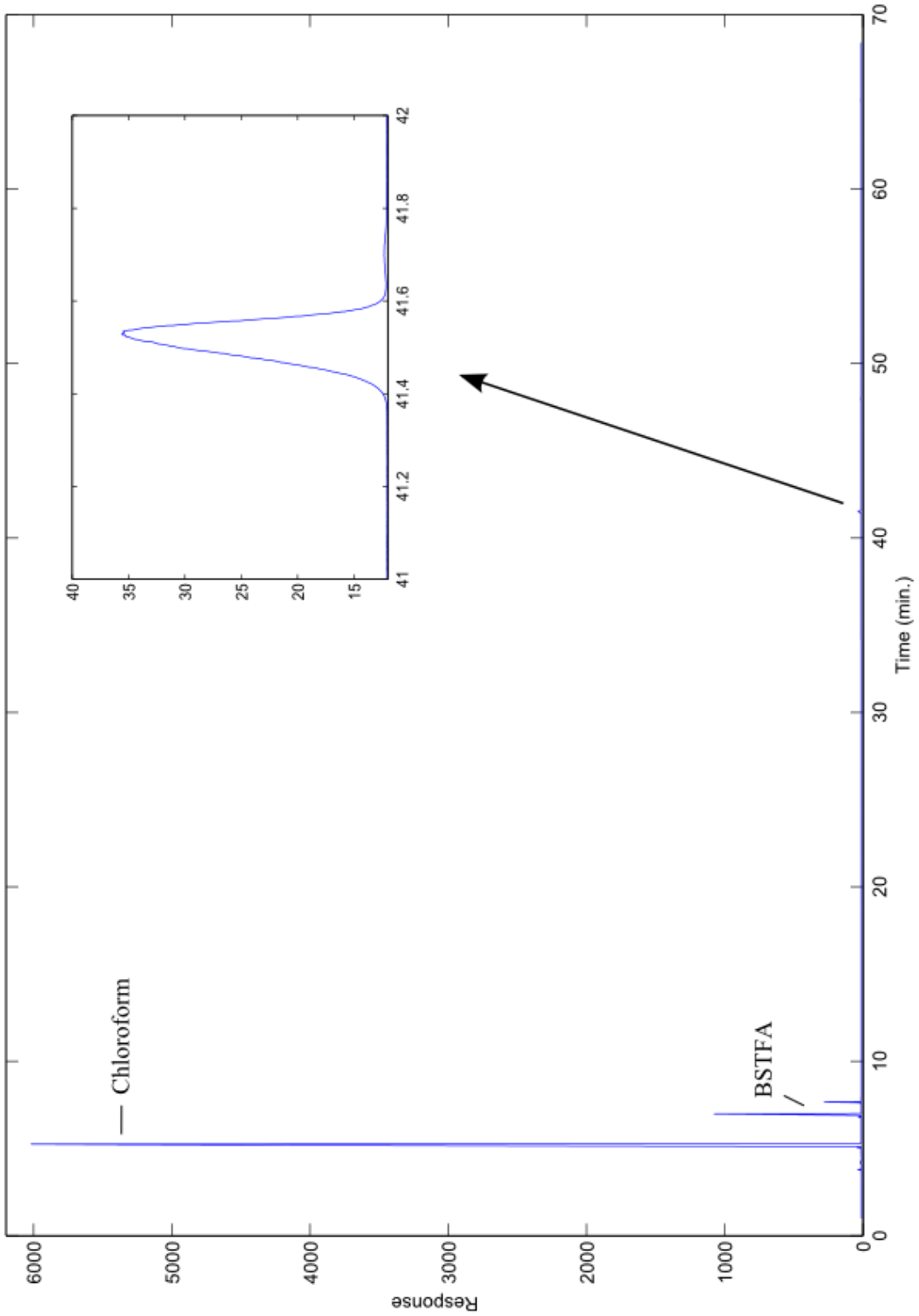

Figure A 2: Gas chromatography measurement of the wax which was extracted with chloroform heated to 50°C. Due to the relatively high concentration of chloroform, the peak caused by the presence of the main component is very small. Even if we exclude the first 10 min. from the graph, only this component really stands out as a component that could potentially be present on the leaf surfaces.

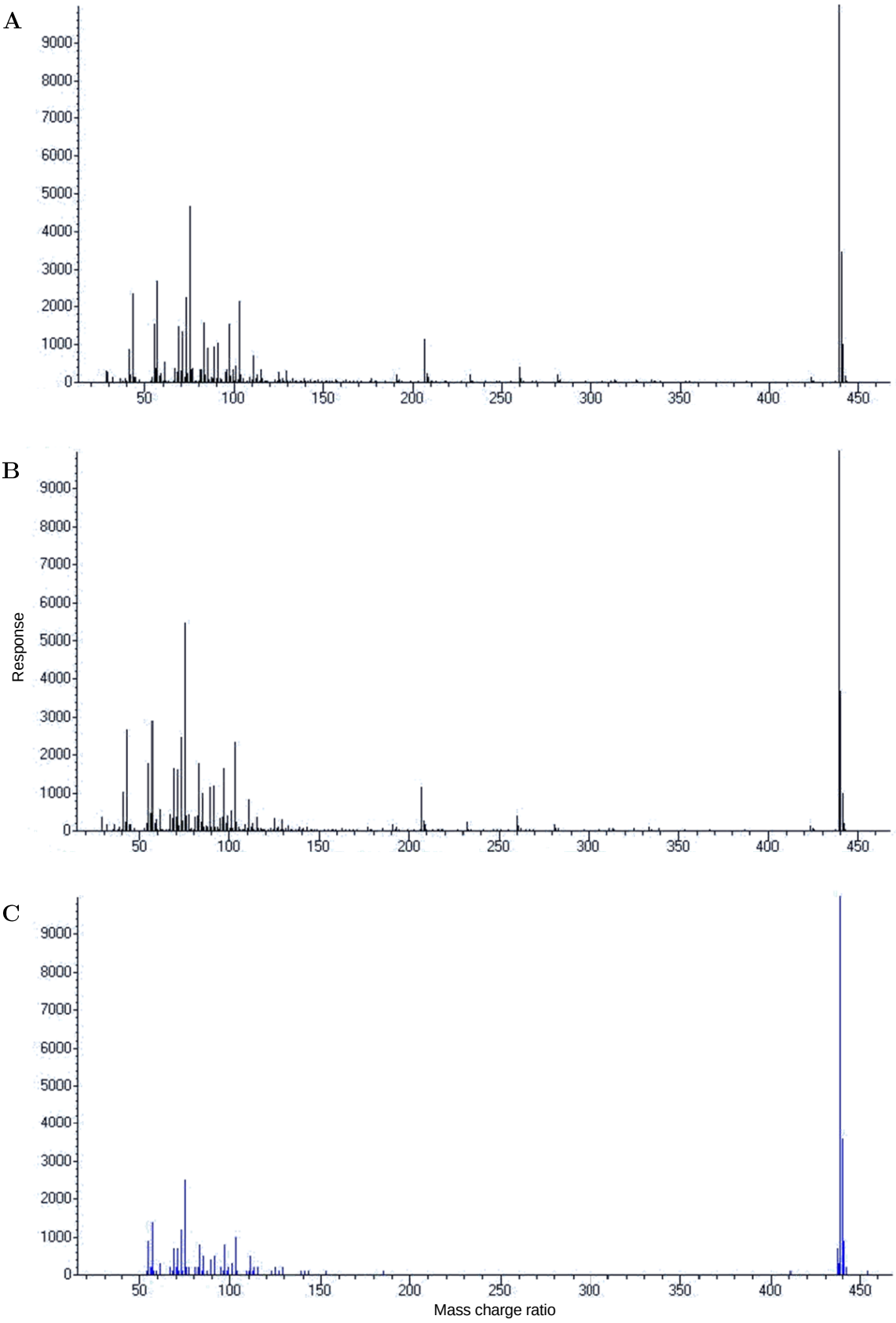

Figure A 3: Mass spectrometry measurement of the wax which is extracted with room temperature chloroform (a) and with chloroform heated to 50°C (b) for the peaks at 41.5 minutes. The bottom figure shows the most comparable component from the database: silane, (hexacosyloxy)trimethyl-.

Appendix 2

Contact angle measurements

Measurement no.	CA left [°]	CA right [°]
1	160,7	161,2
2	159,1	159,2
3	161,8	161,9
4	163,2	163,4
5	164,5	164,6
6	160,7	160,9
7	163,2	163.0
8	164,7	164,4
9	164,2	164,2
10	157,4	157,2
11	160,7	160,8
12	157,4	157,8
13	160,4	160,3
14	162,5	162,5
15	161,8	161,8
16	155,5	155,8
17	156,5	156,6
18	159,8	159,7
19	160,3	160,5
20	161.0	161,1
Average	160.8±2.5	

Table 1: Static contact angles of 15 pieces of Euphorbia myrsinites leaf and the average value with the standard deviation are shown.

Time	1 sec.		5 sec.		10 sec.		30 sec.		1 min.	
CA position	left	right	left	right	left	right	left	right	left	right
1	116.8	117.3	123.8	124.2	125.0	126.6	138.0	137.8	146.1	146.4
2	116.0	117.1	126.6	127.7	145.1	145.2	141.0	141.1	146.0	146.0
3	127.7	128.7	121.4	121.6	135.4	135.1	135.6	135.3	148.9	149.0
4	126.9	127.2	129.8	130.4	130.5	130.0	150.1	150.2	153.4	153.4
5	146.9	146.6	117.4	118.3	114.0	113.6	141.3	140.9	134.8	134.7
6	139.0	138.6	128.0	128.5	134.9	135.5	129.6	128.5	144.9	143.6
7	125.9	124.9	118.9	119.5	132.1	132.3	130.1	130.3	150.0	150.2
8	135.3	135.2	122.7	121.7	138.8	139.1	135.9	136.0	150.3	150.5
9	121.7	122.8	131.4	130.4	136.2	135.6	132.1	131.2	136.2	136.2
10	124.9	126.3	123.9	123.7	127.2	127.1	129.9	129.0	139.3	138.7
11	132.7	132.7	124.0	123.6	123.8	124.1	142.7	142.7	152.4	152.2
12	126.0	124.9	126.1	125.7	147.6	147.5	150.5	150.3	139.1	139.7
13	131.9	131.2	123.8	124.2	126.3	126.9	147.2	146.7	142.2	142.8
14	129.8	130.9	132.4	131.6	122.6	124.2	147.7	147.8	145.9	146.2
15	131.6	130.0	140.8	141.0	126.9	127.3	140.0	140.3	146.8	146.4
Average	128.9±7.6		125.0±4.1		131.6±8.7		139.3±7.1		145.1±5.5	

Table 2: Static contact angle [°] of Euphorbia myrsinites leaves as a function of leaf immersion time in chloroform including the average value and standard deviation.

Measurement no.	CA left [°]	CA right [°]
1	113,4	112
2	106.5	107.9
3	105.2	107.6
4	108.6	109.8
5	108.8	109.8
6	109.9	109.2
7	104.4	107.4
8	113.6	115.5
9	108.2	106.8
10	114	115.1
11	109.5	109.9
12	111.6	111.6
13	116	115.5
14	108.4	112.2
15	106.9	106.8
Average	110.1±3.2	

Table 3: Static contact angle measurements of Euphorbia myrsinites wax on top of a silicon wafer and the average value with standard deviation.

Measurement no.	CA left [°]	CA right [°]
1	148.7	148.9
2	157.8	158.2
3	154.0	154.5
4	152.3	152.3
5	159.7	159.8
Average	154.6±3.9	

Table 4: Static contact angle measurements of Euphorbia myrsinites wax on top of a silicon wafer, deposited out of a higher concentrated wax-chloroform solution. The average value with standard deviation is given in the lower row of the table.

Acknowledgements

Since there are many people who in some way helped me to make this thesis possible, I want to dedicate this final page to them. First of all I would like to thank the entire PIN group for their sociability and kindness. I had a great time working on my master project.

I would like to thank Prof. Harold Zandvliet, for providing me with the opportunity to do my thesis work in his group and for being part of the graduation committee. I also would like to thank Dr. Chao Sun for acting as an external member of the committee. In special thank Stefan, my supervisor, for sharing ideas and regularly checking my progress. Especially his reviewing on my report was very helpful. In addition, I would like to thank Mark for helping me with the scanning electron microscopy measurements and Gregor for helping me with helium ion microscopy measurements. The results gave me plenty of data to work with. Furthermore, I would like to thank Stijn for helping me with the chemical analysis of the wax. I would like to thank Robin, Patrick, Erik and Pantelis for showing me how to work in the lab and of course my roommate Kai for fun conversations between the working hours. Last but not least, I would like to thank my family and friends for all the fun during my studies.